Fouling and its control in membrane distillation for the treatment of reverse osmosis brine

By
Po Zhang

Master of Civil & Environmental Engineering (Advanced) – University of Adelaide – Adelaide – Australia
Bachelor of Chemical Engineering – Beijing University of Chemical Technology – Beijing – China

A thesis submitted to Victoria University – Melbourne – Australia for the degree of Doctor in Philosophy

Institute for Sustainable Industries & Liveable Cities at Victoria University

Melbourne Australia
August 2019

Abstract

Membrane distillation (MD) technology is a promising technology for treating RO brine to enhance overall water recovery and extract valuable salts, thus approaching zero-liquid-discharge. The benefits of MD technology such as no hydraulic pressure restriction, compact design and small carbon footprint by utilising renewable energy or waste heat sources, have created exciting opportunity of integrating MD into desalination systems and ultimately delivering safer, cheaper, more efficient and sustainable desalination operations. However, the lack of understanding of MD membrane fouling and its control are the major obstacles that hamper this technology being realised by industry.

The aim of the present study was to understand the behaviours of MD membrane fouling formation and fouling kinetics in RO brine treatment, and use the knowledge to propose feasible ways to manage fouling in MD industrial applications. The scope of this problem was narrowed to focus on three real RO brines, namely, seawater RO (SWRO) brine, coal seam gas (CSG) RO brine and copper barren RO brine. SWRO brine study was mainly focused on the inorganic scaling, such as $CaCO_3$ and $CaSO_4$. Silica fouling mechanisms were investigated during the study of CSG RO brine. In copper barren RO brine study, the impact of ammonia transfer on the precipitation of metal salts was evaluated. In addition, MD performance was assessed using a commercial oleophobic membrane. The experimental works were undertaken using a bench-scale direct contact membrane distillation (DCMD) apparatus which was specifically constructed for this study.

The key findings from this study include: (1) for brine with the high potential for $CaCO_3$ and $CaSO_4$ precipitation, antiscalant prolonged MD operational time by mitigating salt

precipitation. However, significant homogeneous nucleation of $CaCO_3$ and $CaSO_4$ occurred at a critical brine electrical conductivity (EC) level even in the presence of antiscalant. The rapid formation of crystal deposits was correlated to the pH variation in brine, where pH was an early indicator of rapid flux decline. Although distillate flushing was effective in removing inorganic scaling from membrane surface, organic fouling on the other hand, showed resistance to non-chemical flushing. (2) for brine containing dissolved silica, low hardness and high $NaHCO_3$, Mg^{2+} demonstrated stronger bonding with dissolved silica as compared to Ca^{2+}. The precipitation of magnesium silicates was strongly influenced by the concentration of Mg^{2+} and brine pH. HCO_3^- / CO_3^{2-} on the other hand, showed greater ability to stabilise silica in dissolved form compared with Cl^-. In addition, polymeric silica fouling significantly affected MD performance, demonstrated by rapid flux decline and exponential increase of distillate EC. (3) MD achieved stable performance with negligible fouling over a relative long period of operation for concentrating brine with high dissolved ammonia and metal ions. At above neutral pH, dissolved ammonia reacted with metal ions and formed stable metal-ammonia complexes in soluble form which prevented membrane fouling from metal deposits. (4) antiscalant existed in all three brines did not demonstrate fouling potential in MD membrane in terms of membrane surface attachment nor potential for membrane wetting.

Practical MD fouling management strategies were also evaluated in this study and the key recommendations include: (1) intermittent flushing with distillate water and raw RO brine is effective in removing inorganic salt nucleus from membrane surface. (2) inline cartridge filtration can assist the removal of salt crystals in bulk brine and thereby improve brine water recovery and MD operational time between cleaning events. (3) disodium ethylenediaminetetraacetic acid (Na_2EDTA) treatment in brine can hinder the formation

of Ca / Mg–silicates. However, the key is to avoid sudden temperature decline in MD process which could cause rapid formation of colloidal amorphous silica. (4) oleophobic membrane could be adopted to tackle the high organic containing brines.

Overall, the feasibility of MD for concentrating RO brine was demonstrated in this study. The investigation of MD fouling management strategies, such as cartridge filtration, distillate / raw brine flushing, EDTA / antiscalant treatment and chemical cleaning showed practical implications of sustainable operation of MD process. This study also showed that drastic precipitation of $CaCO_3$ / $CaSO_4$ and polymerised silica have high tendency to cause membrane wetting. Therefore, it is important for industry to determine the critical brine EC level via bench scale / pilot study when concentrating RO brine that has high scaling potential of $CaCO_3$ / $CaSO_4$, and to avoid sudden temperature decline in MD brine recycling stream to mitigate the formation of colloidal amorphous silica.

Declaration

"I, Po Zhang, declare that the PhD thesis entitled **Fouling and its control in membrane distillation for the treatment of reverse osmosis brine** is no more than 100,000 words in length including quotes and exclusive of tables, figures, appendices, bibliography, references and footnotes. This thesis contains no material that has been submitted previously, in whole or in part, for the award of any other academic degree or diploma. Except where otherwise indicated, this thesis is my own work".

Signatu [redacted] Date 12th August 2019

Acknowledgement

It has been a long (9 years as a part-time student) journey to get here. I am grateful that Dr **Eddy Ostarcevic** saw my passion and introduced me to this journey. His life and career advices always encouraged me to stay positive whenever my life situations changed. His enthusiasm in chemical engineering has been an inspiration to me.

My most sincere gratitude goes to my principle supervisor Prof. **Mikel Duke** and associate supervisor Prof. **Stephen Gray** from Institute for Sustainable Industry & Liveable Cities, Victoria University. The comments, ideas and knowledge not only helped me to write this thesis, but more importantly, taught me to think the scientific reasons behind observations and always pay attention to details. The incredible kindness, patience and encouragement helped me to push through the obstacles and stay focused during this study.

I appreciate the supports from Mr **Hiep Le** and Mr **Jason West** allowing me to undertake experimental works and write up the thesis during my employment with Osmoflo Pty Ltd and SA Water.

Lastly, I want to thank my family particularly my wife **Di**, has been extremely supportive of me throughout this journey and has made countless sacrifices to help me to get to this point.

Publications from this research

Zhang P, Knötig P, Gray S and Duke M. Scale reduction and cleaning techniques during direct contact membrane distillation of seawater reverse osmosis brine. Desalination 2015; 374: 20-30.

Zhang P, Pabstmann A, Gray and Duke M. Silica fouling during direct contact membrane distillation of coal seam gas brine with high sodium bicarbonate and low hardness. Desalination 2018; 444: 107-117.

Paper under writing process

Zhang P, Gray S and Duke M. Direct contact membrane distillation for the concentration of reverse osmosis brine from copper processing plant barren leach solution.

Conference presentations

5th – 8th December 2016, Adelaide, South Australia – **International Membrane Science and Technology Conference**. Oral presentation on the seawater RO brine and CSG RO brine minimisation by membrane distillation process.

28th – 30th November 2012, Brisbane, Queensland, **Membrane Society of Australasia Early Career Researchers Symposium**. Poster presentation on the investigation of membrane distillation on seawater RO brine.

Table of Contents

List of Tables

List of Figures

List of common abbreviation

Air gap membrane distillation	AGMD
American society for testing and materials	ASTM
Brackish water reverse osmosis	BWRO
Clean-in-place	CIP
Coal seam gas	CSG
Concentration factor	CF
Coal bed methane	CBM
Capital expenditures	Capex
Direct contact membrane distillation	DCMD
Disc tube reverse osmosis	DTRO
Dissolved organic matters	DOC
Electrical conductivity	EC
Ethylenediaminetetraacetic acid	EDTA
Electrodialysis	ED
Electrodialysis reversal	EDR
Energy dispersive spectroscopy	EDS
Humic acid	HA
Inductively coupled plasma – atomic emission spectroscopy	ICP–AES
Inorganic carbon	IC
Ion product	IP
Liquid entry pressure	LEP
Low-density polyethylene	LDPE

Membrane electrolysis	ME
Membrane distillation	MD
Multi-effect distillation	MED
Multi-stage flash	MSF
Microfiltration	MF
Mechanical vapour compression	MVC
Natural organic matters	NOM
Disodium ethylenediaminetetraacetic acid	Na_2EDTA
Membrane brine concentrator	MBC
Osmoflo brine squeezer	OBS
Operational expenditures	Opex
Polytetrafluoroethylene	PTFE
Polyvinylidene fluoride	PVDF
Polypropylene	PP
Reverse osmosis	RO
Scanning electron microscope	SEM
Stiff and Davis stability index	S&DSI
Saturation index	SI
Specific thermal energy consumption	STEC
Seawater reverse osmosis	SWRO
Sweep gap membrane distillation	SGMD
Total dissolved solids	TDS
Total organic carbon	TOC
Total carbon	TC

Total inorganic carbon	TIC
Tetrasodium ethylenediaminetetraacetic acid	Na_4EDTA
Ultra-high pressure RO	UHP RO
Ultrafiltration	UF
Vacuum membrane distillation	VMD
X-ray diffraction	XRD
Zero liquid discharge	ZLD

Chapter 1 Introduction

1.1 Background

The rising global population and the increasing demand for consumable water are the key factors that have been driving the continuous growth of the global desalination market over the past 30 years. It is estimated that total desalinated water demand will reach 2.92 billion m^3/day by 2030 (Gude et al. 2018). Over the last few years, reverse osmosis (RO) technology has emerged as the fastest growing technology for desalination. In 2017, over 90% of new desalination capacity uses RO as opposed to the traditional thermal distillation technologies (Global Water Intelligence 2017). The main reasons for the success of RO are higher energy efficiency by adopting highly efficient energy recovery system and higher water recovery rate compared to conventional thermal-based desalination technologies. However, as the result of growing interest in RO desalination, disposing large quantity of RO brine at high salinity presents both environmental and financial challenges. Seawater RO (SWRO) desalination is predominantly used for potable water production for large populations located near the coast. This process is typically operated to achieve 40 to 50% water recovery depends on the seawater salinity and temperature, and the remaining 50 to 60% brine solution is usually discharged back to the sea without any treatment. For the world's largest desalination plant, the Sorek SWRO plant (Israel) with capacity of 624,000 m^3/day, it means that more than 524,000 m^3 of brine at salt concentration of ~ 60 g/L will be discharged back into the ocean on a daily basis when plant runs at full capacity. Therefore, significant cost is associated with brine disposal, such as pumping and piping systems. Additionally, the large quantity of

brine could have a strong potential to detrimentally impact on costal ecosystem and species (Morillo et al. 2014).

Brackish water RO (BWRO) process can operate at much higher water recovery than SWRO, from 75 to 90%. A majority of BWRO plants are located at inland areas, and therefore cannot dispose brine into a large water body like SWRO. The BWRO brine disposal cost could reach 30% of total desalination cost depends on the quantity of brine and the characteristics of brine which determines the level of treatment before disposal (Morillo et al. 2014).

RO technology has been successfully implemented in mining, coal seam gas (CSG), and resource industries located at inland of Australia. In these industries, the RO process water recovery range of 75 to 90% depends on the concentrations of total dissolved solids (TDS) in water. The major strategy for inland RO brine management is via evaporation pond. However, the cost of constructing and managing evaporation ponds can be quite substantial (Ahmed et al. 2001), such as double-lined pond with long-term monitoring for groundwater aquafers. Moreover, at industrial site where constructing additional evaporation pond is almost impossible due to the large area required for land storage, RO brine disposal could directly restrict the business from expansion. Therefore, RO brine management represents significant challenge both from economic and environmental perspectives.

Brine volume reduction is one of the possible advanced ways to manage RO brine. Well established current-driven technologies such as electrodialysis (ED) and electrodialysis reversal (EDR) have limited ability to achieve high water recovery from RO brine due to fouling / scaling and high energy cost (Martinetti et al. 2009). Conventional thermal methods such as brine concentrator, crystalliser and thermal evaporators, such as multi-

effect distillation (MED) and multi-stage flash (MSF) are capable of recovering high quality water, and at the same time, achieving high water recovery from RO brine. However, the capital and operating costs often exceed the cost of the RO process and thus, they are not typically used (Martinetti et al. 2009).

Membrane distillation (MD) technology has been identified among several emerging technologies aimed at enhancing overall water recovery and minimising RO brine disposal. MD is a thermal membrane separation process that involves transport of vapour through microporous hydrophobic membranes and operates on the principle of vapour-liquid equilibrium as a basis for molecular separation. MD was first patented in 1963, but it experienced slow growth in desalination application (no commercial installations known) and was taken over by the rapid development of RO technology in the last 40 years. In the last ten years, with the increasing interest in developing the sustainable desalination industry, there has been an accelerated research interest focused on brine management using MD technology attributed to several benefits, such as lower operating pressure compared to RO, capability of utilising the renewable energy (e.g., solar and geothermal) and industrial low grade waste heat, potential to be more compact and versatile compared to conventional thermal-based technologies, and potential for 100% rejection of non-volatile solutes (Tun et al. 2005; Camacho et al. 2013; Deshmukh et al. 2018). Therefore, integrating MD technology into conventional desalination plants could potentially bring positive effects in waste reduction, recovery of valuable salts from brine and carbon footprint reduction (Drioli et al. 2017).

1.2 Problem statement

Despite the advantages mentioned above, MD still needs to overcome several hurdles before this technology can be realised commercially. Among them, membrane fouling is a major operational issue for RO brine treatment.

Sparingly soluble salts such as $CaCO_3$ and $CaSO_4$ are the main salts forming scale in seawater environment. Both salts demonstrate inverse solubility with temperature. When treating SWRO brine with MD, $CaCO_3$ and $CaSO_4$ can easily reach their supersaturation limits and form deposits on membrane surface and thereby affect the performance of MD (e.g., distillate flux). In addition, the dissolved organic matters (DOC) in seawater such as humic substances and polysaccharides could interact with divalent cations and hydrophobic MD membrane, and lead to the intrusion of brine into membrane pores and, thus, irreversibly deteriorating distillate quality (Curcio et al. 2010).

Silica fouling is a major unsolved problem in brackish water desalination process (Milne et al. 2014). Polymerised silica fouling layer has been problematic in RO process as it is very difficult to remove by conventional chemical cleaning approaches (Koo et al. 2001). In MD treatment of CSG RO brine, dissolved silica in CSG produced water could reach its solubility limit at high water recovery and form amorphous silica deposits on membrane surface. Moreover, the alkaline environment of CSG produced water favours the reaction between dissolved silica and Ca^{2+} / Mg^{2+} to form metal silicates which have significantly less solubility than amorphous silica (Sheikholeslami et al. 2001). Thermodynamic software Phreeqc-3 could be used to calculate the supersaturation levels of metal silicates (e.g., Mg_2SiO_4, Ca_2SiO_4) in bulk brine solution, and predict the likelihood of particulates fouling in MD (Lisdonk et al. 2001). In addition, employing

strong chelating agent such as disodium ethylenediaminetetraacetic acid (Na_2EDTA) in brine could form soluble EDTA-Ca / EDTA-Mg complexes inhibiting the formation of metal silicates.

In mining industry, such as copper processing plant, the barren leach solution contains high level of dissolved ammonia which chelates Cu^{2+} and forms soluble metal-ammonia complexes (e.g., $Cu(NH_3)_4^{2+}$) (Richardson 1997; Trevani et al. 2001). Treatment of RO brine from copper barren leach solution using MD can improve overall plant wastewater recycle efficiency by simultaneously recovering ammonia and water while utilising the waste thermal energy from copper processing plant. However, the removal of ammonia from brine solution could lead to the formation of un-complexed Cu^{2+} and cause precipitation of $Cu(OH)_2$ or CuO. Additionally, the presence of high organic content in brine poses a potential risk of membrane organic fouling, particularly the organics with surface tension less than the surface energy of hydrophobic membrane (Naidu et al. 2015; Bansal et al. 2013).

1.3 Significance

So far, limited research works have been conducted in MD fouling, and the works for RO brine treatment are very scarce. Synthetic solution with single foulant was primarily focused in most of the previous studies with short MD run time (< 48 h). In real-world MD application, the existence of complex foulants and fouling mechanisms would make MD fouling difficult to control, which impact on MD long-term operation. Therefore, considerable attention is still required to understand the fouling kinetics of different solution borne components, and determine the treatment limits for various RO brines and importantly, develop cost-effective strategies for managing MD fouling.

Membrane material researchers have applied an oleophobic material onto hydrophobic membrane with the purpose of reducing the adsorption from oils or organics (Wang et al. 2016; Bansal et al. 2013). To the author's best knowledge, the performance of oleophobic membrane under real brine treatment has not been studied in the past. Moreover, the interactions between organics and oleophobic membrane need better understanding in order to define the limits of MD in brine treatment.

1.4 Study objectives

The broad objective of this research is to evaluate MD fouling kinetics and propose viable means to operate MD during the treatment of RO brine. Three RO brines are to be tested in this research. Each of the RO brines has unique compositions. The investigation of these brines is aimed to bring together a set of knowledge in proposing practical ways to operate MD in each context, but also to consider each as an example of the various chemistries that are present in RO brines to give the context of MD more broadly in industry. The specific objectives of each RO brine study were:

SWRO brine

I. Understand the behaviours of $CaCO_3$ and $CaSO_4$ scaling formation;
II. Evaluate the effectiveness of non-chemical cleaning (e.g., distillate / brine flushing) on removal of inorganic and organic compounds, respectively; and
III. Assess techniques including non-chemical cleaning, antiscalants and cartridge filtration to weigh up the best strategies to manage membrane fouling.

CSG RO brine

I. Investigate silica fouling behaviours under the influences of divalent cations (Mg^{2+} and Ca^{2+}), anions (HCO_3^- / CO_3^{2-} and Cl^-) and temperature, respectively;
II. Use Phreeqc–3 software to predict the supersaturation levels of salt species in bulk brine; and
III. Assess the effectiveness of fouling mitigation using Na_2EDTA in brine pretreatment.

Copper barren RO brine

I. Evaluate MD performances using two commercial low-density polyethylene (LDPE) membranes, standard and with oleophobic chemistry, respectively;
II. Assess the behaviour of NH_3 transfer in DCMD and its impact on the stabilities of metal-ammonia complexes; and
III. Evaluate MD foulant removal efficiency using commercial RO cleaning agents in comparison to brine clean.

This thesis contains following chapters: Chapter 2 contains general backgrounds of current technologies of brine minimisation, MD technology and current researches in MD fouling and its mitigation techniques. Chapter 3 describes the experimental methods and analytical techniques. Chapter 4, 5 and 6 present the results of DCMD studies of SWRO RO brine, CSG RO brine and copper barren RO brine, respectively. Chapter 7 concludes the key findings and discusses potential future research necessary in MD fouling in brine treatment.

Chapter 2 Literature review

2.1 RO desalination

2.1.1 Overview

Humans have been searching ways to desalinate salty water to fresh water for centuries. The Greek philosopher Aristotle once observed that "salt water, when it turns into vapour, becomes sweet and the vapour does not form salt water again when it condenses" (Forbes 1970). The phenomenon that Aristotle described is called distillation. Since the 1930s, countries in the Middle East have successfully pioneered and implemented large-scale municipal drinking water distillation (thermal desalination) plants treating seawater using processes called MED and MSF. Another membrane-based desalination technology called RO, an alternative to thermal desalination, has rapidly gained its popularity since the 1960s. RO operates by applying pressure to overcome the osmotic pressure in order to drive water molecules through a semi-permeable membrane where 90–99% of TDS are rejected (Blandin et al. 2013). The semi-permeable membrane separates the feed water into two streams: permeate (purified water) and brine / concentrate (rejected salts and remaining compounds). Today, RO has become the leading technology for new desalination installations (Global Water Intelligence 2017). The main reason for the success of RO technology is due to its lower energy consumption compared with traditional thermal desalination technologies as it avoids the energy intensive phase change essential for distillation. Australia has constructed large-scale SWRO plants in a majority of states, with the total capacity of approximately 534 GL/year (Australian Water Association 2018). Being the driest inhabited continent on earth, SWRO provides Australia a climate-independent source of water for critical human needs.

In addition to seawater treatment, RO technology has been widely implemented in brackish water treatment for industries located in the inland areas. For instance, the CSG or coal bed methane (CBM) industry. Australia is the second highest CSG producer in the world after the US (Hamawand et al. 2013). It is estimated that up to 7,500 GL of CSG produced water, a by-product of CSG extraction process, will be generated from Australian CSG industry in the next 20 years (Hamawand et al. 2013). CSG produced water in Australia contains primarily sodium, bicarbonate and chloride at low calcium and magnesium concentrations, and TDS level range from 500–10,000 mg/L (Millar et al. 2016). CSG produced water is generally unsuitable for land irrigation and has potential to cause surface water, underground and ecosystem damage (Millar et al. 2016). RO is able to separate impurities from CSG produced water before treated water can be conveniently re-used for purposes such as irrigation and potable applications, and at the same time, significantly reduce saline water storage requirements (Khan et al. 2014). The level of activity in the use of RO for the treatment of CSG produced water in Australia suggests that it is a long-term viable option for pursuing the beneficial use of produced water (Fell 2014).

Australia's mining industry that plays an important role in Australia's economy, is another major user of water. In mineral processing, water has been used in various steps to recover valuable metals from ore / raw materials. For instance, it takes about 773,000 L of water to produce a kilogram of gold (Mudd 2007). Mineral processing is largely reliant on the location of ore / raw materials with limited options to mitigate and adapt to regional water scarcity. Szyplinska (2012) stated that over 90% of mineral processing wastewater can be reused by implementing membrane technologies, such as RO and microfiltration (MF). In the last decade, due to the reduction of membrane cost and

environmental drivers, mining companies have invested significant amounts in water infrastructure using RO technology to improve wastewater recovery and reuse. RO processes are not only able to produce clean water for mine process water applications, RO brine stream contains concentrated precious metals that could be fed to the mineral extraction process for further metal recovery that helps negate the investment cost for wastewater treatment and potentially makes a profit for the business (Chester et al. 2016).

2.1.2 Challenges in RO brine management

Despite many benefits that the RO technology can offer, a significant problem concerning the application of RO is brine management. SWRO plants typically operate at 40–50% water recovery and the remaining 50–60% brine at TDS ~ 60 g/L is usually discharged directly into the sea (Giwa et al. 2017). Discharging large quantity of SWRO brine into the sea leads to a significant cost of associated facilities, such as discharge pipe and outfall diffuser systems. On the other hand, brine disposal costs at inland RO plants are higher than that of SWRO plants (Glueckstern and Priel, 1996). The major strategies for discharging brine at inland RO plants are through evaporation ponds and deep-well injection (Glater and Cohen, 2003). For large inland RO plants, the cost of constructing and managing evaporation ponds typically is a significant portion (e.g., 30%) of the total cost of desalination plant (Ahmed et al. 2001). Deep-well injection of RO brine, however, is likely to cause aquifer contamination and well clogging, and therefore it has not been encouraged by the regulators in Australia. Overall, RO brine management has significance both from environmental and economic aspects.

2.1.3 Advantages and shortcomings of brine minimisation technologies

One of the approaches for RO brine management is brine volume reduction to achieve high overall water recovery from desalination process. Brine volume reduction processes include the use of thermal-based technologies, pressure-driven and electrical potential-driven membranes (Lee et al. 2018). Table 2.1 summarises the main features of brine concentration technologies. As shown in Table 2.1, the major drawback for conventional thermal-driven desalination technologies (MVC, MED, MSF) is the requirement of high thermal energy, and they normally require an external steam supply (e.g., from power plant steam turbine). Pressure-driven technologies (UHPRO, DTRO, SWRO) typically consume high electric energy due to high osmotic pressure of brine. Several innovative pressure-driven brine concentration technologies, such as OBS and MBC, are in their early stage of industrial applications and considerable research is still needed to reduce these system's capital (Capex) and operational expenditures (Opex). In addition, the major drawback for electrochemical technologies (ED, EDR) treating RO brine is the fouling of ion exchange membrane which can lead to high energy consumption and poor separation efficiency (Table 2.1).

In the last decade, there has been an exponential growth in MD research (Thomas et al. 2017). MD is a thermal membrane separation process that involves transport of vapour through microporous hydrophobic membranes and operates on the principle of vapour-liquid equilibrium as the basis for molecular separation. The most attractive feature of MD is potential for 100% rejection of non-volatile solutes and production of high purity distillate (Tun et al. 2005). Compared to RO process, MD can operate at reasonable flux at much lower pressure (e.g., < 3 bar) due to its reduced sensitivity to brine TDS concentration. Unlike polyamide RO membranes that do not tolerate chlorine, MD

membranes (Section 2.2) can tolerate chlorine and other oxidising agents which is a great advantage for MD biofouling management (Cath et al. 2003; Nguyen et al. 2015). MD employs compact microporous membranes with large membrane areas instead of large vapour chambers used in conventional thermal technologies, and this feature leads to a lower cost and smaller footprint of MD system (Hsu et al. 2002). In addition, the high membrane area to volume ratio in MD allows it to operate at lower temperature with respect to conventional thermal technologies, and to exploit the advantages of modularity and operational simplicity for applications in integrated membrane systems (Al-Obaidani et al. 2008).

Table 2.1 Summary of separation principle, operating conditions, typical concentrate TDS, energy consumption and comparisons of brine concentration technologies.

Technology	Separation principle	Operating conditions	Typical concentrate TDS (mg/L)	Energy consumption (kWh/m^3)		Technology maturity, limitations and economic considerations	Ref.
				Electrical	Thermal		
SWRO	Pressure-driven membrane separation	< 82 bar	< 65,000	3–6	–	• Proven technology • Limited on maximum operating pressure / TDS • Moderate capital and operational costs	Subramani and Jacangelo 2014, Rioyo et al. 2017
Ultra-high pressure (UHP) RO	Pressure-driven membrane separation	< 120 bar	< 150,000	Data not available		• Early stage of industrial adoption • High capital costs for overall system due to high operating pressure • High operational costs due to high electric energy consumption	www.dow.com, Alsogair 2017
Disc tube (DT) RO	Pressure-driven membrane separation	< 120 bar	< 150,000	Data not available		• Early stage of industrial adoption • High capital costs for overall system due to high operating pressure • High operational costs due to high electric energy consumption	www.pallwater.com, Karlapudi 2015
Osmoflo brine squeezer (OBS)	Pressure-driven membrane separation	< 82 bar	< 150,000	6–8	–	• Early stage of industrial adoption • Patented technology	www.osmoflo.com, Le 2017
Membrane brine concentrator (MBC)	Forward osmosis (FO) and pressure-driven membrane separation	< 82 bar	< 160,000	6–15	–	• Early stage of industrial adoption in small scale system • Patented technology • Relative complex process	www.modernwater.com, Mehta and Nicoll 2018

Table 2.1 (continued) Summary of separation principle, operating conditions, typical concentrate TDS, energy consumption and comparisons of brine concentration technologies.

Technology	Separation principle	Operating conditions	Typical concentrate TDS (mg/L)	Energy consumption (kWh/m^3)		Technology maturity, limitations and economic considerations	Ref.
				Electrical	Thermal		
Mechanical vapour compression (MVC)	Thermal-based distillation	~ 70 °C	< 60,000	7–15	–	• Proven technology • High capital cost for large system. So far only considered for zero liquid discharge (ZLD) applications • High operational cost due to high electric energy consumption	Rioyo et al. 2017, Stillwell et al. 2016, Lee et al. 2018
MED/MSF	Thermal-based distillation	70–120 °C	< 100,000	2–5	30–120	• Proven technology in seawater desalination • High thermal energy requirement • High capital and operational costs • Heat-exchanger fouling at high temperature and TDS	Stillwell et al. 2016, Giwa et al. 2017
MD	Thermal-based distillation	35–90 °C	< 150,000	1.5–4	4–200	• Pilot plant scale • High thermal energy requirement • Lack of custom-made membranes	Stillwell et al. 2016, Duong et al. 2015, Mericq et al. 2010, Dow et al. 2016, Woldemariam et al. 2016
ED / EDR	Electric potential-driven membrane separation	10–35 °C	< 100,000	Up to 15	–	• Proven technology but only pilot studies in brine minimisation • Pre-treatment process is required to mitigate fouling at ion-exchange membrane • High capital and operational costs	Tsiakis et al. 2005, Oztekin et al. 2016

2.2 MD and its configurations

In MD process, the membrane acts as a physical support and does not contribute to the process selectivity (Khayet et al. 2004). The ideal MD membrane should be porous and hydrophobic in nature. The common MD membrane materials, such as polytetrafluoroethylene (PTFE), polyvinylidene fluoride (PVDF), polypropylene (PP), and polyethylene (PE) (Thomas et al. 2017; Alklaibi et al. 2004) have porous structure at mean pore size of 0.1–0.5 μm and porosity of 0.65–0.95 (Zhang et al. 2009) in order to facilitate the vapour permeation. Due to the hydrophobic nature of these membranes, liquid water cannot penetrate the membrane pores unless the applied hydraulic pressure exceeds the liquid entry pressure (LEP). Traditionally, MD contains four major configurations, namely, DCMD, air gap MD (AGMD), sweep gas MD (SGMD), and vacuum MD (VMD) (Figure 2.1). More recently, several novel MD configurations have also been studied with the view of improving MD thermal efficiency and flux, and these configurations include vacuum air-gap MD (VAMD) (Abu-Zeid et al. 2016), permeate-gap MD (PGMD) (Khalifa et al. 2017) or liquid-gap MD (LGMD) (Ugrozov et al. 2003) and material gap MD (MGMD) (Francis et al. 2013).

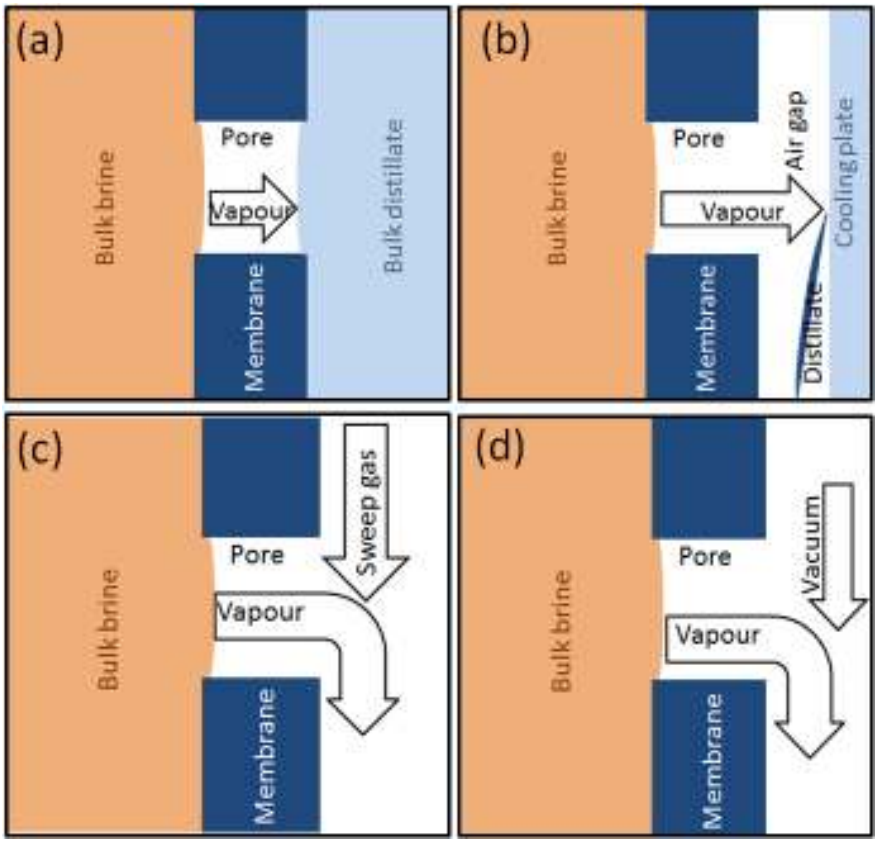

Figure 2.1 Traditional MD configurations: (a) DCMD; (b) AGMD; (c) SGMD and; (d) VMD.

Among all the MD configurations shown in Figure 2.1, DCMD is the simplest configuration and has been widely used by researchers in both lab and pilot scales (Thomas et al. 2017). DCMD does not require a vacuum pump as in VMD, nor condenser as in SGMD or cooling surface as in AGMD, and the distillation process can be carried out in any desired membrane configuration, such as flat-sheet, spiral-wound, capillaries and hollow-fibers (Al-Obaidani et al. 2008). DCMD with short flow path is regarded as the most suitable MD configuration that can achieve the highest distillate flux compared with others (Duong et al. 2016; Hwang et al. 2011; Zhang et al. 2013). Although DCMD is not as thermally efficient as compared to other MD configurations, at an industrial site with abundant low grade waste heat (e.g., ≈ 40 °C), maximising distillate flux thereby minimising MD system's Capex is deemed more important than thermal efficiency (Dow et al. 2016; Dow et al. 2013).

In DCMD process, the non-volatile solutes (e.g., dissolved salts) contained in the brine are completely retained by the membrane. Due to both mass and heat transfer effects, the membrane salt concentration (C_{mf}) is higher and membrane surface temperature (T_{mf}) is lower than the bulk brine solution and this is called concentration and temperature polarisation phenomenon, respectively (Figure 2.2). Higher concentrations of organic / colloidal compounds and dissolved salts at the membrane surface could lead to the adherence of organic / colloidal compounds and salt deposition (when the salt solubility decreases along with temperature drop) on the MD membrane surface. The main techniques that are currently applied for reducing the effects of concentration and temperature polarisations are increasing flow velocity and placing spacers in the flow channels to promote turbulence both sides of the membrane (Zhang et al. 2009).

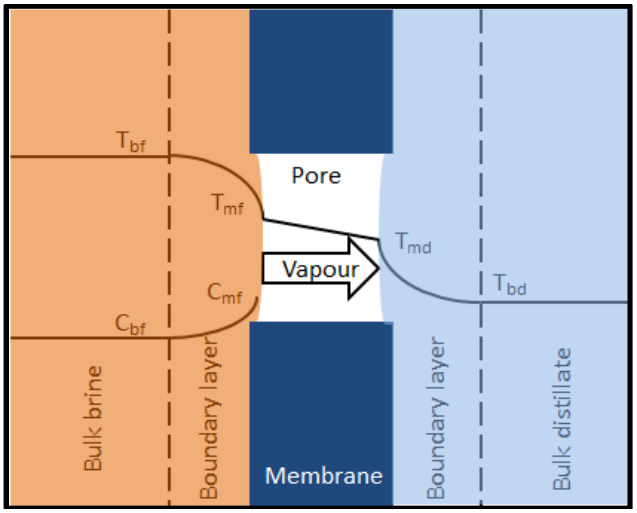

Figure 2.2 DCMD process heat and mass transfer.

2.3 MD fouling

2.3.1 Overview

Researchers have recognised that MD fouling and wetting are the major operational issues for concentrating hyper-saline RO brine (Bouchrit et al. 2015). MD fouling is the

accumulation of unwanted materials on the membrane surface or inside the pores, and this could pose a very detrimental effect on MD long-term stable operation (Gryta 2008). MD fouling can alter the hydrophobicity of membrane surface, leading to the intrusion of brine into membrane pores and, thus, deteriorating distillate quality (Gryta 2008). This phenomenon is called membrane wetting. It is believed that the fouling mechanisms in MD are significantly different to RO due to larger pores and diffusion pathways in MD process (Lawson et al. 1997). The fouling layer in MD may not be as compact as it is in RO process, and the lack of hydraulic pressure in MD may help to improve membrane cleaning efficiency (Hausmann et al. 2013; Zhong et al. 2016).

2.3.2 $CaCO_3$ and $CaSO_4$ scaling

The main salts that responsible for membrane scaling for both seawater and brackish water treatments are calcium crystals, such as $CaCO_3$ and $CaSO_4$. Both salts are sparingly soluble in water and have inverse solubility with temperature. Scaling formation on membrane involves both crystallisation and hydrodynamic transport mechanisms (Oh et al. 2009). Crystallisation includes two pathways, namely surface (heterogeneous) crystallisation and bulk (homogeneous) crystallisation which are illustrated in Figure 2.3 below.

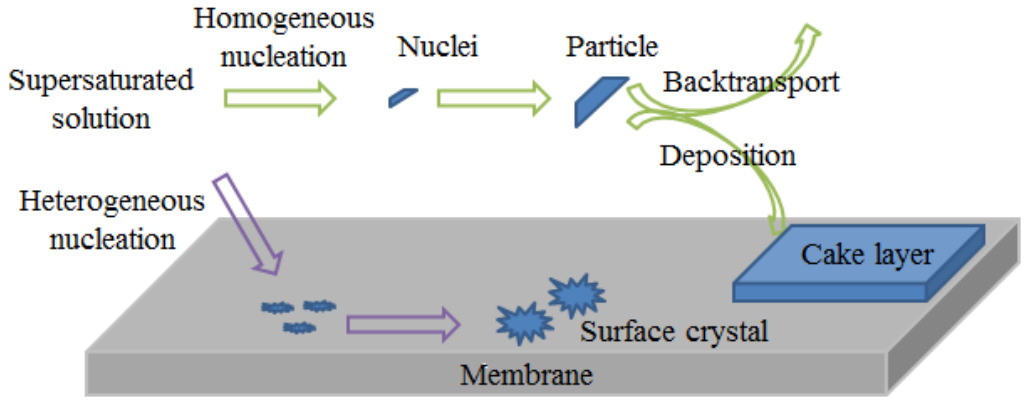

Figure 2.3 Scale formation mechanisms in MD process.

The precipitation of $CaCO_3$ in heated solution was described by He et al. (2009) as below:

$$2HCO_3^- \overset{\text{Heat}}{\longleftrightarrow} H_2O + CO_2 \uparrow + CO_3^{2-} \quad (2.1)$$

$$Ca^{2+} + CO_3^{2-} \rightarrow CaCO_3 \downarrow \quad (2.2)$$

or when combined:

$$2HCO_3^- + Ca^{2+} \overset{Heat}{\longrightarrow} H_2O + CO_2 \uparrow + CaCO_3 \downarrow \quad (2.3)$$

In MD process, heating the feed solution causes the decomposition of HCO_3^- (Equation 2.1) and the formation of $CaCO_3$ (Equation 2.2).

The crystal deposits not only reduce the MD membrane effective operational area but also increase the heat resistance between the bulk side of brine solution and membrane surface which inhibits vapour flux transfer through the membrane (Hausmann et al. 2014). Gryta (2007) proposed that when $CaCO_3$ precipitation firstly forms it partly blocks membrane pores. Then, water evaporation takes place on wetted crystal surfaces creating the possibility of heterogeneous crystallisation and the growth of crystallites in the direction of the vapour phase. As a result, a new area of pores is wetted and the total area of wetted pores grows. Gryta named this phenomenon “water-logging” (Figure 2.4). Gryta also

suggested that acid rinsing solution dissolved $CaCO_3$, and at the same time, caused the penetration of solution into the pores filled with the $CaCO_3$ deposits, which further enabled the wettability of the consecutive adjacent pores.

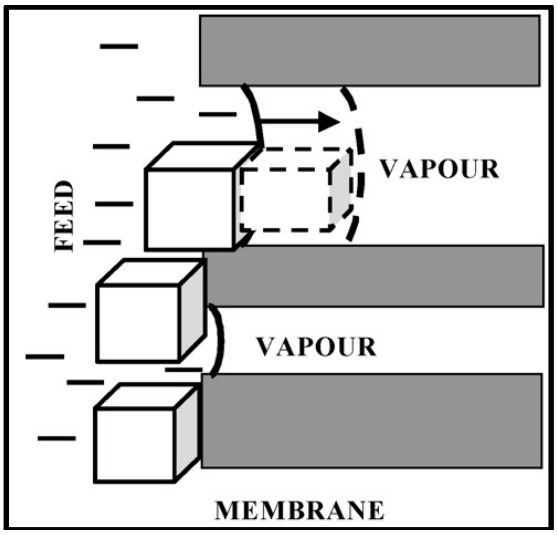

Figure 2.4 Wettability of hydrophobic membrane caused by heterogonous salt crystallisation inside the pores during MD process. (water-logging mechanism described by Gryta 2007).

Nghiem and Cath (2010) studied $CaSO_4$ scaling in DCMD process, and reported that precipitation occurred as thin needle shaped crystals at feed temperature of 40 °C, whist larger $CaSO_4$ crystals were formed at feed temperature of 60 °C. Nghiem suggested that once $CaSO_4$ nucleation occurs, the $CaSO_4$ crystals can grow rapidly and completely inhibit water vapour transfer. In addition, other studies have reported that $CaSO_4$ can grow perpendicularly and penetrate into the pore interior resulting in a damage of the MD module and membrane wetting (Gryta 2008; Yu et al. 2013).

In a mixed $CaCO_3$–$CaSO_4$ system, the solubility of $CaCO_3$ / $CaSO_4$ may be different as compared to the pure salt system (Sheikholeslami and Ong 2003). Therefore, it is important to understand the supersaturation level of $CaCO_3$ / $CaSO_4$ in real RO brine. Research has employed a computer program, Phreeqc, to predict the supersaturation

levels of Ca and Mg salts in solution (Lisdonk et al. 2001; Waly et al. 2012). Phreeqc uses the Debye Huckel-Jones Davies equation for calculation of the activity-coefficients to allow the prediction of the supersaturation level of a wide range of inorganic sparingly soluble salts (Lisdonk et al. 2001). The behaviour of salt precipitation was found consistent with thermodynamic equilibrium calculations with this software (Greenlee et al. 2010).

2.3.2 Silica fouling

Silica fouling is a major unsolved problem in brackish water desalination process (Milne et al. 2014). Dissolved silica in water exists as orthosilicic acid ($Si(OH)_4$) and silicate anions ($H_2SiO_3^{2-}$, $H_2SiO_3^-$) (Milne et al. 2014). The equilibrium reactions of orthosilicic acid in solution were described by Weres et al. (1980) as below:

$$Si(OH)_4 \leftrightarrow SiO(OH)_3^- + H^+ \quad (2.4)$$

$$Si(OH)_3^- \leftrightarrow SiO(OH)_2^{2-} + H^+ \quad (2.5)$$

As can be seen in Equation 2.4 and 2.5, the solubility of silica is strongly pH dependent. Either high or low degrees of ionisation of dissolved silica prevents silica polymerisation (Sheikholeslami et al. 1999). Sheikholeslami et al. (2001) stated that the optimum armorphous silica solubility occurs at pH > 9.5 or < 6.5 since dissolved silica exists in solution predominantly in either neutral or anionic species. When the concentration of dissolved silica exceeds its solubility (at a given temperature and pH), silica polymerisation (heterogeneous nucleation) will occur and form colloidal amorphous silica. This process was described below by Ning (2002):

$$nSi(OH)_4 \rightarrow (OH)_3Si - O - Si(OH)_3 \text{ dimer} \rightarrow \text{oligomers} \rightarrow \text{colloidal amorphous silica} \quad (2.6)$$

The colloidal amorphous silica deposited on membrane surface will further dehydrate and finally become a glasslike scale which is very difficult to remove by conventional chemical cleaning approaches (Koo et al. 2001). Therefore, RO system generally operates at silica concentration below 150 mg/L to mitigate silica fouling (Bremere et al. 2000).

Temperature is another important factor that influences silica solubility. When the temperature of the solution increases, it leads to an increase of silica solubility (Demadis 2010), and this favours MD process operating at higher concentration of silica as compared to RO. However, MD temperature and concentration polarisations (Figure 2.2) could promote silica supersaturation near the membrane surface and cause precipitation of colloidal amorphous silica.

Dissolved silica in CSG produced water varies from site to site, although it may not be very high in produced water, but can easily exceed the solubility in a RO–MD hybrid system operating at high water recovery. Duong et al. (2015) performed a pilot study on concentrating CSG RO brine using Aquastill's (Sittard, The Netherlands) spiral-wound AGMD system. This study demonstrated stable operation of MD system at 80% of RO brine recovery (overall recovery of 95%), and salt rejection of 99.5%. However, concerns were raised that membrane fouling due to silica and calcium carbonate may restrict efficiency of MD long-term operation. Zhong et al. (2016) evaluated silica fouling with synthetic CSG produced water using a submerged VMD system equipped with capillary hydrophobic PP membranes. The synthetic solutions employed in Zhong's study were silica rich (200 mg/L) with high Mg^{2+} (62.5–200 mg/L) and Ca^{2+} (40–300 mg/L), but low

$NaHCO_3$ (1.2 g/L). The submerged VMD was operated at 70 ˚C under constant TDS concentration at 37.2 g/L and pressure of – 95 kPa. Membrane wetting was observed in Zhong's study. They also reported that calcite and magnesium silicates were the major foulants on the membrane.

CSG produced water in Australia contains predominantly $NaHCO_3$ / Na_2CO_3 and NaCl (Millar et al. 2016). In terms of the effect of anions (e.g., CO_3^-, Cl^-) on silica solubility, research has reported contrasting observations. Koo et al. (2001) concluded that CO_3^- was more significant in facilitating silica polymerisation as compared to Cl^-, while Marshall et al. (1980) reported that use of carbonate salts increased amorphous silica solubility as compared to chloride salts.

2.3.3 Conclusion and gaps in knowledge

Previous studies have revealed that fouling from $CaCO_3$ / $CaSO_4$ and silica have various impacts on MD performance, such as flux decline, membrane damage as well as membrane wetting (Gryta 2007; Nghiem and Cath 2010; Zhong et al. 2016). Synthetic single salt solutions were predominantly adopted in those studies. SWRO brine is a mixed $CaCO_3$–$CaSO_4$ system also contains natural organic matters (NOM) such as polysaccharides and humic acid (HA). It is expected that the scaling kinetics are quite different compared to single salt system. For instance, the solubility of $CaCO_3$ / $CaSO_4$ could be increased in a mixed $CaCO_3$–$CaSO_4$ system in respect to the pure salt systems (Sheikholeslami and Ong 2003). In addition, the presence of NOM in seawater could reduce the heterogeneous nucleation of $CaCO_3$ / $CaSO_4$, and cause salt crystals to be less "sticky" to hydrophobic membrane compared to the pure salt crystals (Curcio et al. 2010;

Hoch et al. 2000). Therefore, it is important to study the kinetics of $CaCO_3$ and $CaSO_4$ scaling in MD with real SWRO brine.

MD fouling studies on CSG produced water are scarce. Duong et al. (2015) suggested that the likely foulants were silica and calcium carbonate, but they did not further explore the kinetics of the foulant formation in MD process. Zhong et al. (2016) reported that the formation of calcite and magnesium silicates which subsequently led to membrane wetting. The submerged VMD adopted in Zhong's study is considered more sensitive to membrane wetting due to the hydrostatic pressure drop across the membrane which acts as a driving force for liquid into the membrane pores. Moreover, the high temperature (70 ºC) used in Zhong's study could promote metal silicate formation as metal silicates have inversed solubility with temperature. In addition, research has shown contrasting observations for the effect of anions (e.g., CO_3^-, Cl^-) on silica solubility (Koo et al. 2001; Marshall et al. 1980). Overall, there is still a need for understanding the influence of divalent cations (Mg^{2+} and Ca^{2+}) and anions (HCO_3^- / CO_3^{2-} and Cl^-) on silica fouling in MD for CSG RO brine treatment.

2.4 Dissolved gases in MD

2.4.1 CO_2 and NH_3

Dissolved gases, such as CO_2 and NH_3 present in MD feed play an active role in changing solution pH and subsequently influencing solubility of salts. The transfer of dissolved gas across membrane could compete with water vapour; therefore, reduce overall vapour flux (Warsinger et al. 2015). Dissolved CO_2 / NH_3 transfer across membrane also increases distillate electric conductivity (EC) by re-forming HCO_3^- / NH_4^+ on the distillate side (Equation 2.8 and 2.9). At the beginning of MD process, the rapid dissociation of HCO_3^-

to CO_2 due to elevated temperature is likely to decrease pH in MD feed due to the CO_2 formation rate being greater than the CO_2 degassing rate. As the MD process continues, CO_2 degassing from MD feed could gradually increase the pH of the MD feed and facilitate the formation of $CaCO_3$ (He et al. 2009). High temperature of MD will also assist NH_3 diffusion through membrane pores due to the endothermic nature of the dissociation of NH_4^+ (Xie et al. 2009) (Equation 2.8).

2.4.2 Cu–NH_3–CO_2 system

The copper barren wastewater of copper processing plant contains significant amount of dissolved CO_2 and NH_3 as the plant process uses ammonium carbonate ($(NH_4)_2CO_3$) and ammonium hydroxide (NH_4OH) as copper leaching agents in a hydrometallurgical process to extract copper from metal scraps. Ammonia reacts with copper and forms stable and water soluble copper ammine complex (e.g., $Cu(NH_3)_4^{2+}$) in alkaline solution, and this reaction is described in Equation 2.7 (Richardson 1997).

$$Cu + 2NH_4OH + (NH_3)_2CO_3 \rightarrow Cu(NH_3)_4CO_3 + 2H_2O \quad (2.7)$$

Then, the pregnant leach solution is steam stripped, and the final product cupric oxide (CuO) is precipitated and NH_3 and CO_2 are recovered in this step. Following the CuO removal in a thickener, the barren leach solution is cooled to 30 °C through several heat exchangers before being treated by ultrafiltration (UF) and RO. Five equilibrium reactions exist in the Cu–NH_3–CO_2 system in copper barren RO brine, the dissociation of ammonia (Equation 2.8), carbon dioxide (Equation 2.9), bicarbonate (Equation 2.10) and the formation of carbamate (Equation 2.11) as well as copper-ammonia complexes (Equation 2.12).

$$NH_4^+ + OH^- \leftrightarrow NH_3 + H_2O \quad (2.8)$$

$$CO_2 + H_2O \leftrightarrow HCO_3^- + H^+ \quad (2.9)$$

$$HCO_3^- \leftrightarrow CO_3^{2-} + H^+ \quad (2.10)$$

$$NH_3 + HCO_3^- \leftrightarrow NHCOO^- + H_2O \quad (2.11)$$

$$Cu(NH_3)_n{}^{2+} + NH_3 \leftrightarrow Cu(NH_3)_{n-1}{}^{2+} \quad n = 0 - 4 \quad (2.12)$$

Ammonia stripping efficiency in MD is strongly related to feed solution pH (Qu et al. 2013), and this is due to the increasing pH value of the aqueous solution making the dissociation equilibration move towards yielding greater amount of NH_3 (Equation 2.8). Ammonia removal from brine would simultaneously reduce brine pH and form HCO_3^- (Equation 2.10 and 2.11), therefore, encouraging CO_2 diffusion through membrane pores (Equation 2.9). Cu^{2+} forms a number of soluble amine complexes in the ammonia system (Equation 2.12), and the most stable complex is tetra-amine ($Cu(NH_3)_4^{2+}$) which is the predominant copper-ammonia species at solution pH > 8.3 (Trevani et al. 2001).

2.4.3 Conclusion and gaps in knowledge

The degassing of dissolved CO_2 and NH_3 in MD process leads to changes in solution pH which subsequently influences the solubility of salts (Warsinger et al. 2015). So far, MD performance has not been studied in brine containing a Cu–NH_3–CO_2 system. In Cu–NH_3–CO_2 system, with NH_3 being removed from brine along with reduced brine pH (Equation 2.8), $Cu(NH_3)_4^{2+}$ forms in equilibrium with other less stable copper-ammonia species (Equation 2.12), and ultimately the un-complexed Cu^{2+} could appear in solution and precipitate as $Cu(OH)_2$ or CuO. Concentrating RO brine of a copper barren leach

solution using MD process can improve the overall plant wastewater recycle efficiency by simultaneously recovering ammonia and water. In addition, the heat source from barren leach stream at 65–80 °C can be utilised to provide thermal energy for MD which makes this process more attractive than other brine concentration technologies. Therefore, it is of great interest to assess MD performance in treating copper barren RO brine.

2.5 Fouling mitigation in MD

2.5.1 Overview

Developing a technically feasible and potentially cost-effective solution to manage MD fouling and wetting is a major research goal to have MD commercialised for brine treatment. In recent years, research has been undertaken to address MD fouling / wetting, and some fouling mitigation approaches were based on the lessons learned from mature water treatment technologies (e.g., UF / RO) as well as other industries (e.g., geothermal energy). These fouling mitigation approaches include antiscalant addition, cartridge filtration to remove salt crystals from bulk feed, flushing with deionised water to remove salt nuclei from membrane surface, chemical cleaning and fabricating special membrane to resist fouling.

2.5.2 Antiscalant

Antiscalant is considered effective in inhibiting crystal deposit build up during RO process and for high temperature processes, such as MED and MSF. Antiscalant mitigates membrane scaling by selecting crystal morphology nucleation, retarding the rate of crystal growth and changing the agglomeration tendency of crystals (Gloede et al. 2008). Another advantage of using antiscalant in these processes is due to its low cost, and low

dosage typically at 1–10 mg/L (He et al. 2009). Commercial antiscalants that are used in RO processes generally contain polyphosphates, organophosphonates, and polyelectrolytes (Gryta 2012). Gryta (2012) investigated $CaCO_3$ scaling in DCMD by introducing commercial polyphosphate based antiscalcant into tap water with added HCO_3^- and Ca^{2+}. Gryta discovered that polyphosphate significantly reduced $CaCO_3$ deposit layer on PP membrane surface compared with no use of antiscalant. With antiscalant dosing, $CaCO_3$ deposits were only on the membrane surface, and could be completely removed by acid cleaning using 3–5 wt.% HCl solutions. He et al. (2009) studied five commercial antiscalants for mitigating $CaCO_3$ and $CaSO_4$ scaling in DCMD process using supersaturated synthetic solutions. At $CaCO_3$ saturation index (SI) = 10.7, 3.0 mg/L of antiscalant containing organo-phosphorus compound from Genesys International Ltd. (Minneapolis, MN) extended the $CaCO_3$ precipitation from 9 to 255 min. It was reported that polyacrylic acid and sodium polyacrylate based antiscalant were more effective for inhibiting $CaSO_4$ scaling. None of those antiscalants in He's study caused PP membrane pore wetting at concentration of 20 mg/L. Hasson et al. (2003) studied RO process comparing five commercial antiscalants for inhibition of $CaSO_4$ precipitation, and concluded that the effectiveness of antiscalant was not impacted by the shear stress induced by pump impellers when recycling RO brine back to the feed tank. This finding is encouraging for MD process as it predominately operates in brine recycling mode to maintain high thermal efficiency (Duong et al. 2015) and for minimising the footprint (or Capex) of the system.

2.5.3 Cartridge filtration

In a DCMD pilot study, the use of a cartridge filter was found to be effective at reducing scaling during the treatment of a real groundwater RO brine by placing the filter in the

hottest region of the hot cycle (after heat exchanger, but before membrane) which inhibited $CaCO_3$ scale formation on the membrane enabling much higher water recoveries to be achieved (Dow et al. 2010). He et al. (2009) reported that the formation of $CaCO_3$ / $CaSO_4$ that occurred in DCMD was predominantly in the hot bulk feed rather at the boundary layer near membrane surface. It was found that the 5 µm filter was blocked by the $CaCO_3$ / $CaSO_4$ at inlet of MD module while only minor blockage occurred when the filter was installed at the outlet of module. The micro-filter used in He's study had a small surface area (diameter of 47 mm), therefore, it experienced excessive pressure drop during the run due to filter blockage. This finding suggests that cartridge filters used in RO brine treatment should be of sufficient surface area to prevent frequent filter change-out.

2.5.4 Membrane flushing

Membrane forward flushing using permeate water has been widely implemented in RO process purging brine from membrane modules, and at the same time removing deposits such as $CaCO_3$ and $CaSO_4$ from the membrane surface. Nghiem and Cath (2010) applied intermittent membrane flushing in a MD study using MilliQ water to remove $CaSO_4$ from membrane surface. Due to the long induction time of $CaSO_4$ crystallisation compared to $CaCO_3$, the intention of membrane flushing was to remove $CaSO_4$ nuclei prior to the formation of $CaSO_4$ large crystals on the membrane surface. Nghiem and Cath (2010) reported that although $CaSO_4$ scaling in DCMD can be effectively extended by regular flushing, $CaSO_4$ crystallisation eventually occurred on membrane surface at high $CaSO_4$ concentration.

2.5.5 Oleophobic membrane

During recent developments of new MD membranes, researchers have applied an oleophobic coating onto hydrophobic membrane with the purpose of reducing membrane wettability from adsorbing oils or dissolved organics (Wang et al. 2016; Bansal et al. 2013). This novel approach used oleophobic material that was made of fluorinated polymer with low surface energy, and covered or completely encapsulated the fibrils and nodes of the hydrophobic membrane to reduce membrane surface energy below the surface tension of the challenge materials (e.g., oil and grease) which in turn prevented the challenge material from fouling the membrane surface (Bansal et al. 2013). It is expected that oleophobic membrane can also effectively prevent membrane fouling from other organics, such as HA, organic antiscalant and organic flocculant.

2.5.6 Chemical cleaning

Another main technique that is currently being applied for membrane fouling control is membrane cleaning using commercial available chemicals (Gryta 2008). NaOH cleans organic foulants from membrane by hydrolysis and solubilisation (Ang et al. 2006). Meng et al. (2014) conducted NaOH (pH = 10) rinse for 15 min on the PVDF MD membrane fouled by HA-Ca complexes, and restored the membrane hydrophobicity to 97% of its original value. Tetrasodium ethylenediaminetetraacetic acid (Na_4EDTA) as a strong metal chelating agent at alkaline pH (Nowack et al. 1996), can form stable complexes with divalent cations such as Ca^{2+} and Cu^{2+}, and help break down the scaling layers from membrane surface. In addition, studies of UF and RO processes have shown that feed water treatment with Na_4EDTA addition can form soluble EDTA–Ca complexes, and effectively mitigate the membrane fouling caused by HA–Ca complexes (Hao et al. 2011;

Lee et al. 2005). HCl is effective for removing inorganic metal compounds (e.g., $CaCO_3$, $Cu(OH)_2$) that are readily soluble at low pH value. MD studies conducted by Gryta (2005, 2007, 2009) suggested that HCl cleaning was effective to remove the majority of $CaCO_3$ / $CaSO_4$ scale from PP hollow fiber membrane surfaces at various concentrations (2–5 wt.%). However, the effectiveness of acid cleaning is strongly dependent on the location of scale. For scale deposited inside membrane pores, repeated acid cleaning and rinsing could eventually lead to pore wetting (Gryta 2007).

2.5.7 Conclusion and gaps in knowledge

Commercial antiscalants have demonstrated effectiveness in mitigating MD fouling caused by $CaCO_3$ and $CaSO_4$ using supersaturated synthetic solutions (He et al. 2009). Antiscalant exists in SWRO brine at ~ 10 mg/L could be conveniently utilised in MD process to achieve high water recovery at no additional cost of chemical. However, at high water recovery, the concentration of antiscalant in MD feed could reach > 50 mg/L which is the typical maximum concentration for RO process specified by the antiscalant manufacturers. Organic antiscalants are generally displayed as water-like polar property and low surface tension (He et al. 2009). Hence, the surfactant effects of antiscalants may lead to membrane wetting in MD process. The kinetics of scale formation in the presence of antiscalant in SWRO brine has not been investigated in previous MD studies.

The use of a cartridge filter was found to be effective at removing $CaCO_3$ from feed solution in groundwater RO brine treatment using MD (Dow et al. 2010). So far, this method has not been explored in MD process treating SWRO brine where the predominant crystal deposits are $CaCO_3$ and $CaSO_4$.

Deionised water flushing was effective in removing crystal deposits (e.g., $CaCO_3$ and $CaSO_4$) from membrane in MD process (Nghiem and Cath 2010). However, research has not investigated the effectiveness of membrane flushing using distillate (MD product). In SWRO brine, $CaCO_3$–$CaSO_4$ deposits lose its strength and become less adherent and more readily removed under the influence of NOM and antiscalant (Falini et al. 2009; Gryta 2009). Therefore, it is expected that distillate flushing could also achieve good level of crystal removal.

Recent development of oleophobic membrane has showed the potential for preventing organic fouling in MD (Bansal et al. 2013). To the author's best knowledge, MD fouling for brine treatment using oleophobic membrane has not previously been undertaken. Aquastill (Sittard, The Netherlands) has recently adopted a commercial oleophobic membrane for MD application, and this presents an opportunity of assessing the performance of oleophobic membrane treating copper barren RO brine at high organic content.

In RO process, Na_4EDTA pre-treatment effectively mitigated the membrane fouling caused by HA–Ca complexes (Hao et al. 2011; Lee et al. 2005). With low hardness in CSG produced water, EDTA addition could be adopted in MD as a cost-effective solution to inhibit $CaCO_3$ and magnesium silicate formation thereby increasing water recovery from CSG RO brine.

2.6 Summary of literature review

Large SWRO plants have been constructed in major Australia's coastal cities to tackle potable water shortage problems for urban populations. RO technology has also been rapidly adopted by Australia's major industries located at inland areas, such as CSG and

mineral processing. The search for environmentally friendly and cost-effective brine minimisation technology is considered as a key challenge for management of brine concentrates. MD technology has great potential in brine minimisation, such as near complete rejection of non-volatile solutes, lower hydraulic pressure compared to pressure-driven technologies and lower operating temperature compared to thermal-driven technologies. However, MD fouling and wetting are major obstacles that hamper this technology being realised by industry.

$CaCO_3$ and $CaSO_4$ are the major salts that responsible for membrane scaling in SWRO process. Research of $CaCO_3$ / $CaSO_4$ scaling in MD process has been predominantly focused on synthetic single salt solutions. SWRO brine is a mixed $CaCO_3$–$CaSO_4$ system which also contains antiscalant and NOM. The scaling kinetics of actual SWRO brine in MD process can be quite different compared to single salt system.

Silica fouling is another unsolved problem in brackish water desalination process. Silica / metal silicates fouling was reported during CSG produced water treatment using MD (Duong et al. 2015). So far, research has not investigated the kinetics of silica fouling in MD, particularly under the influence of divalent cations (Mg^{2+} and Ca^{2+}) and anions (HCO_3^- / CO_3^{2-} and Cl^-). Thermodynamic software Phreeqc has been successfully employed to calculate the supersaturation levels of Ca and Mg salts in solution (Lisdonk et al. 2001; Waly et al. 2012). Phreeqc could also be used to predict the fouling potential of metal silicates in MD process.

Copper barren wastewater from copper processing plant contains significant level of dissolved ammonia which reacts with copper and forms copper ammine complex (e.g., $Cu(NH_3)_4^{2+}$) in alkaline solution. MD process can simultaneously recover ammonia and

water while utilising the waste heat source from barren leach stream. However, the stability of copper amine complex and fouling potential of Cu salts in MD process need to be understood.

All three brines (SWRO brine, CSG RO brine and copper barren RO brine) contain commercial antiscalant which was introduced in RO process as a cost-effective solution to mitigate crystal deposit build up on RO membrane. Organic antiscalant at high concentration (e.g., > 50 mg/L) could enhance the adherence of antiscalant onto membrane surface and subsequently lead to MD membrane wetting. Therefore, it is important to assess the antiscalant fouling potential in MD process from the perspectives of membrane surface attachment and membrane wetting.

In the aspect of MD fouling management, several techniques may be implemented. For instance, cartridge filtration could remove $CaCO_3$ and $CaSO_4$ crystals from the bulk SWRO brine. In addition, $CaCO_3$ and $CaSO_4$ crystals, under the influence of antiscalant and NOM are more readily removed from membrane surface compared to pure salts. Therefore, intermittent distillate / brine flushing could assist crystal nuclei removal which may warrant a long-term MD operation without chemical cleaning. For brine containing a low hardness level (e.g., CSG RO brine), EDTA addition could be adopted in MD feed to form soluble EDTA–Ca / EDTA–Mg complexes thereby inhibiting the formation of metal silicates. Moreover, newly proposed oleophobic membrane could be used in MD to mitigate organic fouling while treating RO brine at high organic content (e.g., copper barren RO brine).

Chapter 3 Experimental methods

3.1 Bench-scale DCMD apparatus

A bench-scale DCMD apparatus was constructed for this study. The flow diagram of the DCMD apparatus is shown in Figure 3.1. The apparatus contained a feed water section and a distillate water section. Feed water was withdrawn from the 15 L feed container (6) and transferred to the DCMD module (3) through a heating unit (2). Feed water container was placed on a Velp Scientifica^{TM} F20500162 magnetic stirrer (Thermal Scientific, USA) under 400 rpm magnetic stirring to provide agitation during experiments to prevent precipitated solids from settling at the bottom of container. The heating unit consisted of a hot water bath and coil. The hot water bath temperature was set at a fixed value during experiments by a TH6 thermoregulator (Ratek Instruments, Australia). The coil was made of ¼ inch 316L stainless steel tube and was submerged inside the hot water bath. The feed water was then recirculated to feed water container via the DCMD module (3). Distillate from the membrane was collected in the 15 L distillate container (5) and then withdrawn from the container and transferred back to the DCMD module (3) through a cooler (8) to remove the heat from the process. Distillate temperature at the cooler outlet was controlled to a set value by a TH5 thermoregulator and a RC1 immersion cooler (Ratek Instruments, Australia). Liquid transfer within this apparatus was achieved by a double-headed peristaltic pump (1a and 1b) (Masterflex, Cole-Parmer, USA). The 5 µm cartridge filter (4) (PXP.Zs05–10–PW, SUEZ, France) and membrane cleaning lines were installed to explore the operating potential and response to cleaning in this study. The distillate overflow line was to allow the permeated distillate product to be continuously cycled back to the feed container in order to maintain constant brine TDS during treatment of SWRO

brine and CSG RO brine where TDS in brines were predominantly dissolved inorganic salts (Table 3.1 and Table 3.2).

Four RS Pro Type K thermocouples (TT) (RS Components, Australia) measured the fluid temperature at the DCMD module inlets and outlets. The outputs from thermocouples were recorded at 5 min interval in a computer via a TC–08 multichannel datalogger (Pico Technology, UK). Orion 5–star portable EC meters (ECT) (Thermal Scientific, USA) measured the feed water and distillate qualities. Continuous monitoring of the distillate EC provided a means to detect wetting of the membrane during experiments and ensure that the membrane remained intact. An Orion 5–star portable pH meter (pHT) (Thermal Scientific, USA) measured feed water pH in the feed water container. A Defender® 3000 balance (Ohaus, USA) of range 0–30kg was used to measure the instantaneous distillate water quantity. As a visual indication, a Model 232.30 pressure gauge (PI) (WIKA, Australia) of range 0–100 kPa was installed to measure hot feed pressure into the DCMD module. This was done to ensure operating pressure was under critical values that lead to compression of the membrane or pore wetting and subsequent loss of performance (Zhang et al. 2013). Pressures were measured less than 5 kPa in all experiments of this study, and significant membrane compression is not anticipated at these pressures (Zhang et al. 2012). Thermal insulation foam was applied on both feed container (including lid) as well as hot side tubing to minimise heat loss and water evaporation (Figure 3.2).

.

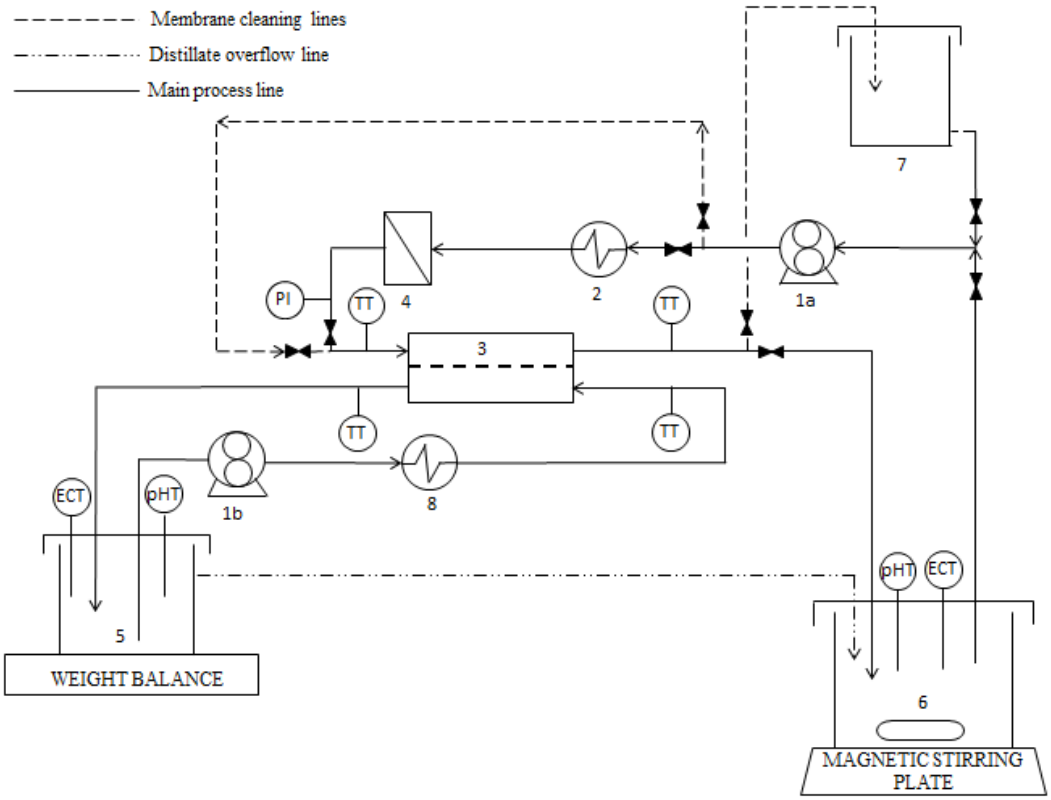

Figure 3.1 Bench-scale DCMD apparatus flow diagram: 1a and 1b—double-headed peristaltic pump; 2—heater; 3—DCMD module; 4—cartridge filter; 5—distillate container; 6—feed container; 7—cleaning container; 8 — cooler.

Figure 3.2 Bench-scale DCMD apparatus.

3.1.1 DCMD module

A flat-sheet DCMD module is the key component in this apparatus. As shown in Figure 3.3, the DCMD module housing was made of two transparent acrylic plates (30 mm thickness) to facilitate visual observation of membrane surface fouling / wetting phenomenon during the experiments. Silicon rubber gaskets (1.5 mm thickness) were placed at each side of the membrane to create flow channels for brine and distillate, respectively. Silicon rubber gaskets also acted as sealant purpose to prevent water leakage from DCMD module. Membrane was sandwiched between acrylic plates by eight of 316L stainless steel bolts (Figure 3.4). All bolts and nuts were tightened using a torque wrench set at 15 N·m to create equal flow channel spaces for brine and distillate, respectively. To enhance heat and mass transfer in MD process, Dow Filmtec^{TM} SW30–4040 RO membrane feed mesh spacers (28 mil thickness) were placed at 45° to the flow direction (diamond arrangement) in membrane brine and distillate channels, respectively (Figure 3.4) (Phattaranawik et al. 2003). As can be seen in Figure 3.3, brine / distillate solution was fed through a horizontal flow channel (12 mm diameter), and entered membrane flow channel via four vertical ports (12 mm diameter). Brine and distillate in countercurrent flow mode inside DCMD module. The effective membrane area of the MD module used in this study was 0.0169 m^2 (130 mm × 130 mm). The design drawing of DCMD acrylic plate can be seen in Appendix A.

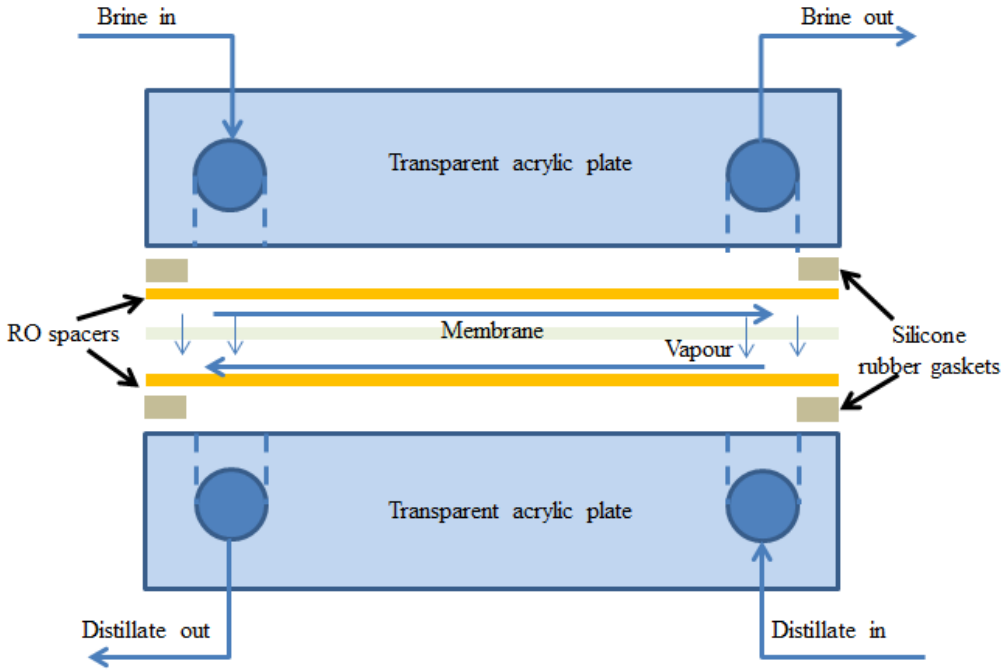

Figure 3.3 Configuration of DCMD module.

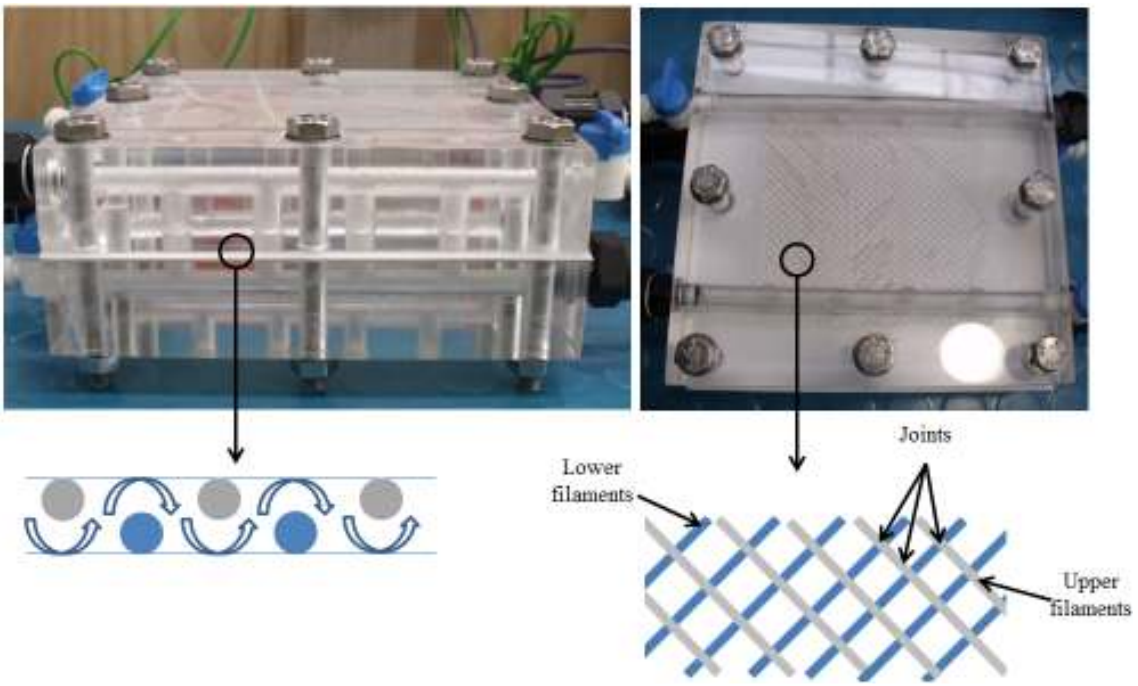

Figure 3.4 DCMD module, net spacer and flow direction in spacer filled channel.

3.1.2 Microporous membrane

PTFE membranes were adopted for the treatment of SWRO brine and CSG RO brine due to their high hydrophobicity, low thermal conductivity, good chemical stability and high

porosity (Zhang et al. 2009). PTFE membrane was acquired from Changqi Co. Ltd, China, and was made of an active PTFE layer on top of PP scrim supporting sub-layer. According to the supplier's membrane specification, the nominal pore size and membrane active layer thickness was 0.5 µm and approximately 35 µm, respectively. Membrane air permeability of 1.4×10^{-3} mol m^{-2} Pa^{-1} s^{-1} specified by manufacturer indicated that high vapour flux could be obtained.

Two types of commercial MD membranes provided by Aquastill Pty Ltd (Sittard, The Netherlands) were adopted in copper barren RO brine test. The first type of membrane, namely standard PE membrane, is fabricated with LDPE with no backing material, and has nominal pore size of 0.3 µm, thickness of 76 µm, porosity of 85%, and thermal conductivity of 1.35 W/m·K according to the supplier's membrane specification. The second type of membrane was an oleophobic PE membrane, with an oleophobic modification applied to the standard PE membrane to improve the membrane resistance against wetting and fouling.

3.2 Analytical methods

3.2.1 Membrane surface characterisation by Scanning Electron Microscope (SEM)–Energy Dispersive Spectroscopy (EDS) and X-ray Diffraction (XRD) analysis

Membrane samples were prepared by firstly removing the residual liquid on membrane surface by tilting the membrane sheet and draining the liquid. The membrane samples were then dried in dust-free atmospheric environment over 15 d prior to analysis. Care

was taken when handling membrane samples to ensure no additional force was applied on the scaling layer that may have led to breaking of the scaling layer from the surface.

The membrane surface was coated with gold in vacuum before the morphology and compositions of membrane fouling layer were observed using Zeiss Supra 55VP FEG SEM coupled with Oxford X-Max 20 EDS at an accelerating voltage 20 keV and a working distance 10 mm. Membrane samples from copper barren RO brine test in Section 6.5 were not coated with any conductive coating.

XRD was also performed to detect crystal deposits on membrane surfaces. XRD samples were recorded with a PANalytical's X'Pert X-ray Diffraction apparatus (40 keV, 30 mA) with Cu Kα radiation (λ = 1.548 Å) in the range of 2θ = 5-50° using steps of 0.05° and a scanning rate of 0.02° $mins^{-1}$.

3.2.2 Metal ions analysis by Inductively Coupled Plasma (ICP)–Atomic Emission Spectroscopy (AES) tests

Metal ion concentrations in solution were determined by a Model ICPE-9000 ICP-AES (Shimadzu, Japan). The ICP master stock calibration solution was prepared by mixing 50 ml of multielement standard solution (27 metal components and each at 0.5 mg/L) with standard solutions (1000 mg/L) of Al–2.2 ml, Fe–2.25 ml, Na–25 ml, Ca–5ml, Mg–5ml, K–2.5ml and Sr–2.25 ml, respectively. Then, master stock calibration solution was diluted by demineralised water at five difference ratios (1:400, 1:80, 1:16, 1:3 and 2:1) for ICP calibration. All standard solutions were acquired from CPAChem Ltd (Stara Zagora, Bulgaria). In this study, the distillate water samples were directly measured by ICP while brine samples were diluted by demineralised water at 1: 20 ratio before the

test. All samples were filtered by 0.45 µm nitrocellulose membrane and acidified by 1 ml of nitric acid (69 wt.%) and 1ml of hydrochloric acid (37 wt.%) before analysis.

3.2.3 Hardness analysis by titration tests

Titration tests were performed on SWRO brine samples to determine the total alkalinity, hardness and calcium concentrations. Alkalinity titration was conducted according to Standard HACH method 8203 (phenolphthalein and total method). A 5 ml of 0.45 µm filtered brine sample was diluted to 25 ml using demineralised water, and subsequently titrated by 0.16 M H_2SO_4 cartridge.

Total hardness and calcium titrations were based on Standard EDTA titration (Clesceri et al. 1998). Due to the high concentration of hardness in brine, 0.1 M EDTA titrant was prepared by dissolving 37.23 g of Na_2EDTA in 1 L of demineralised water. pH buffer solution was prepared by dissolving 1.179 g of Na_2EDTA and 780 mg of $MgSO_4 \times 7H_2O$ in 50 ml of demineralised water, and the solution was added with 16.9 g of NH_4Cl and 143 ml of ammonia hydroxide solution (30 wt.%), and subsequently diluted to 250 ml with demineralised water. A 0.45 µm filtered brine sample at 4 ml was diluted to 50 ml using demineralised water and followed by the titration. The hardness was calculated as follows:

$$\text{Total hardness} = \frac{V_t B_{CaCO_3} \cdot 1000}{V_{sample}} \left(\frac{mg}{L} \text{as } CaCO_3\right) \quad (3.1)$$

Where V_t is the volume (ml) of titrant solution and V_{sample} is the actual brine volume (4 ml). B represents the equivalent mass (mg) of $CaCO_3$ to 1 ml of 0.1 M EDTA titrant, and the value is 10.

Titration of calcium was performed using 0.01 M lab grade EDTA solution and the calcium concentration was calculated as follows:

$$Ca^{2+} = \frac{V_t B_{CaCO_3} \cdot 400}{V_{sample}} \left(\frac{mg}{L} \text{as } CaCO_3\right) \quad (3.2)$$

Where V_t is the volume (ml) of titrant solution and V_{sample} is the actual brine volume (4 ml). B represents the equivalent mass (mg) of $CaCO_3$ to 1 ml of 0.01 M EDTA titrant, and the value is 1.

3.2.4 Dissolved silica analysis by Silicomolybdate tests

In CSG RO brine test, Silicomolybdate method (HACH 8185) was used to measure the dissolved silica in samples. All samples were filtered by 0.22 µm nitrocellulose membrane before spectrophotometer analysis to remove possible colloidal and salt precipitates in solutions. For brine samples, a 15-fold dilution was applied to avoid interferences from HCO_3^- and ionic strength (Nghiem et al. 2015). A HACH spectrophotometer DR1900 was used to measure light absorbance at 452 nm. All containers used in this test were made of PE to prevent possible silica leaching from glass containers.

3.2.5 Dissolved ammonia analysis by Nesslerisation tests

Ammonia ion specific meter HI-93733 (Hanna, USA) was used to measure the dissolved ammonia concentration in the solution. This method is based on American society for testing and materials (ASTM) Manual of Water and Environmental Technology, D1426-92 Nesslerisation method. The reaction between dissolved ammonia and reagents HI-93733-01(Hanna, USA) causes a yellow tint and the intensity of colour is determined by a diode photocell. This analysis was adopted in copper barren RO brine test.

3.2.6 Total organic carbon (TOC) analysis

TOC analysis was performed using a Sievers InnovOx Laboratory TOC Analyser (SUEZ, France). Samples were preserved by addition of H_2SO_4 to pH < 2 and stored at 4 °C until analysis. Analyses were conducted in TOC mode (TOC = total carbon (TC) – total inorganic carbon (TIC)). TOC calibration up to 100 mg/L was made using potassium hydrogen phthalate and inorganic carbon (IC) calibration using anhydrous sodium carbonate.

3.3 Phreeqc–3 calculation

In CSG RO brine test, Phreeqc–3 software (Lisdonk et al. 2001) was chosen to calculate SI of inorganic salts, particularly metal silicates in brine.

The SI is defined as:

$$SI = \log\left(\frac{IAP}{K_{sp}}\right) \tag{3.3}$$

Where the IAP is the ion activity product and K_{sp} is the solubility product. When SI > 0, the compound is supersaturated and there is a risk of precipitation. The activity of water a_{H_2O}, in Phreeqc–3 was calculated from an approximation that is based on Raoult's law.

$$a_{H_2O} = 1 - 0.017 \sum_{i=1}^{N_{aq}} m_i \tag{3.4}$$

Where i is a certain aqueous species, N_{aq} is the total number of aqueous species and m_i is the molarity of the i^{th} aqueous specie in solution. The water vapour pressure of the salt solution was calculated using

$$p = p^0 a_{H_2O}\, x_{water} \tag{3.5}$$

Where p (Pa) is water vapour pressure in salt solution, p^0 (Pa) is pure water vapour pressure and x_{water} is the molar fraction of water in salt solution.

The vapour pressure of pure water is calculated from Antoine Equation which has been applied to MD study previously (Duong et al. 2016).

$$p^0 = \exp(23.1964 - \frac{3816.44}{T-46.13}) \quad (3.6)$$

Where T (K) is the water temperature.

3.4 Energy assessment

In copper barren RO brine test, the waste heat requirement for the bench-scale DCMD process was calculated per unit of distillate generated defined by the specific thermal energy consumption (STEC) as follows (Saffarini et al. 2012):

$$STEC = \frac{\dot{m}_{hot}\ C_p\ (T_{hot} - T_{sys})}{JA} \quad (3.7)$$

Where $\dot{m}_{hot}$ is the hot brine feed flow rate (0.02 kg/s), C_p is the specific heat capacity of the feed water (4.18 kJ/kg·K), T_{hot} is the DCMD inlet temperature (60 °C) and T_{sys} is the temperature at heater inlet which in this study was approximately same as the temperature in the feed container (55 °C). J is the distillate flux and A is the membrane area (0.0169 m^2).

3.5 UHP RO apparatus

In copper barren RO brine test, with the view of insufficient waste heat to supply the thermal energy requirement of DCMD system operates at high water recovery, a bench-scale UHP RO apparatus was acquired from MDS America Pty Ltd (CA, USA) to assess

the feasibility of RO brine minimisation using a hybrid high pressure UHP RO + MD process. The aim of this test was to concentrate RO brine by 3 folds using UHP RO apparatus.

As can be seen in Figure 3.5, the RO module contained a stainless steel housing (7) at pressure rating of 1,500 psi (103.5 bar). A custom-made spiral-wound polyamide membrane element (43 mm diameter, and 250 mm long) with surface area of 0.4 m^2 was equipped inside RO housing. RO feed pressure was supplied by a low pressure centrifugal pump (3) and a high pressure piston pump (5) Model 231 (CAT pump, USA) at the design flowrate of 4.9–8.7 L/min. A 5 μm cartridge filter (4) was installed at the suction side of piston pump. During the test, RO brine was fed to the apparatus from a 1,000 L bulky tank (1), and continuously recirculated to the feed tank while permeate was collected in product tank (2). RO feed pressure was maintained at 100 bar in this test via a needle valve (6) installed at brine outlet. RO feed and permeate conditions (e.g., flow, pressure, temperature, pH and EC) were manually recorded throughout the run, and membrane fouling / scaling was assessed by calculating normalised permeate flux changes using FTNorm.xls software (Dow Chemical, USA).

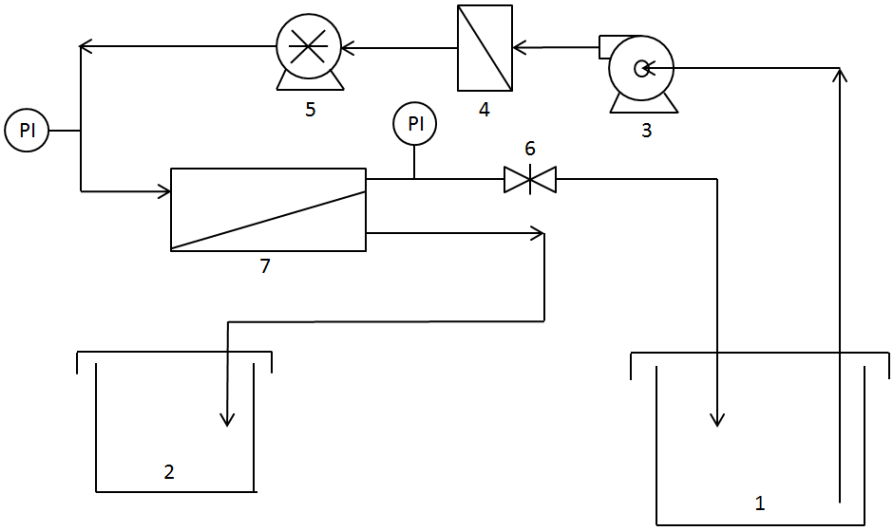

Figure 3.5 High pressure RO apparatus flow diagram: 1—feed tank; 2—permeate tank; 3—low pressure RO feed pump; 4—cartridge filter; 5—piston pump; 6—needle valve; 7—RO module.

Figure 3.6 Bench-scale UHP RO apparatus.

3.6 Characteristics of RO brine solutions

3.6.1 SWRO brine

SWRO brine was obtained from a SWRO plant located at Whyalla, South Australia. The plant was built to provide desalinated water for iron ore mining operations. The single-pass RO system operates at 40% recovery at feed flow of 500 m^3/hr. The plant uses MF as pre-treatment to RO. To prevent salt precipitation on the RO membranes in normal operation, commercial antiscalant Flocon 190 (BWA Water Additives UK Ltd), a solution of an organic phosphonate acid is dosed prior to RO at an optimised dosing rate 2.0 mg/L. The compositions of raw seawater and SWRO brine determined by laboratory analysis in the Australian Water Quality Center are summarised in Table 3.1 below.

Table 3.1 Raw seawater and SWRO brine main components.

Parameter	Raw seawater (mg/L)[a]	SWRO brine (mg/L)[b]
Ca^{2+}	537 – 623	895 – 1038
Mg^{2+}	1530 – 1810	2550 – 3017
Cl^-	20,800 – 23,700	34,667 – 39,500
Na^+	11,500 – 14,800	19,167 – 24,667
HCO_3^-	155 – 156	258 – 260
SO_4^{2-}	4290 – 7590	7150 – 12,650
TDS	37,000 – 41,000	61,667 – 68,333
EC	55,200 – 61,300 µS/cm	90,100 – 98,000 µS/cm

[a]Temperature: 25 °C, pH - 8.1. Individual ion concentration varies subject to low and high tides.
[b]Recovery factor: 40%.

3.6.2 CSG RO brine

The CSG produced water was collected from a CSG well in Gloucester (New South Wales, Australia) and kept under ambient temperature at around 25 °C prior to experiments. CSG produced water was first desalinated using an RO test rig which contained a 1 µm cartridge filter and RO vessel equipped with single brackish water RO membrane TML20–400 (Toray Co., Japan). RO brine from the test rig was continuously

recirculated to the feed tank, and RO process stopped at 45% water recovery of CSG produced water to avoid salt precipitation in the feed tank. The concentrated retentate in feed tank was used as MD feed in this test. The characteristics of CSG RO brine are listed in Table 3.2 and solution ionic strength was calculated as 0.2 M.

Table 3.2 Characteristics of RO brine at 45% recovery of CSG produced water.

Parameters	
EC	17.8 mS/cm
TDS	10,173 mg/L
pH	8.6
TOC	5.7 mg/L
HCO_3^- as $CaCO_3$	6,840 mg/L
CO_3^{2-} as $CaCO_3$	980 mg/L
Total alkalinity as $CaCO_3$	7,820 mg/L
Ca^{2+}	5 mg/L
Mg^{2+}	4.3 mg/L
Na^+	4,180 mg/L
Cl^-	900 mg/L
K^+	8 mg/L
Iron	0.03 mg/L
Aluminum	< 0.01 mg/L
Dissolved silica	32 mg/L
SO_4^{2-}	8 mg/L

3.6.3 Copper barren RO brine

The copper barren RO brine was collected from a copper processing plant (Adchem Pty Ltd) located at Burra, South Australia. The three-stage RO system operates at water recovery of 85%, and brine flowrate of 4 m^3/h. RO brine was stored at ambient temperature around 20 °C throughout this study. The compositions of RO brine are listed in Table 3.3 below. As it is shown in Figure 3.7, the RO brine present as tinted blue color which was attributed to the high concentration of dissolved copper ions (Table 3.3).

Table 3.3 Characteristics of RO brine from barren leach solution.

Parameters	
pH	9.1
Aluminum	0.3 mg/L
Calcium	1.5 mg/L
Magnesium	2 mg/L
Potassium	17 mg/L
Total iron	0.3 mg/L
Chromium	0.02 mg/L
Sodium	3,000 mg/L
Sulphate	1,200 mg/L
Silica	1.1 mg/L
Strontium	0.01 mg/L
Copper	120 mg/L
Total ammonia	2,180mg/L
Bicarbonate (as $CaCO_3$)	778 mg/L
Chloride	7,600 mg/L
TOC	47 mg/L
TDS	11,420 mg/L
EC	27,900 µS/cm

Figure 3.7 Copper barren RO brine.

3.7 SWRO brine DCMD test

DCMD experiments were initially conducted in batch mode to understand the precipitation mechanisms of sparingly soluble salts in together with flux behaviour as a function of concentration. 11 kg of SWRO brine was added to the feed container with no

further addition of antiscalant. The process was then operated continuously to concentrate the brine solution with feed and distillate inlet temperatures of 50 and 25 °C, respectively. Feed and distillate circulation flowrates were maintained at 1,000 ml/min (cross flow rate = 0.075 m/s) throughout the experiment. At the completion of each experiment, the bench apparatus was recirculated with NaOH solution at pH = 12 followed by HCl solution at pH = 2 for 30 min (each) to remove any residual organic and inorganic matter left in system. Demineralised water was then used to rinse the apparatus until pH and EC at the system outlet had same readings as the system inlet. At the beginning of each experiment, demineralised water was used to operate DCMD for membrane activation under same experimental conditions (e.g., temperature, flowrate) until consistent flux was achieved over 2 hours. Distillate flux, J_i ($L/m^2 \cdot h$), was calculated by:

$$J_i = \frac{\Delta m \cdot 1000}{\Delta t \cdot A \cdot \rho} \ (L/m^2 \cdot h) \tag{3.8}$$

Where membrane area, A = 0.0169 m^2, Δm is the distillate weight (kg) collected over the time period of Δt (h). ρ is the distillate density 997.04 kg/m^3 at 25 °C.

A continuous mode DCMD experiment was also carried out to simulate a more realistic process where the hot feed would have a constant TDS concentration. To achieve this mode, the distillate overflowed from distillate container to the feed container throughout the experiment in order to maintain constant TDS in the feed container. Demineralised water was added to the feed container occasionally during experiment to replace the water lost due to evaporation. Operational parameters such as temperature and flowrate were identical to batch mode experiments. Grab samples were taken at the distillate overflow line and distillate flux was calculated by:

$$J_i = \frac{m_{overflow} \cdot 6000}{\rho \cdot A} \ (L/m^2 \cdot h) \quad (3.9)$$

Where membrane area, A = 0.00169 m^2, $m_{overflow}$ is the weight (kg) of distillate over a 10 min period. Distillate was captured at the bottom of an overflow pipe to the feed container, and immediately weighted by a balance that had a minimum resolution of 10 mg. ρ is the distillate density of 997.04 kg/m^3 at 25 °C. The flux data presented in this test are normalised flux (J_i/J_0), which is the instantaneous flux J_i over the initial flux J_0. The purpose of normalised flux is to provide comparable and presentable results of flux decline and recovery due to SWRO brine used in this study at EC range of 90 to 98 mS/cm (Table 3.1), which lead to the slight variation of initial flux J_0.

3.7.1 Membrane scaling process in batch mode operation

Four batch mode experiments were conducted at identical process conditions as described above. Each experiment was terminated at different normalised flux reduction ratio. Membranes were then removed from the DCMD module and surface scaling analysis was conducted. The surface scaling morphologies and structures were compared to reveal the membrane scaling process in terms of various concentrations of TDS in SWRO brine.

3.7.2 Estimation of seawater vapour pressure

Raoult's law was used to estimate the vapour pressure of seawater as a first approximation. Sharqawy et al (2010) developed an equation below to estimate seawater vapour pressure neglecting effects of concentration polarisation:

$$\frac{p_v}{p_{v,sw}} = 1 + 0.57357 \times \frac{S}{1000 - S} \quad (3.10)$$

Where p_v is vapour pressure of pure water in Pa and $p_{v,sw}$ is vapour pressure (Pa) of seawater for salinity S in g/kg.

3.7.3 Salt precipitation test with antiscalant

Salt precipitation tests were conducted to evaluate the antiscalant efficiency for inhibiting Ca related scale formation under DCMD process conditions. A commercial SWRO antiscalant Flocon 190 was investigated in this study. According to the manufacturer's specification, Flocon 190 is effective in controlling carbonate and sulphate scale forming salts on membrane surfaces. The pH of Flocon 190 was between 10 and 11. Based on the ionic composition reported in Table 3.1, synthetic SWRO brine was prepared by mixing laboratory grade salts (Na_2SO_4, $MgCl_2$ x $6H_2O$, KCl and NaCl) and synthetic sea salt S9883 acquired from Sigma-Aldrich in 500 ml of demineralised water at ambient temperature. Synthetic SWRO brine was prepared according to the ionic composition of the real SWRO brine for a final TDS concentration of 184 g/L (Table 3.4), and this is equivalent to 2.7-fold concentration of raw SWRO brine (Table 3.1). At room temperature, mixed salts were added to two beakers contained demineralised water at temperature of 50 °C. The solutions were stirred for 10 min under controlled temperature of 50 °C and then Flocon 190 was added to one beaker at 10 mg/L to simulate the dosing regime used for the RO process. During the following 2 h of mixing, titration analysis was conducted to determine HCO_3^-, Ca^{2+} concentration. The concentration of Mg^{2+} was calculated by the difference between total hardness and calcium hardness from the titration results. In order to minimise the undissolved salts contained in sample water, a small amount of sample water (e.g., 5–10 mL) was withdrawn near the liquid surface for analysis after each pre-determined time interval. All samples were filtered through 0.45

μm filter prior to the titration analysis to identify the soluble ions in solution. The efficiency of antiscalant on scale inhibition was compared according to the titration results. The salt precipitation process with antiscalant dosing was explored via observing the concentration changes of HCO_3^-, Ca^{2+} and Mg^{2+} in brine solution.

Table 3.4 Compositions of synthetic SWRO brine in 500 ml solution.

Salt	Mass (g)
Synthetic sea salt	79.17
$CaCl_2 \times 2H_2O$	1.46
Na_2SO_4	5.01
$MgCl_2 \times 2H_2O$	8.54
KCl	0.44
NaCl	8.73

3.7.4 Analysis of crystal deposits on cartridge filter

Analysis of the hot feed side cartridge filter can reveal the possible crystal deposits. Cartridge filter analysis was performed by immersing the cartridge filter in demineralised water overnight following DCMD experiments, to dissolve scaling compounds from the surface. Then, the final solution was conducted by ICP-AES analysis.

3.8 CSG RO brine DCMD test

In this test, both feed and distillate flows were operated at a fixed flowrate of 1,000 ml/min (cross flow rate = 0.075 m/s). Feed and distillate inlet temperatures were controlled at 50 and 25 °C, respectively. DCMD experiment was first performed over 150 h on CSG RO brine under batch mode operation. The purposes of this experiment were to assess DCMD performance over a relative prolonged period, and to identify membrane foulants at high water recovery. Due to the volume constraint of feed container, during this experiment, the feed container was restocked occasionally with fresh CSG RO brine. A 5 μm cartridge filter was used in the brine stream.

Synthetic CSG RO brine DCMD experiments were carried out without the cartridge filter in order to understand the overall chemistry in brine and its influence on DCMD performance. The effect of Ca^{2+} and Mg^{2+} on silica fouling was assessed first. As shown in Table 3.5, two brine solutions with different concentrations of Mg^{2+} were employed in this test. Brine solution Mg4.3 contained 4.3 mg/L of Mg^{2+} as actual CSG RO brine (Table 3.2), while brine solution Mg30 contained 30 mg/L of Mg^{2+}. $NaHCO_3$ concentration was adjusted in synthetic solutions to ensure it maintained at same ionic strength as actual CSG RO brine (Table 3.2). Compared to the actual RO brine, the additional $NaHCO_3$ (< 0.01 M) in synthetic solutions was considered to have negligible effect on the purpose of this test.

In this test, 7.2 L of brine was treated in batch mode to 80% brine recovery (overall recovery of 91%). A 24 h of continuous mode operation (recirculating distillate to feed) was applied in Mg30 test to allow sufficient time for salts to form under supersaturated condition thereby avoid misinterpreting of foulants by examining the membrane surface immediately after batch mode operation. Concentrations of Mg^{2+}, Ca^{2+} and dissolved silica in brine were measured throughout the experiments via grab samples.

Table 3.5 Composition of synthetic CSG RO brines.

Brine	I (M)	HCO_3^- (mg/L)	Ca^{2+} (mg/L)	Mg^{2+} (mg/L)	Na^+ (mg/L)	SO_4^{2-} (mg/L)	Cl^- (mg/L)	SiO_2 (mg/L)
Mg4.3	0.2	9,522	5	4.3	4,901	8	1,037	32
Mg30	0.2	9,392	5	30	4,852	8	1,037	32

Synthetic CSG RO brines were prepared from analytical grade salts (NaCl, Na_2SO_4, $CaCl_2 \cdot 2H_2O$, $MgCl_2 \cdot 6H_2O$, $NaHCO_3$ and Na_2O_3Si). All analytical grade salts were acquired from Sigma-Aldrich. Trivalent metal ions such as Fe^{3+} and Al^{3+} were not considered as part of this study due to the concentrations being either very low or

undetectable in CSG produced water. Moreover, membrane surface EDS analysis results shown later in Section 5.1 revealed that membrane fouling deposits did not contain Fe^{3+} / Al^{3+}. Organic components were also not simulated in synthetic CSG RO brine due to the ability of organics (e.g., HA) to possibly form complexes with cations (e.g., Ca^{2+}) as well as to react with hydrophobic membrane by adsorption (Jermann et al. 2007; Tijing et al. 2015). Such behaviour would impact on the main purpose of this study that is to identify silica interaction kinetics with hardness ions and their subsequent effect on MD fouling.

Synthetic hardness-free CSG RO brines were also prepared to investigate the effect of anions (HCO_3^- / CO_3^{2-} and Cl^-) on silica polymerisation and the influence of polymerised silica on DCMD performance. The brines used in this test are given in Table 3.6. Brine solution NaCl0M contained only $NaHCO_3$ at 0.2 M, while brine solution NaCl0.1M contained $NaHCO_3$ and NaCl each at 0.1 M. Each brine solution contained dissolved silica concentration at 140 mg/L in order to promote supersaturation of silica (Bremere et al. 2000). In this test, 7.2 L of brine was treated in batch mode to 80% brine recovery, followed by 35 h of continuous mode operation to allow dissolved silica reaching equilibrium state in brine (Gryta 2005). Brine pH was maintained during experiments using 1 N NaOH and HCl, respectively. Dissolved silica concentrations in brine were measured throughout the experiments via grab samples.

Table 3.6 Composition of synthetic hardness-free CSG RO brine.

Brine	I (M)	$NaHCO_3$ (M)	NaCl (M)	$NaHCO_3$ (mg/L)	NaCl (mg/L)	SiO_2 (mg/L)	pH
NaCl0M	0.2	0.2	-	16,800	-	140	9.15±0.05
NaCl0.1M	0.2	0.1	0.1	8,400	5,844	140	9.15±0.05

Prior to each experiment, synthetic CSG RO brines were filtered through 0.45 µm filter to remove any particulates present in solution. At the end of each experiment, the system was emptied by slowly purging the tubing with air, then the used membrane was removed for analysis and a new membrane was installed for brine loop (MD hot cycle) clean. Brine loop was cleaned by recirculating 3.2 wt.% HCl (1 L) and then 4.0 wt.% NaOH (1 L) for 30 min at 1000 ml/min, respectively, to dissolve possible precipitates in the system such as metal silicates, amorphous silica and hardness scales. Pre- and post-flushing with demineralised water was performed for each chemical clean.

3.8.1 Amorphous silica solubility tests

Amorphous silica solubility tests were performed in PE containers placed on a magnetic stirrer hot plate and maintained at 25, 55 and 65 ˚C, respectively. According to Table 3.2, the molar ratio between HCO_3^- / CO_3^{2-} and Cl^- is approximately of 5.8 : 1. The same ratio of $NaHCO_3$ and NaCl was applied to synthetic brine solutions containing 100 g/L $NaHCO_3$ and 12 g/L NaCl to simulate approximately 88% CSG produced water recovery where stable MD performance was obtained prior to rapid flux decline (Section 5.1). Filtered synthetic brine was heated to the desired temperature, then Na_2O_3Si was added to solution at a stirring speed of 400 rpm for 10 min then the stirring speed was reduced to 100 rpm. The mass of Na_2O_3Si added to solution was selected to achieve initial dissolved silica concentration of 450 mg/L at 25 ˚C and 900 mg/L at 55 and 65 ˚C, each at about 3.5 times of dissolved amorphous silica equilibrium concentration in low ionic strength solution (Gunnarsson and Arnórsson 1999). High initial concentrations were chosen to promote rapid colloidal silica formation by homogenous nucleation (Bremere et al. 2000). The dissolved silica concentration was measured at every 24 h period following addition of Na_2O_3Si.

3.8.2 Scale inhibition tests

Two proprietary RO antiscalants were selected for this study, namely antiscalant A and B. Antiscalant A is a phosphonate based inorganic inhibitor, and antiscalant B is an organic polymer based inhibitor. According to the manufacturers, both antiscalants are suitable for thermal desalination application and specifically designed for silica scale inhibition and are also effective to inhibit other scales such as $CaSO_4$ and $CaCO_3$. Antiscalant was added in brine solution to obtain a concentration of 10 mg/L, which is about the antiscalant concentration in RO brine (He et al. 2009). In the Na_2EDTA study, the stoichiometric amount of Na_2EDTA was introduced to synthetic brine prior to mixing of $CaCl_2$ and $MgCl_2$ solutions. The effectiveness of antiscalants and Na_2EDTA was assessed through the mass loss of Mg^{2+}, Ca^{2+} and dissolved silica in MD brine at the end of each experiment via ICP-AES analysis.

3.9 Copper barren RO brine DCMD test

A 5 µm cartridge filter was installed at the DCMD module brine inlet. The process was operated with feed and distillate inlet temperature of 60 and 30 °C, respectively. Feed and distillate circulation flowrates were maintained at 1,200 ml/min (cross flwo rate = 0.09 m/s) throughout the experiments.

To assess the performances (e.g., distillate flux, membrane fouling) of standard PE and oleophobic PE membranes under high water recovery, 17 kg of brine was progressively concentrated under batch mode operation until brine concentration factor (CF) = 5 (overall recovery of 97%) was reached. The value of CF was calculated by following equation:

$$CF = \frac{m_{f,i}}{m_{f,i} - m_p} \quad (3.11)$$

Where $m_{f,i}$ is the initial feed water weight (kg) and m_p is the distillate water weight (kg).

Then, the experiment was converted to constant CF mode for 72 h of operation where raw RO brine was added to the feed container in small batches while MD brine was removed occasionally from feed container to maintain constant brine CF = 5 throughout the experiment.

To investigate the stability of copper-ammonia complexes and the impact of copper salts precipitation on DCMD performance, 300 ml of demineralised water was used to compensate water in MD feed at interval of 3-4 h during 74 h of constant CF mode operation with the expectation of that ammonia removal from MD feed would eventually lead to precipitation of copper salts.

3.9.1 Membrane cleaning tests

Upon the completion of constant CF mode (CF = 5) experiment with demineralised water top up, the membrane was removed and prepared at sample size of 4 cm × 4 cm for cleaning tests. The membrane sample was immersed in the 2 L beaker for 1 h at 40 °C with stirring speed of 200 rpm. Membrane sample was cleaned by alkaline solution which contained 1 wt.% NaOH and 1 wt.% Na_4EDTA followed by 1 wt.% HCl. Between each cleans, the membrane sample was soaked in 40 °C demineralised water for 10 min with stirring. All analytical grade chemicals were acquired from Sigma-Aldrich in this test. The same cleaning protocol was applied to the membrane sample which was cleaned with raw RO brine except at cleaning temperature of 60 °C. It was expected that dissolved ammonia in RO brine could extract copper from crystal lattice or react with Cu^{2+},

subsequently enhancing copper salt solubility in solution. The effectiveness of different cleans were accessed by SEM-EDS analysis.

Chapter 4 DCMD of SWRO brine

The main objective of this test was to investigate the scale (e.g., $CaCO_3$ and $CaSO_4$) formation behaviour on MD membranes when treating SWRO brine (Table 3.1). In addition, techniques such as chemical free membrane cleaning (e.g., distillate / raw RO brine flushing), antiscalants and cartridge filtration were studied to weigh up the best strategies to manage membrane fouling.

4.1 PTFE membrane

Figure 4.1 presents the SEM images of active layer and support layer of PTFE membrane employed in this study. It is shown in Figure 4.1a and 4.1b, the PTFE active layer contains continuous fibrils conjoined by nodes with various sizes, and the membrane pores are present as the irregular interstices between fibrils. The morphology of PTFE membrane is determined by the stretching technique applied in the membrane fabrication process (Lalia et al. 2015). The island-like nodes shown in Figure 4.1b could act as the nucleation site for crystal growth which eventually leads to the damage of PTFE fibrils (Guillen-Burrieza et al. 2013; 2014). PTFE membrane active layer appears highly porous (Figure 4.1a and 4.1b); however, the vapour transport across membrane could be influenced by the PP scrim support layer. Higher porosity of support layer means more active membrane area for mass transport, hence higher vapour flux. Thicker support layer on the other hand, tends to trap more distillate water molecules and adsorb more heat supplied by the hot feed, thus increasing the temperature polarisation.

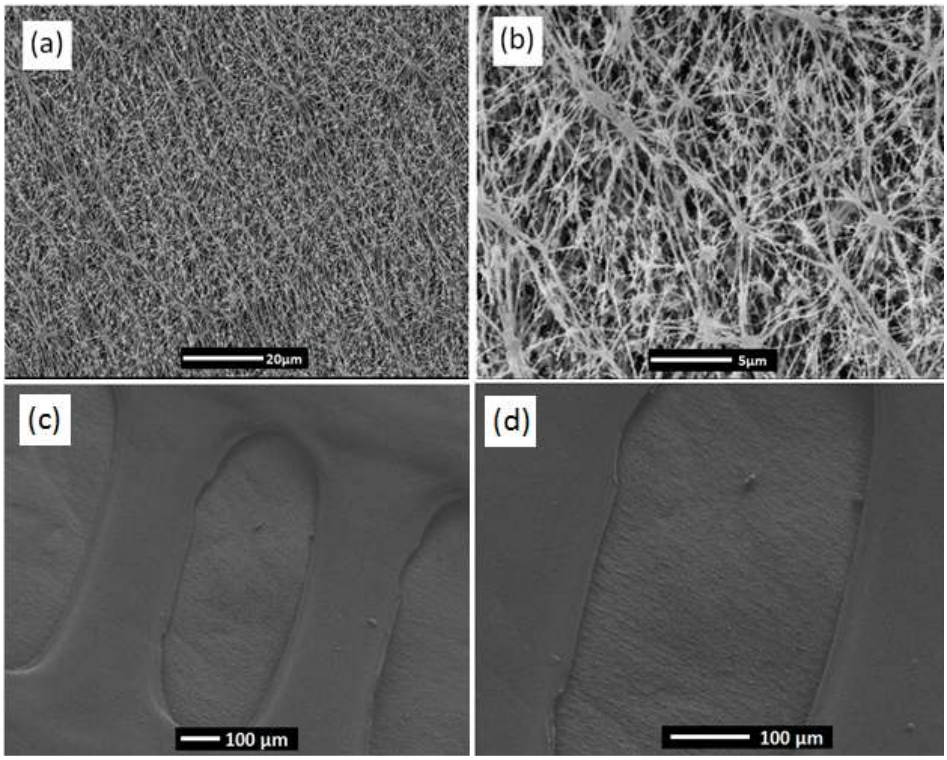

Figure 4.1 SEM images of virgin PTFE membrane: (a) and (b) are for active layer; (c) and (d) are for support layer.

4.2 DCMD batch mode operation

Results of batch mode DCMD experiments on SWRO brine (Table 3.1) are shown in Figure 4.2. In this test, the brine feed cartridge filter was not installed.

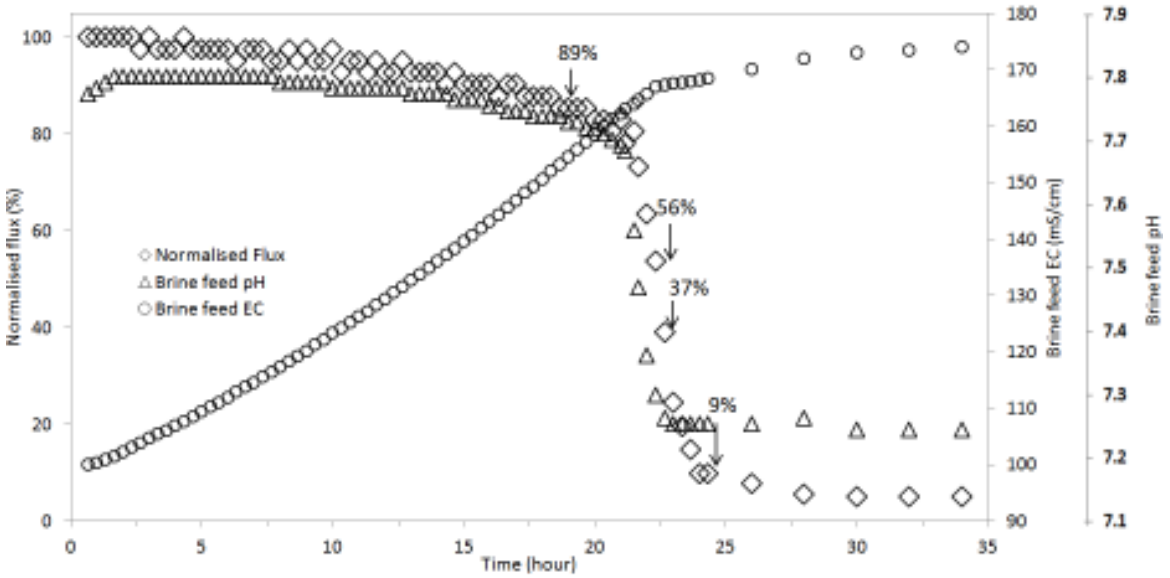

Figure 4.2 Normalised flux, brine feed EC and pH as function of run time for DCMD batch mode operation on SWRO brine. Experimental conditions: initial SWRO brine weight = 11 kg; T_f = 50 ˚C; T_d = 25 ˚C; Q_f= Q_d = 1000 ml/min (cross flow = 0.075 m/s); total run time = 34 h; initial flux J_0 = 25 L/m^2·h; cartridge filter was not used in the brine feed stream. Four experiments stopped at normalised flux of 89, 56, 37 and 9%, respectively and membranes analysed by SEM.

A gradual distillate flux decline occurred during the first 21 h of operation, with the hot feed EC increasing from 98 to 160 mS/cm (Figure 4.2). Over this period, a 20% flux decrease was observed and an average flux of 23 L/m^2·h was achieved. Flux decline may be due to rising salinity which reduces vapour pressure according to Raoult's law (Equation 3.4). The calculated flux decline due to increased TDS in brine feed suppressing the vapour pressure was approximately 3%. The resulting 17% difference between the observed flux decline and the theoretical 3% decline in driving force is likely due to the effects of partial membrane scaling and increased viscosity of brine feed which can both reduce mixing near the surface leading to increased temperature polarisation. Figure 4.3 illustrates the viscosity of sodium chloride solution at 1 atm under different temperatures (McCain 1990). According to the correlation presented in Figure 4.3, the NaCl solution viscosity increased by approximately 30% from TDS of 5 to 15 wt.% at 50 °C. The majority of the flux decline appears to be linked more to either increased fluid

viscosity (and in turn increased temperature polarisation due to reduced surface mixing) or due to scale build up on the membrane surface adding thermal and hydraulic resistance.

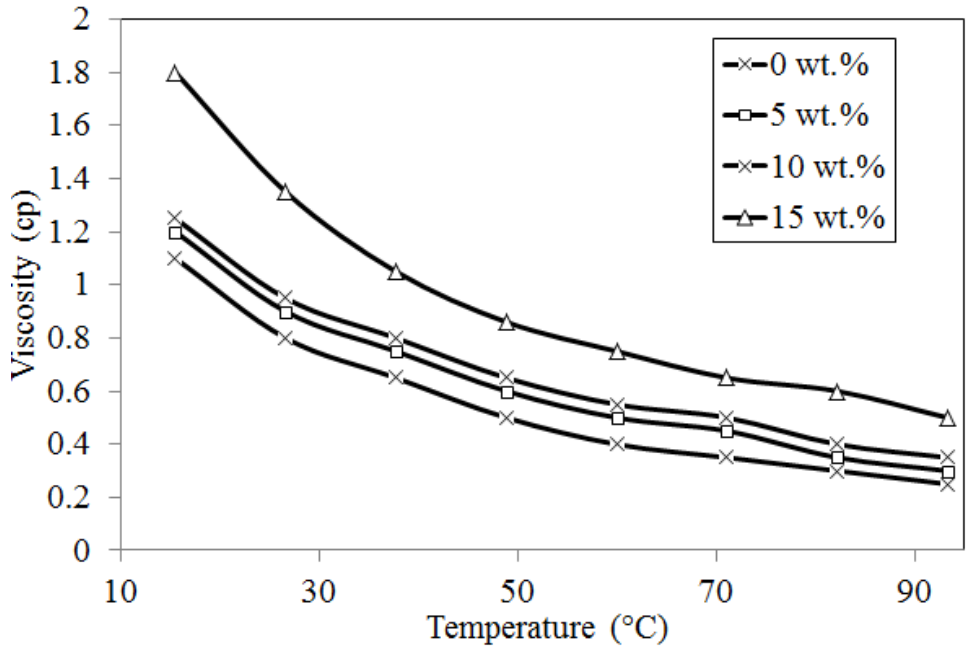

Figure 4.3 Viscosity of sodium chloride solutions as a function of temperature and salinity (wt.%) at 1 atm (data withdrawn from McCain 1990).

However, also shown in Figure 4.2, a significant flux drop that occurred at a brine EC of 160 mS/cm after 21 h of operation. The normalised flux rapidly reduced by 90% over 2.5 h. This dramatic flux drop suggests severe salt precipitation at the membrane surface blocking water transport through the membrane. After 24 h of operation, the normalised flux reduced to 9% with brine water recovery of 45%. From this point, flux slowly declined to 5% at the end of this experiment with SWRO brine EC at 175 mS/cm. The 'milky' appearance of the brine solution and white deposits occurred in brine suggested that a significant amount of sparingly soluble salts were precipitated with some still in suspension (Figure 4.4a and 4.4b). Visual inspection of the membrane surface revealed that the membrane was covered with white crystal deposits (Figure 4.4c). It was suspected that salt crystals rapidly covered the membrane surface and almost stopped distillate

production within just a few hours. Despite this, continuous monitoring of distillate EC confirmed that membrane pore wetting did not result from the severe membrane scaling. The distillate EC measured less than 5.0 µS/cm during the entire run, indicating the membrane provided almost complete rejection of non-volatile solutes in SWRO brine.

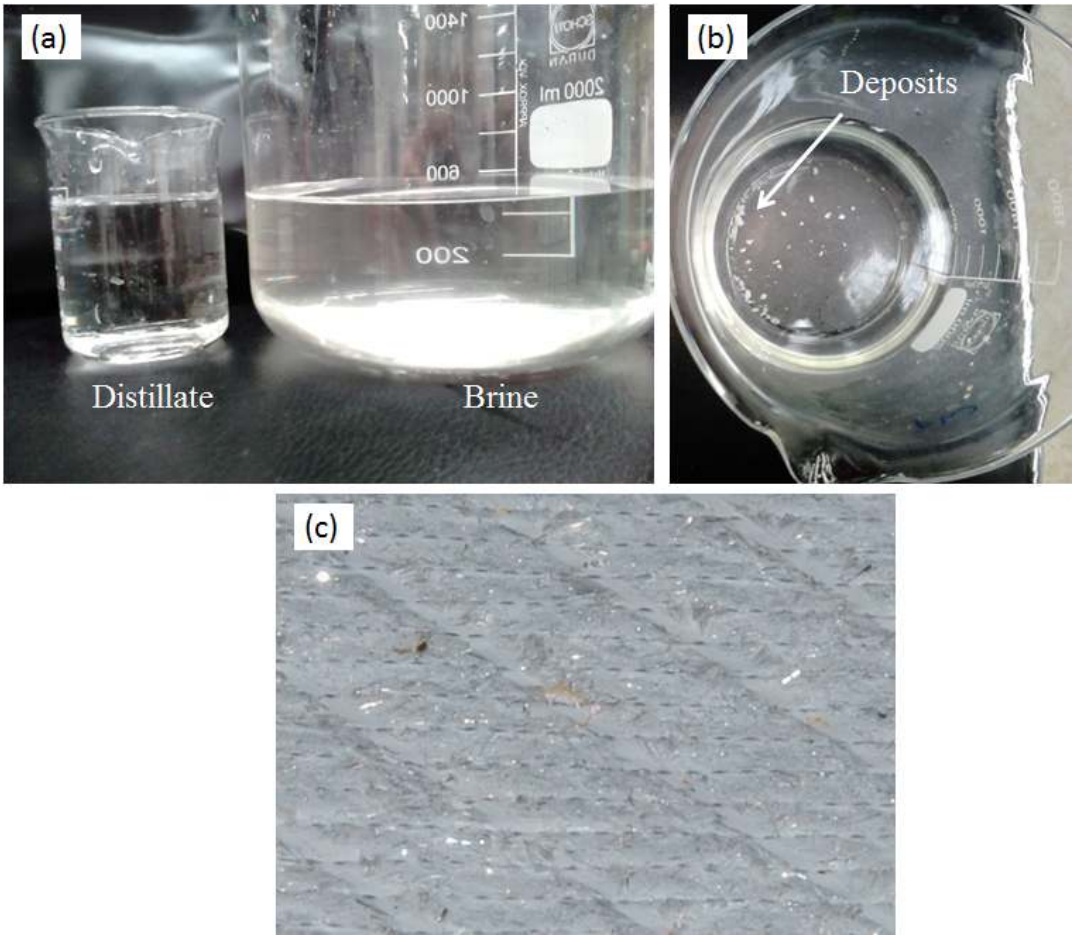

Figure 4.4 Batch mode DCMD on SWRO brine to brine EC of 175 mS/cm: (a) illustrates brine and distillate solutions at the end of experiment; (b) illustrates crystal deposits in brine and (c) shows crystal deposits on membrane surface.

Four experiments were conducted at identical process conditions marked with water recoveries on Figure 4.2. Each of the experiments were terminated at different filtration times corresponding to various normalised flux reduction ratios and water recoveries. The membrane at each time was removed from DCMD module for SEM analysis after each experiment. SEM micrograph Figure 4.5 reveals that the membrane surface operating at

89% of the initial flux appeared smooth with no obvious precipitate when compared with virgin membrane SEM micrograph (Figure 4.5). This is evidence that membrane scaling was negligible at normalised flux of 89% and sparingly soluble salts were still in solution. Figure 4.5c and 4.5d on the other hand, show significant crystal deposits on the membrane surfaces at normalised flux of 56 and 37%, respectively. Needle-shaped crystals covered the membrane surface area. The crystals could be $CaSO_4$, as studies have reported that $CaSO_4$ can grow directly on and cover on membrane surfaces which will completely stop flux (Nghiem et al. 2011). In Figure 4.5e, the scaling layer appears to have become thick and highly compacted, where only 9% of normalised flux was obtained.

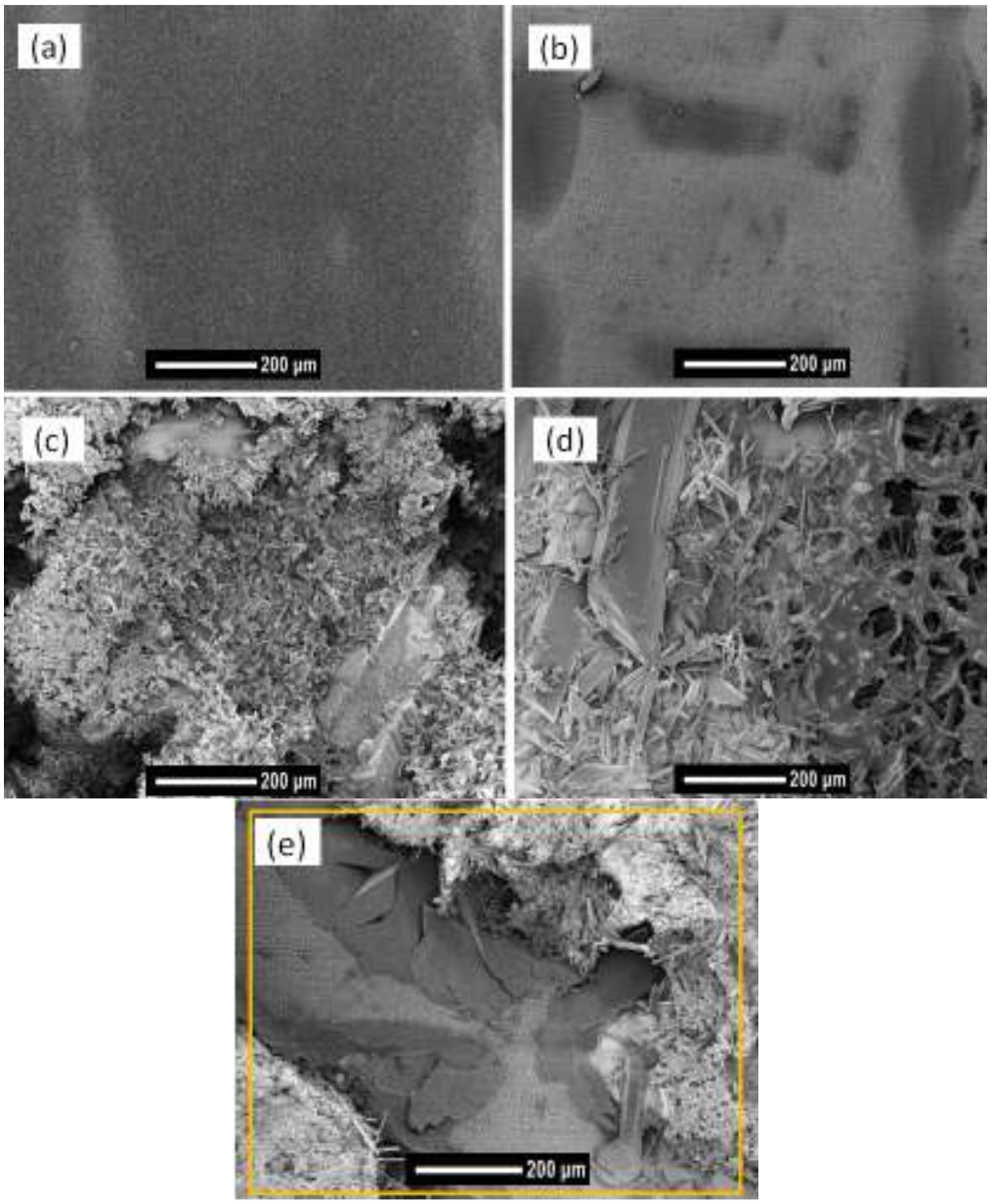

Figure 4.5 SEM micrographs of membrane surface where experiment terminated at normalised flux of (a) virgin membrane; (b) 89%; (c) 56%; (d) 37%; and (e) 9%.

Elements on membrane sample in Figure 4.5e were analysed using EDS and results are shown in Table 4.1, where the major elements present on the membrane can be seen. The most significant peak was attributed to F, which would predominantly come from the PTFE membrane as no significant levels of F are expected to come from the solution. Results also show significant peaks such as O, S, Cl and Ca with small peaks of Na and C. The element Na and Cl can be explained from the residual brine solution at the

membrane surface since the PTFE membrane does not contain the elements Na nor Cl. The element C can be attributed to the PTFE membrane or carbonate salts. Additionally, the Ca in the scale was measured as 11 mol %, while S was 5 mol % being only 45% of the Ca value. The molar ratio of Ca^{2+} : SO_4^{2-} in raw SWRO brine is 1 : 2.7 (Table 3.1). However results here show that more than half of the Ca not associated with S, this indicates that the Ca related crystals on membrane surface possibly contain $CaCO_3$.

Table 4.1 EDS analysis results of the membrane surface (circled in Figure 4.5e) where experiment terminated at normalised flux of 9%.

Element	C	F	Na	Ca	Cl	S	O	Si
mol %	9	37	6	11	25	5	6	1

4.3 Behaviour of $CaCO_3$ scaling

Previous studies on alkaline scaling in DCMD batching experiments with synthetic supersaturated $CaCO_3$ solution reported that pH changed in brine feed could be associated with precipitation of $CaCO_3$ as described by Equations 2.1 and 2.2. Continuous pH monitoring of the brine feed in Figure 4.2 revealed that pH followed almost the same pattern as the normalised flux, where pH declined slightly in advance to flux decline. In Figure 4.2, brine feed pH gradually declined from 7.80 to 7.65 over the first 21 h of operation, followed by a dramatic drop over the next 2.5 h. The pH value then stabilised at 7.25 after 23 h of operation when normalised flux was at 10%. Titration analysis was conducted to investigate the behaviour of Ca^{2+} and HCO_3^- over 5 h where significant flux reduction occurred within this period.

Figure 4.6 shows the change in the key components in Equations 2.1 and 2.2 during the DCMD batch mode operation. During the first 21 h of operation, the process was governed by the slow dissociation of HCO_3^- due to heated feed brine and high HCO_3^-

concentration. The concentration of HCO_3^- and dissolved CO_2 was maintained in brine solution with only a small amount of CO_2 degassed from solution according to Equation 2.1. This explains the gradual pH decline in Figure 4.2. After 21 h of operation, severe concentration reductions for Ca^{2+} and HCO_3^- occurred indicating that $CaCO_3$ crystals precipitated from the supersaturated state (Figure 4.6, Figure 4.5b to d). According to Equations 2.1 and 2.2, rapid formation of $CaCO_3$ would result in a high HCO_3^- dissociation rate and thus rapid CO_3^{2-} and CO_2 production following. CO_2 generation was faster than the degassing rate. Therefore, it re-dissolved and reacted in water to become H_2CO_3 which reduced the pH of the feed solution between 21 to 23 h of operation (Figure 4.2). The pH then remained constant when the generation of CO_2 slowed after 23 h of operation and a constant level of H_2CO_3 remained in solution. It was also noticed that Ca^{2+} dropped 1 h after the sudden decrease of HCO_3^- (Figure 4.2). A possible explanation for this is that the size of $CaCO_3$ / $CaSO_4$ nuclei at early of crystallisation was small and therefore not effectively removed by 0.45 μm filter prior to titration test (Oh et al. 2009). During the period between 21 to 23 h of operation, the concentrations of Ca^{2+} and HCO^{3-} were reduced by 660 and 166 mg/L (as $CaCO_3$), respectively. According to Equation 2.1 and 2.2, besides $CaCO_3$ formation, there was still an additional 409 mg/L Ca^{2+} (as $CaCO_3$) reduction not associated with HCO_3^-. It is likely that $CaSO_4$ scale was also formed during this period. It is estimated that $CaSO_4$-$CaCO_3$ precipitates in the bulk brine solution contained 52 mol % of $CaSO_4$. Compared with the results shown in Table 4.1 where the molar ratio of S is 45% of the Ca value, 7 mol % of the precipitated $CaSO_4$ expected from MD feed solution over time hasn't been accounted for by the composition membrane scaling layer, possibly because part of $CaSO_4$ was precipitated at feed tank or still in suspension mode at bulk feed solution (Figure 4.4b) when experiment was terminated.

Overall, results in Figure 4.6 indicate that pH monitoring of the brine solution can be adopted to capture the early stages of membrane alkaline scaling.

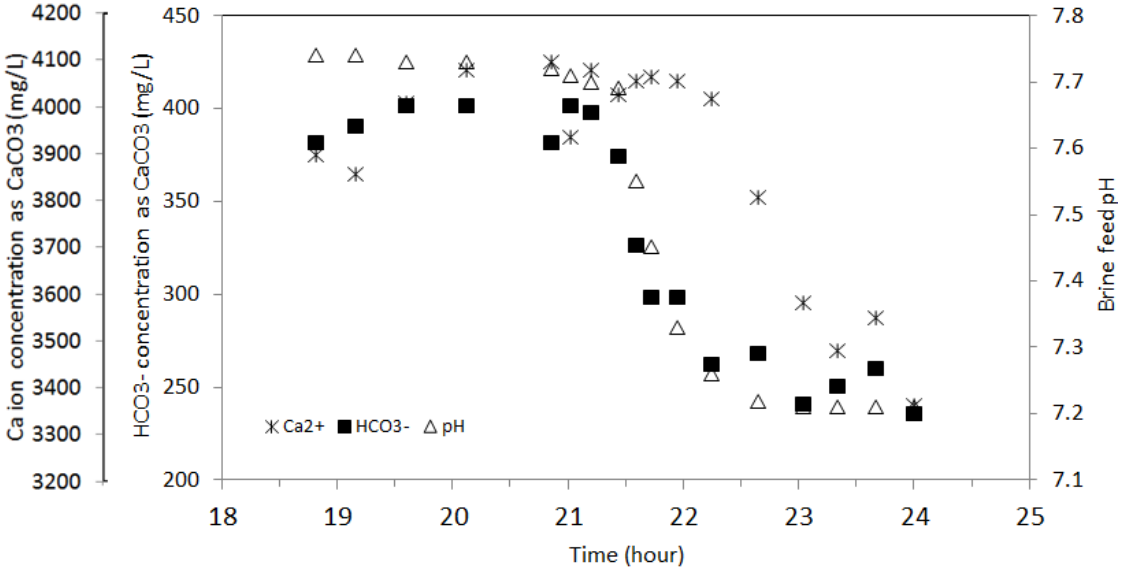

Figure 4.6 Behaviour of brine feed pH, HCO_3^- and Ca^{2+} as function of time for DCMD batch mode operation on SWRO brine. Experimental conditions: initial SWRO brine weight = 11 kg; T_f = 50 ˚C; T_d = 25 ˚C; Q_f = Q_d = 1000 ml/min (cross flow = 0.075 m/s); total run time = 24.3 h; cartridge filter was not used in the brine feed stream.

Figure 4.7 illustrates that the distillate EC and normalised flux as part of a separate run. EC always remained below 2.2 µS/cm prior to the dramatic flux reduction. The distillate EC increased to 5.8 µS/cm at the same time as the normalised flux declined from 85 to 60%. The change in EC could be due to accumulated CO_2 at bulk brine solution, which transported through the membrane and produced HCO_3^- on the distillate side as indicated by an EC rise. CO_2 in the distillate degassed quickly once the feed CO_2 was removed via Equation 2.2. He et al. (2009) studied $CaCO_3$ scaling with tap water feed during DCMD. It was reported that feed water pH reduction was associated with rapid CO_2 production and formation of $CaCO_3$. However, distillate pH behaviour was not monitored in that study. The dramatic flux decline in this run occurred in Figure 4.7 is 2 h earlier than results shown for the run in Figure 4.2. This is due to different batch of SWRO brines

used in experiments with slight deviation of EC (Table 4.1). In both experiments, rapid flux decline occurred at feed brine EC of approximately 160 mS/cm.

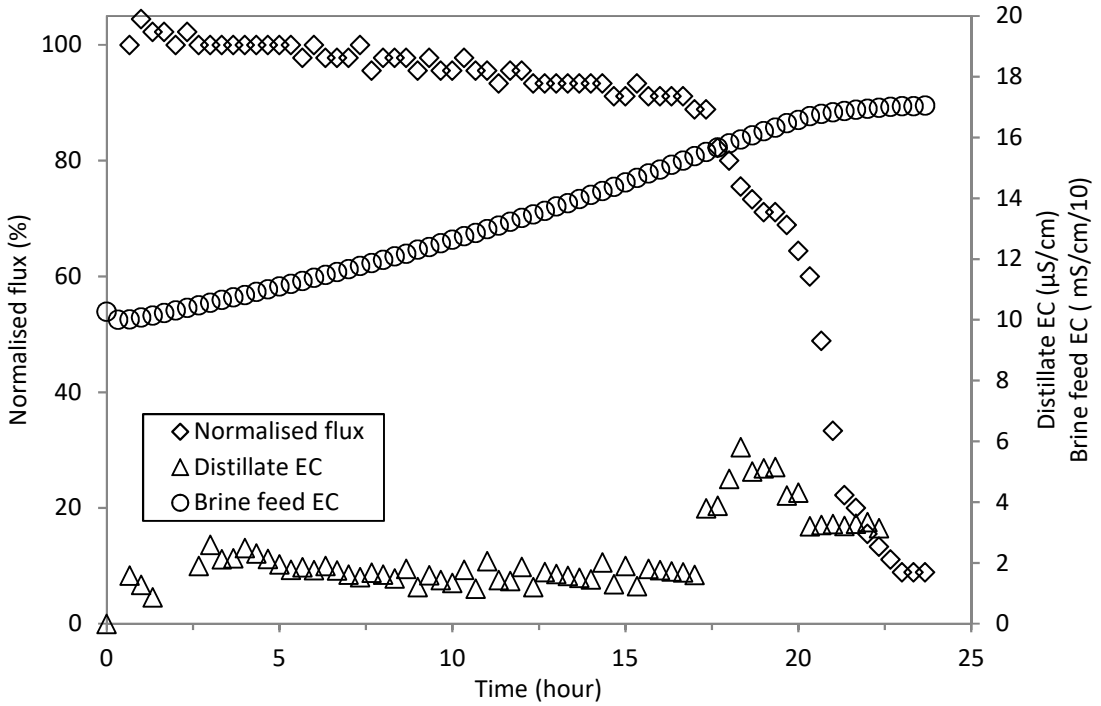

Figure 4.7 Behaviour of distillate EC, brine feed EC and normalised flux as function of time for DCMD batch mode operation on SWRO brine. Experimental conditions: initial SWRO brine weight = 11 kg; T_f = 50 °C; T_d = 25 °C; Q_f = Q_d = 1000 ml/min (cross flow rate = 0.075 m/s); total run time = 24.3 h; cartridge filter was not used in the brine feed stream.

4.4 DCMD continuous mode operation

DCMD was performed in continuous mode to simulate industrial conditions in which SWRO brine from RO processing is directly treated with MD where constant TDS conditions are present in the hot cycle. It was suspected that with long-term operation at supersaturated conditions, even with the existence of antiscalant, the salts dissolved in the hot feed solution may precipitate from the feed solution which could also have a significant influence on membrane wetting and flux reduction (Gryta 2008).

Stiff and Davis Stability Index (S&DSI) is often used for waters with ionic strength greater than 0.3 to predict potential calcium carbonate scaling. Antiscalant manufacturer's software Flodose (version 4.0 from BWA Water Additives) was used to calculate S&DSI using ASTM method D 4582–91. A negative S&DSI indicates that $CaCO_3$ tends to dissolve, while a positive S&DSI indicates that $CaCO_3$ tends to precipitate.

The SWRO brine was initially concentrated to 120 mS/cm under the batch mode at recovery and S&DSI of 35% and 1.24, respectively. MD brine was then used as hot feed solution for 50 h continuous mode operation. It was shown in Figure 4.8 that distillate EC reached 8 µS/cm at the end of batch mode operation. After 25 h of continuous mode operation, distillate EC stabilised at 1.5 µS/cm, which equated to the true distillate EC produced from the DCMD process. The gradual decline of distillate EC shown in Figure 4.8 was likely due to slow degassing of CO_2 as discussed in Chapter 4.3. The membrane therefore provided greater than 99.9% rejection of salt, and membrane pore wetting was not observed. It was also noted that distillate flux only had a minor reduction with increased operational time. Membrane flux achieved average of 24 $L/m^2 \cdot h$ between 20 to 26 h of operational time compared with average flux of 23 $L/m^2 \cdot h$ between 43 to 50 h of operation (Figure 4.8). Membrane surface SEM analysis was performed at the end of the experiment and micrographs are shown in Figure 4.9. Figure 4.9b at the wider scale indicates that the majority of membrane surfaces were free of crystal deposits. Higher magnification micrograph (Figure 4.9a) shows that small non-porous patches were formed on the membrane surface. This suggested that antiscalant at approximately 5.0 mg/L in 120 mS/cm brine was effectively keeping salts in a supersaturated condition over 50 h. As shown in Figure 4.2 and Figure 4.5, salt precipitation will occur when brine TDS concentration reaches a critical EC level of 160 mS/cm even in the presence of antiscalant.

These small non-porous patches could be explained by the adsorption of dissolved organic matters (e.g., protein, polysaccharide). Previous works have shown that the hydrophobic character of MD membranes enhance the adsorption of organic matter onto membrane surfaces (Gryta 2008; Hausmann et al. 2013). Proteins were found to be an important component in the buildup of fouling layer shown in studies on dairy solutions (Hausmann et al. 2013; Falini et al. 2009). It is suggested that possible organic fouling contributed to the flux decline for 120 mS/cm feed during continuous mode operation.

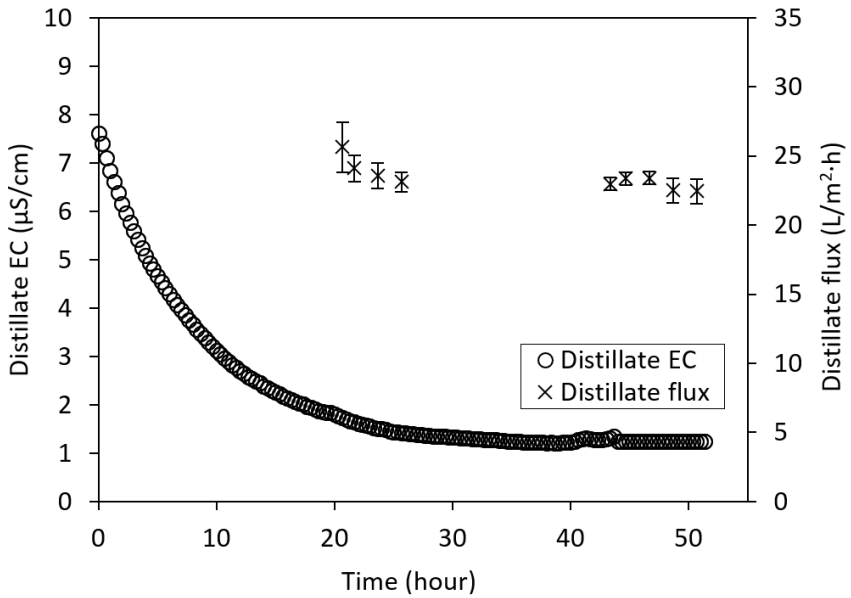

Figure 4.8 DCMD continuous mode operation on SWRO brine: behaviour of distillate conductivity and flux as a function of time. Experimental conditions: initial SWRO brine weight = 3 kg; T_f = 50 °C; T_d = 20 °C; Q_f = Q_d = 1000 ml/min (cross flow = 0.075 m/s); feed EC = 120 mS/cm; cartridge filter was not used in the brine feed. Error bar represents the standard deviation of replicate measurements (n = 3).

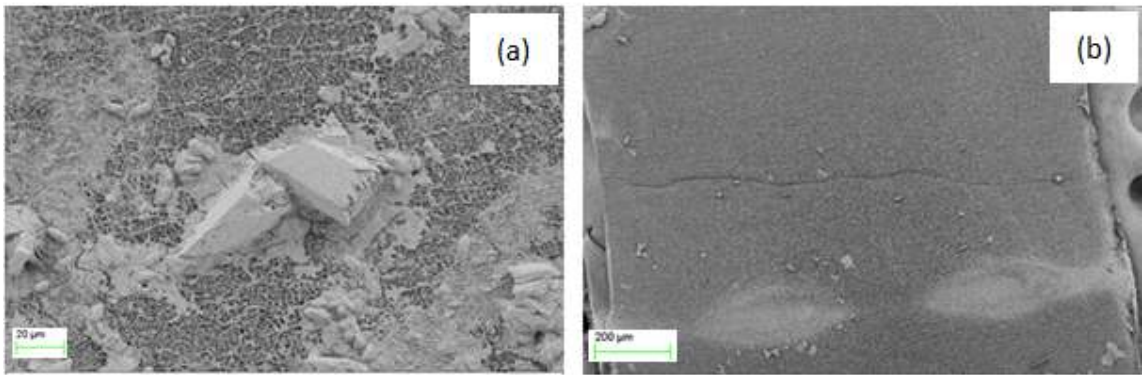

Figure 4.9 SEM micrographs of PTFE membrane surface. SEM micrographs (a) and (b) are for 120 mS/cm feed. Experimental conditions: initial SWRO brine weight = 3 kg; T_f = 50 °C; T_d = 20 °C; Q_f=Q_d = 1000 ml/min (cross flow = 0.075 m/s). cartridge filter was not used in the brine feed stream.

4.5 Mitigation of DCMD scaling

4.5.1 Effect of antiscalant to mitigate calcium salts precipitation

The batch and continuous test results demonstrated that antiscalants were participating in minimising scaling at higher salinities. Therefore it is of interest to explore the effect of antiscalant in more detail. Figure 4.10 shows the effect of antiscalant (Flocon 190) to mitigate the precipitation of calcium related salts for SWRO brine in a non-membrane beaker experiment at temperature of 50 °C with synthetic SWRO brine with a TDS concentration of 184 g/L equivalent to the brine solution at approximately 80% seawater recovery. Titration results shown in Figure 4.10 begin with 10 min after mixed salts were added to beakers. Figure 4.10a shows a solution without Flocon 190 added. Concentrations of HCO_3^- and Ca^{2+} rapidly decreased during the first 80 min of the beaker experiment, where pH followed the same pattern as HCO_3^-. This indicated that a significant amount of $CaCO_3$ was generated following Equation 2.1 and 2.2. The reduced pH was caused by the fast production of CO_2 by the rapid conversion of HCO_3^- following Equation 2.1 in the first 80 min. Following Equation 2.2, Ca^{2+} continued to decline from 100 min where HCO_3^- appeared stabilised leading to the precipitation of $CaCO_3$. This is in agreement with a previous study (Gryta 2007) that reported low $CaCO_3$ nucleation induction times once supersaturation conditions are reached. The precipitation of $CaCO_3$ could also form complexes with Mg^{2+}, as reduced concentration of Mg^{2+} in solution was observed. The pH was slightly raised towards the end of the experiment due to slower generation of CO_2 via Equation 2.1 which can be due to degassing of CO_2 from solution

or the progress of Equation 2.2 to form $CaCO_3$ since the decline of Ca^{2+} was also observed.

Figure 4.10b illustrates that with a Flocon 190 concentration of 10 mg/L, concentrations of HCO_3^- , Ca^{2+} and Mg^{2+} remained relative constant over 2 h of operation. The concentration of HCO_3^- slightly reduced from 795 to 782 mg/L during the test and CO_2 was generated according to Equation 2.1. When the saturation of dissolved CO_2 in solution was reached, CO_2 was degassed which favoured a slight increase of pH from 7.2 to 7.4 (Figure 4.10b). It appears that Flocon 190 is very effective at inhibiting the nucleation of calcium related sparingly soluble salts. Flocon 190 already contained in the SWRO brine helps to retard salt precipitation in DCMD experiments (Figure 4.2).

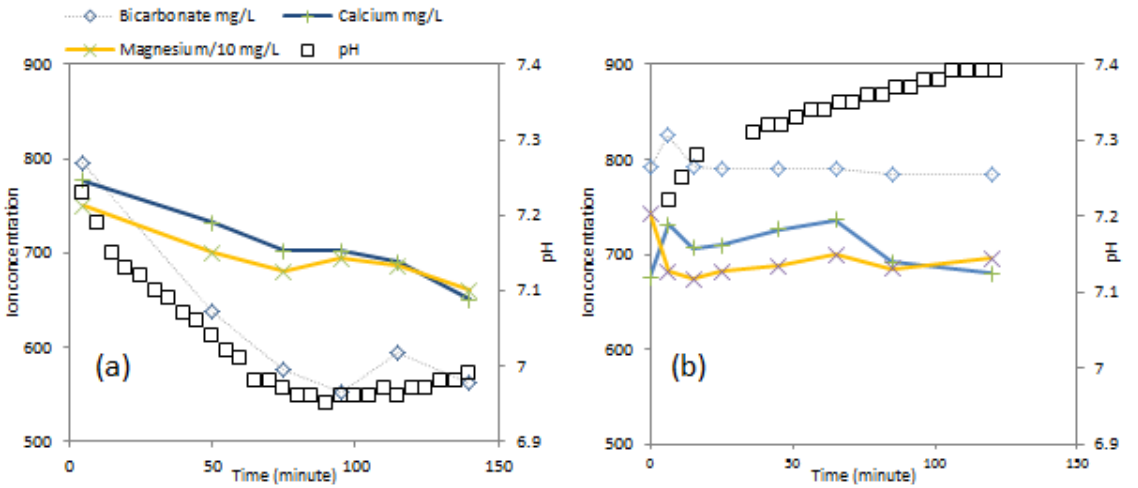

Figure 4.10 Behaviour of, pH, Ca^{2+}, HCO^{3-} and Mg^{2+} as function of time in beaker experiments: (a) without Flocon 190 (b) with Flocon 190 concentration of 10 mg/L. Experimental conditions: T = 50 °C; TDS = 184 g/L.

4.5.2 Addition of cartridge filter to mitigate MD scaling

MD testing in Figure 4.2 and Figure 4.5 show that scaling occurred at higher concentrations indicating coupling with a filter to remove precipitating salts will further improve water recovery potential. A 0.45 µm cartridge filter to capture soluble salts was

used in a batch mode experiment. The experiment was terminated after 27 h of operation at a normalised flux of 8.6% and brine EC of 191 mS/cm. The experiment achieved 60% water recovery of SWRO brine. The 'milky' color observed when no filter was used was not observed in the brine solution at the end of this experiment. In contrast, the experiment without the cartridge filter installed in Section 4.2 achieved 9% normalised flux when the brine EC and water recovery were 171 mS/cm and 45%, respectively. The cartridge filter appeared to effectively remove salt crystals, and significantly improved DCMD operational time and water recovery. The cartridge filter element was then removed from the filter housing and submerged into demineralised water overnight. ICP analysis was employed on the solution, and results are shown in Table 4.2. Results from ICP are in agreement with the membrane surface analysis in Table 4.1 that significant amounts of Ca and S related salts were formed. It indicated that the majority crystal deposits formed on the cartridge filter were $CaCO_3$ and $CaSO_4$. The molar proportion of S to Ca from the ICP results was 63%, indicating the majority of the scale in the filter was made of $CaSO_4$. Small amounts of Ba, K, Fe and Sr were also attached to $CaCO_3$-$CaSO_4$ and could have formed crystal complexes (Falini et al. 2009).

Table 4.2 ICP results of cartridge filter submerged solution.

Element	Ba	Ca	Fe	K	Mg	Na	S	Sr
mol %	0.0002	50	0.002	0.15	0.66	17	32	0.06

4.5.3 Effect of distillate water flushing

Results in Section 4.2 showed that loosely packed crystal deposits on the membrane at normalised flux of 56% (Figure 4.5). The membrane surface was covered by a thicker, more compact scaling layer when normalised flux declined to 9% (Figure 4.5e). Therefore, it is hypothesised that dissolution of crystal deposits on DCMD membrane by

an applied cleaning routine during the early stage of scaling could restore the membrane flux substantially. Figure 4.11 shows the normalised flux and EC before and after distillate water flushing. The experiment was stopped when the normalised flux reached 58.7%. Distillate with EC of 3.7 µS/cm was then circulated on the feed side of the module for 20 min to clean the membrane. Distillate flushing successfully restored membrane flux to 98% of the original flux value. After distillate flushing, the EC of permeate was 2.13 µS/cm during the following experiment which indicates the cleaning did not cause membrane wetting. Results from XRD analysis (Figure 4.12a and 4.12b) revealed that identical membrane surface characteristics of virgin membrane and membrane cleaned with distillate water, and crystal peaks disappeared below the detectable limits on membrane with distillate flushing. SEM images confirmed the formation of amorphous deposits on membrane surface before the clean (Figure 4.12c), while the entire membrane surface was almost free of deposits after distillate flushing (Figure 4.12d).

At the completion of this experiment, distillate was used to flush the brine feed side including heat exchange 316SS tube and cartridge filter. It was observed that white salt precipitates were carried to the MD module by flushing water, and large undissolved precipitates were trapped in the feed spacer. The feed side was then recirculated with NaOH and HCl solution (pH = 12 and 2, respectively), followed by a final distillate flushing. It was noticed that salt precipitates in the feed spacer were dissolved during chemical cleaning. The same readings of pH and EC at the brine feed inlet and outlet were obtained within 5 min of final distillate flushing at flowrate of 1000 ml/min. Compared with MD module cleaning, a separate cleaning loop and cleaning regime may be required for the MD pre-treatment system in order to optimise MD performance.

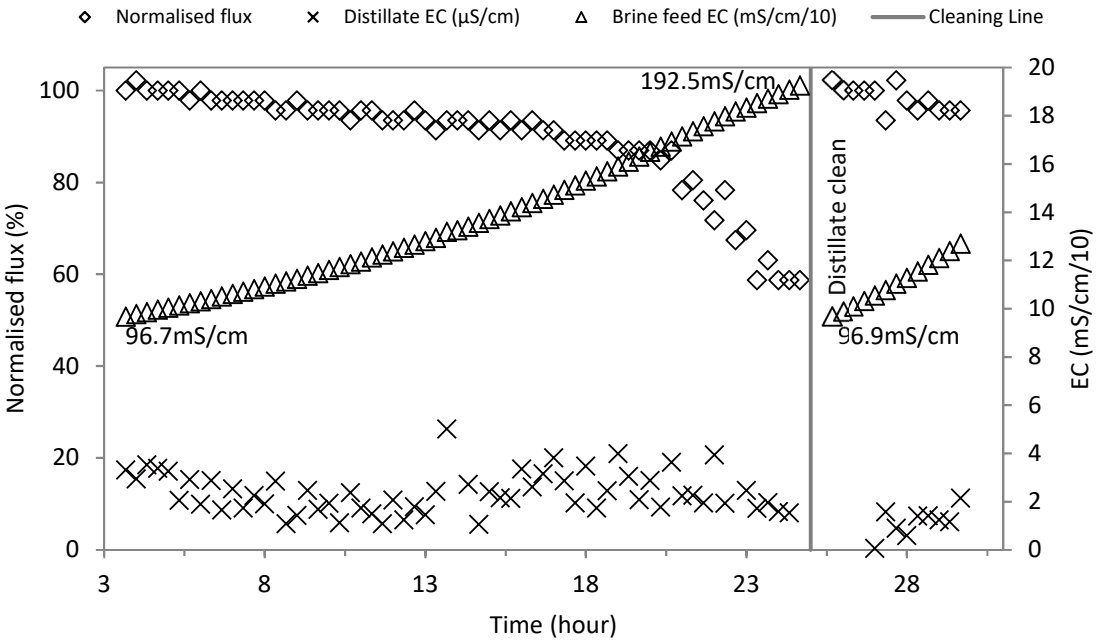

Figure 4.11 Normalised flux, distillate EC and corresponding brine feed EC at function of time with 0.45 µm cartridge filter installed. Distillate flushing after 25 h of operation. Experimental conditions: initial SWRO brine weight = 11 kg; T_f = 50 °C; T_d = 25 °C; Q_f = Q_d = 1000 ml/min (cross flow = 0.075 m/s).

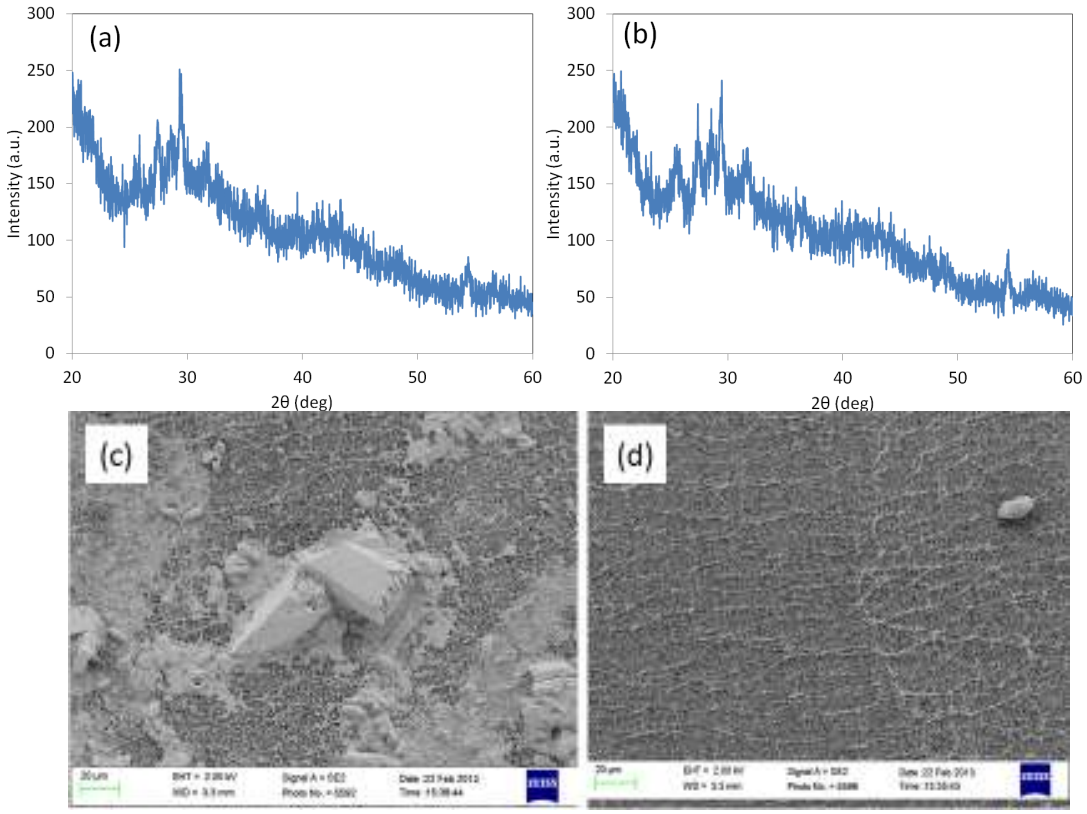

Figure 4.12 XRD analysis on PTFE membrane: (a) virgin membrane and (b) fouled PTFE membrane after distillate flushing, respectively. SEM imagines of PTFE membrane: (c) before distillate flushing and (d) after distillate flushing, respectively.

In another batch mode DCMD experiment where distillate flushing was conducted at normalised flux reached 60%. After the distillate flushing, the experiment was resumed with the same brine prior to the flushing at EC of 175 mS/cm. It can be seen in Figure 4.13 that distillate flushing restored normalised flux to 78%. However, flux decline occurred at the start of continuous mode operation, and it aggravated after 10 h when there was a sudden increase of distillate EC (Figure 4.13). The experiment was terminated after 13 h of continuous mode operation when distillate ceased production while brine and distillate EC reached 235 and 6 mS/cm, respectively. Distillate flushing was performed again at the end of this test. During flushing, it was noticed that crystalline deposits on membrane surface were removed, while several small patches on membrane surface turned clear so that the PP scrim could be seen, and this was a sign of membrane wetting phenomena. It was speculated that massive precipitation of salts particularly needle-shaped $CaSO_4$ possibly penetrated into the pore interior resulting in a damage of the membrane and membrane wetting (Gryta 2008; Yu et al. 2013).

Results present in Figure 4.11 and Figure 4.13 suggest that operating SWRO brine at moderate water recovery (prior to drastic salt precipitation) can mitigate the risk of membrane wetting. It is worth noting that distillate flushing could dissolve $CaCO_3$ which formed inside membrane pores, and accelerate membrane wetting process (Gryta 2008). The impact of distillate flushing in SWRO brine treatment over long-term operation requires further investigation.

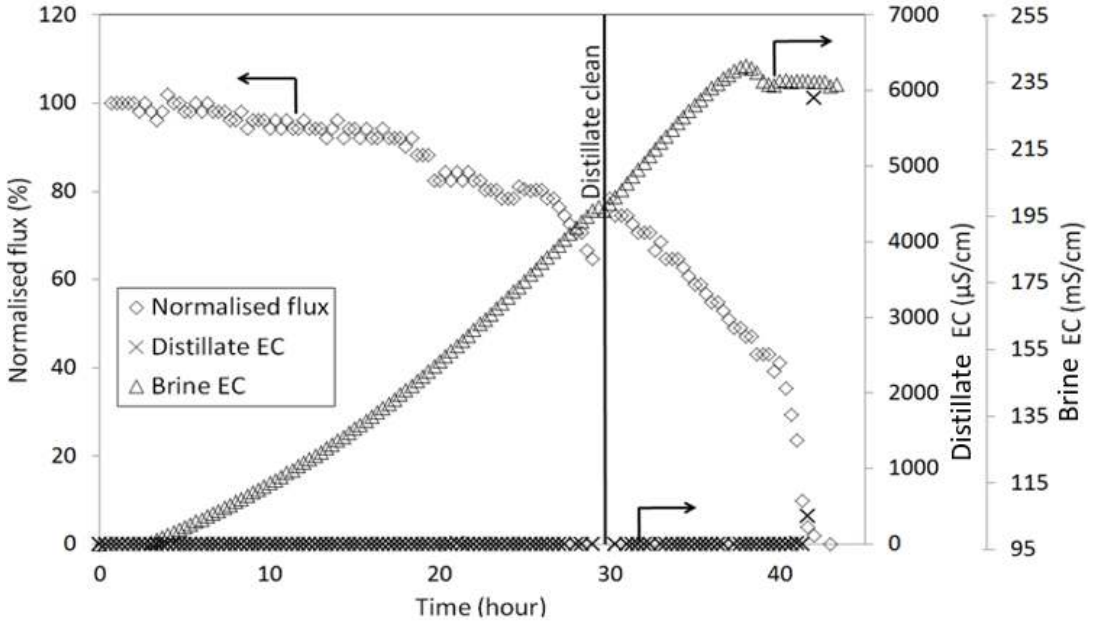

Figure 4.13 Normalised flux, distillate EC and brine EC at function of time with 0.45 µm cartridge filter installed. Distillate flushing after 28 h of operation, and experiment resumed with the same brine post flushing.

4.5.4 SWRO brine flushing

It was expected that intermittent membrane flushing with raw SWRO brine could also achieve a level of crystal deposit removal, and it was likely to minimise the consumption of valuable distillate product in industrial applications. The batch mode experiment was carried out until normalised flux reached approximately 55% and a water recovery of 50%. Then, the experiment was stopped and 4 L of raw SWRO brine (90 mS/cm) was introduced to the DCMD module at a flowrate of 1,000 ml/min and 30 min of recirculation at ambient temperature. The brine feed side and feed container were drained and re-filled with raw SWRO brine for the next run. The overall experiment was terminated after 133 h of operation. Data loggers were interrupted by the failure of the local internet network connection during the 3rd and 4th batch, but the experiment still continued and was valid. Figure 4.14 shows the normalised flux at the beginning of each run following SWRO brine flushing gradually declined from 100 to 84.4%. While

restoring performance was significant, over time it became less effective. The projected results from antiscalant software showed that $CaSO_4$ SI in SWRO brine was 36%. SI of $CaSO_4$ was calculated by Flodose ASTM method 4692–87. SI is defined as the Ion Product (IP) for the scale forming species divided by the calculated solubility constant (Ksp) for the species. SI greater than 100% indicates tendency for precipitation of salt, while SI less than 100% indicates salt tends to dissolve. $CaSO_4$ SI less than 100% indicate less tendency for precipitation of $CaSO_4$. This explains the effectiveness of brine flushing where $CaSO_4$ precipitates could be partially dissolved by the brine solution. Results indicated that crystal deposits were not removed completely by SWRO brine flush. The residual crystal deposits on the membrane after each flushing could potentially act as nucleation sites for sparingly soluble salts to accelerate salt crystallisation in the following batch. Multiple raw SWRO brine flushing did not cause membrane pore wetting and the product EC was less than 8 μS/cm. In comparison with virgin membrane surface (Figure 4.15b), Figure 4.15a revealed that small size crystals existed on the membrane surface after brine cleaning at the beginning of 6^{th} batch. The crystal layer was more compact and therefore contributed to flux resistance. Larger salt crystals are likely to be developed on those nucleation sites with continuous operation. From this work, it seems that distillate flushing is better at reversing scaling, but to reduce wasting distillate a SWRO brine flushing can be performed more often to also clean the membrane. A cleaning program of regular SWRO brine cleans and occasional distillate water clean could conserve the consumption of distillate water while maintaining high flux performance.

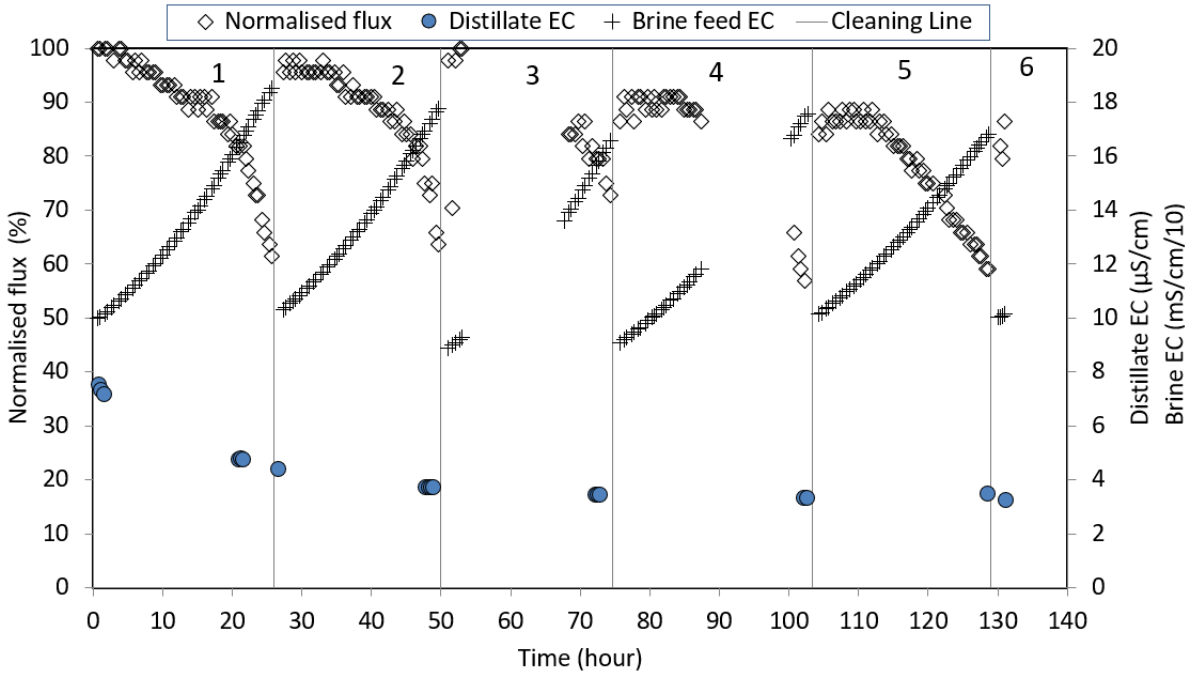

Figure 4.14 Normalised flux, distillate EC and corresponding brine feed EC at function of time with 0.45 µm cartridge filter installed. Raw SWRO brine flushing conducted at normalised flux of 55%. Experimental conditions: initial SWRO brine weight = 11 kg; T_f = 50 ˚C; T_d = 25 ˚C; Q_f = Q_d = 1,000 ml/min.

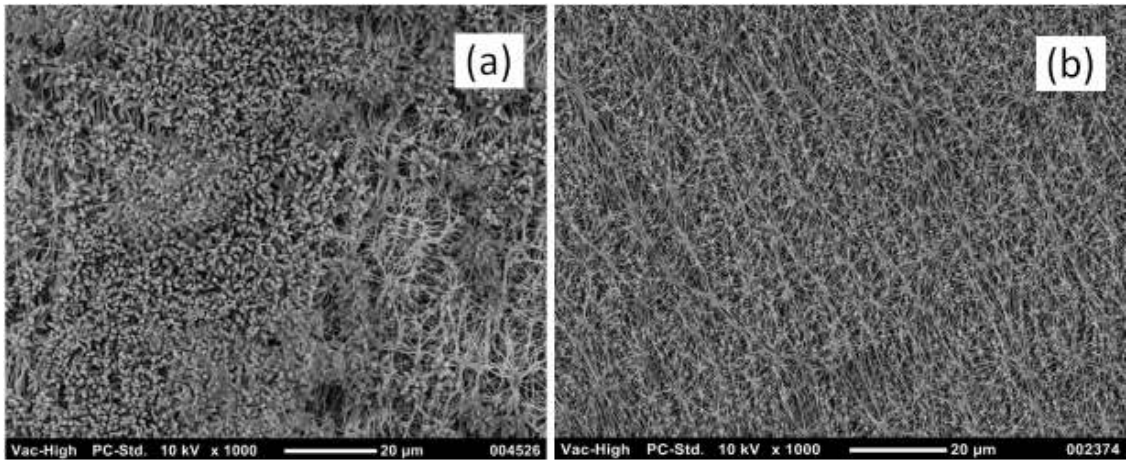

Figure 4.15 SEM micrographs of membrane surface (a) at end of experiment post SWRO brine flushing and (b) virgin membrane. Experimental conditions: initial SWRO brine weight = 11 kg; T_f = 50 °C; T_d = 25 °C; Q_f = Q_d = 1,000 ml/min (cross flow = 0.075 m/s).

4.6 Conclusion

This study investigated the SWRO brine minimisation at bench scale DCMD process.

Results demonstrated that MD is a technically viable technology for concentrating SWRO

brine up to EC = 160 mS/cm with < 20% flux drop (average flux above 20 L/m^2·h) and no requirement of pre-treatment. Commercial SWRO antiscalant was attributed to reduced scaling of calcium related salts in MD in the supersaturated conditions. Negligible flux decline was noticed when operating continuous mode DCMD at brine EC = 120 mS/cm for 50 h at antiscalant concentration about 5 mg/L.

Scaling study revealed that distillate flux reduction was mainly caused by precipitation of $CaCO_3$ and $CaSO_4$ under supersaturation conditions in the bulk brine solution. Even with the existence of antiscalant, the kinetics of $CaCO_3$ and $CaSO_4$ crystallisation were fast once brine TDS concentration reached a critical level. The rapid deposition of $CaCO_3$ and $CaSO_4$ formed a thick and highly compacted scaling layer which dramatically reduced the normalised flux to < 10% within 4 h of operation. It was also noticed that the precipitation of calcium salts was correlated to the pH variation in brine solution; therefore, industry could adopt brine pH monitoring as an early indicator of rapid flux decline.

In terms of managing MD fouling in SWRO brine treatment, in-line cartridge filtration can effectively remove salt crystals formed in brine solution and improve DCMD operational time and water recovery. In addition, membrane flushing with distillate water and raw SWRO brine restored distillate flux where distillate flushing showed near-complete restoration of original flux conditions. However, organic fouling showed resistance to non-chemical flushing. Antiscalant at about 7 mg/L (50% brine recovery) did not cause membrane wetting over long-term MD operation. However, the un-managed severe salt precipitation showed strong tendency to cause membrane wetting.

Overall, this study showed that homogeneous nucleation was the predominate mechanism that led to membrane scaling by $CaCO_3$ and $CaSO_4$ when TDS concentration at RO brine reached a critical EC level. On the other hand, membrane surface was free of crystal deposits while operating MD below the critical EC level over 50 h. Therefore, it is a key for industry to determine the critical brine EC level via bench scale / pilot study when concentrating RO brine that has high scaling potential for $CaCO_3$ and $CaSO_4$. This study also showed that by managing cleaning before the onset of severe precipitation on the membrane, wetting can be avoided and distillate EC remains low (e.g., < 5 μS/cm). Therefore, industry can adopt the cleaning regime consisting of distillate and RO brine flushing of the MD membrane to minimise the chemical cleaning frequency and chemical consumption.

Following the test of SWRO brine, the results present in Chapter 5 are related to a CSG RO brine treatment using DCMD process where the kinetics of silica fouling was the primary research goal in this test.

Chapter 5 DCMD of CSG RO brine

In this test, DCMD performance and membrane fouling were assessed over a relative long period of operation for concentrating CSG RO brine (Table 3.2). The influence of divalent cations (Mg^{2+} and Ca^{2+}), anions (HCO_3^- / CO_3^{2-} and Cl^-) and temperature on silica fouling were examined individually. Thermodynamic software Phreeqc–3 was chosen to calculate the SI of inorganic salts particularly metal silicates in bulk brine solution and thereby predict the likelihood of particulates fouling in MD. Moreover, the efficiencies of MD silica fouling control using commercial RO antiscalants and Na_2EDTA were assessed.

5.1 DCMD batch mode operation on CSG RO brine

Results of batch mode DCMD with CSG RO brine are shown in Figure 5.1. In this test, a 5 µm cartridge filter was installed in the brine feed stream. The experiment was terminated after 150 h of operation at brine EC of 85 mS/cm and brine recovery of 90% (overall recovery of 95%). A total of 72 L CSG RO brine was processed in this experiment. The RO–DCMD hybrid process obtained 152 L product water from 160 L CSG produced water. It is shown in Figure 5.1, DCMD obtained initial distillate flux of 21.0 $L/m^2 \cdot h$, as overall recovery reached 88%, both bulk brine water activity and distillate flux reduced by 3%, reflecting a similar decrease in the bulk brine partial vapour pressure (Equation 3.5 and 3.6). This suggests that distillate flux decline was mainly attributed to the reduced partial pressure of water in brine due to increased molar fraction of salts. Thereafter, distillate flux deviated from water activity and declined by 13% and reached 18.3 $L/m^2 \cdot h$ at the end of experiment (Figure 5.1) with water molar fraction decreasing by 2%. As shown in Figure 4.3, NaCl solution viscosity increases approximately 3% from

TDS of 5 wt.% to 10 wt.% at 50 °C (MaCain 1990), distillate flux decline here could be linked to the increased brine viscosity which aggravated concentration and temperature polarisations at the membrane surface. Additionally, membrane scaling by salt supersaturation at higher recovery could contribute to flux losses.

It is noteworthy that at the beginning of the experiment, brine pH reduced along with increased distillate EC, and maximum distillate flux at 21.5 $L/m^2 \cdot h$ occurred at 5 h of operation (Figure 5.1). This was mainly due to high dissociation rate of HCO_3^- to CO_2 ($2HCO_3^- \leftrightarrow CO_3^{2-} + CO_2 + H_2O$) in brine when the brine was heated. CO_2 from brine travelled to the distillate side through membrane pores and subsequently increased distillate EC. The fast degassing rate of CO_2 at the beginning of experiment through the membrane pores also competed with water vapour, thus, reducing the distillate production rate and delayed the occurrence of maximum distillate flux. Similar behaviours were reported by Duong et al. (2015). As can be seen in Figure 5.1, distillate EC slightly increased after 125 h of operation along with distillate flux and brine pH decline. The increased distillate EC was speculated due to the formation of magnesium silicates, and this is further discussed in Section 5.2.1. The formation of magnesium silicates corresponds to brine pH decline due to OH^- reacting with Mg^{2+} and dissolved silica. The reduction of OH^- also led to hydrolysis of CO_3^{2-} and CO_2 production ($CO_3^{2-} + H_2O \leftrightarrow 2OH^- + CO_2$), and subsequently increased distillate EC.

Phreeqc–3 thermodynamic calculations revealed possible salts that supersaturated in brine solution at 90% overall recovery and 50 ˚C, namely talc ($Mg_3Si_4O_{10}(OH)_2$, SI = 10.3), quartz (SiO_2, SI =1.1), dolomite ($CaMg(CO_3)_2$, SI =4.4), chrysotile ($Mg_3Si_2O_5(OH)_4$, SI = 4.7), calcite ($CaCO_3$, SI = 4.7) and aragonite ($CaCO_3$, SI = 1.7). At

high SI, the induction period of salt nucleation can be significantly reduced, and will have an influence on the risk of membrane scaling. Quartz is a form of crystalline silica, and it has over 10 times lower solubility than amorphous silica. Iler (1979) has shown that formation of quartz in solution is kinetically unfavourable, and suggested that whatever the origin of silica in water, it initially precipitates as amorphous silica or silicates, following which amorphous silica undergoes a very slow kinetic process to form crystalline silica. Therefore, the formation of quartz was unlikely during this test. SEM analysis of the brine side of the membrane was performed and results are shown in Figure 5.2. Figure 5.2a at the wider scale shows the membrane surface was mostly free of deposits. Higher magnification (Figure 5.2b) shows amorphous deposits on the membrane surface with the majority of deposits having particle sizes of about 1 μm, so those precipitates would not be expected to be removed by the 5 μm cartridge filter installed in the brine cycle if they existed in bulk brine. EDS analysis on Figure 5.2b indicated the presence of C, O, Mg, Ca, Si, and Na, suggesting the possible foulants were magnesium / calcium silicates and $CaCO_3$. The presence of Na could be due to NaCl formation among the other salts on the membrane surface during drying out of the membranes where NaCl could be trapped inside other foulants or just simply inside wetted pores (Nguyen and Lee 2015).

Overall, this experiment demonstrated that CSG produced water can be treated with DCMD over a relative long period of operation at overall recovery above 90% and without significant flux decline, and with EC rejection above 99.9%. This could be attributed to CSG produced water consisting of low hardness but being rich in $NaHCO_3$ / Na_2CO_3 and NaCl. A series of experiments were conducted on synthetic solutions to understand interactions of dissolved silica, Mg^{2+} and Ca^{2+} in DCMD process.

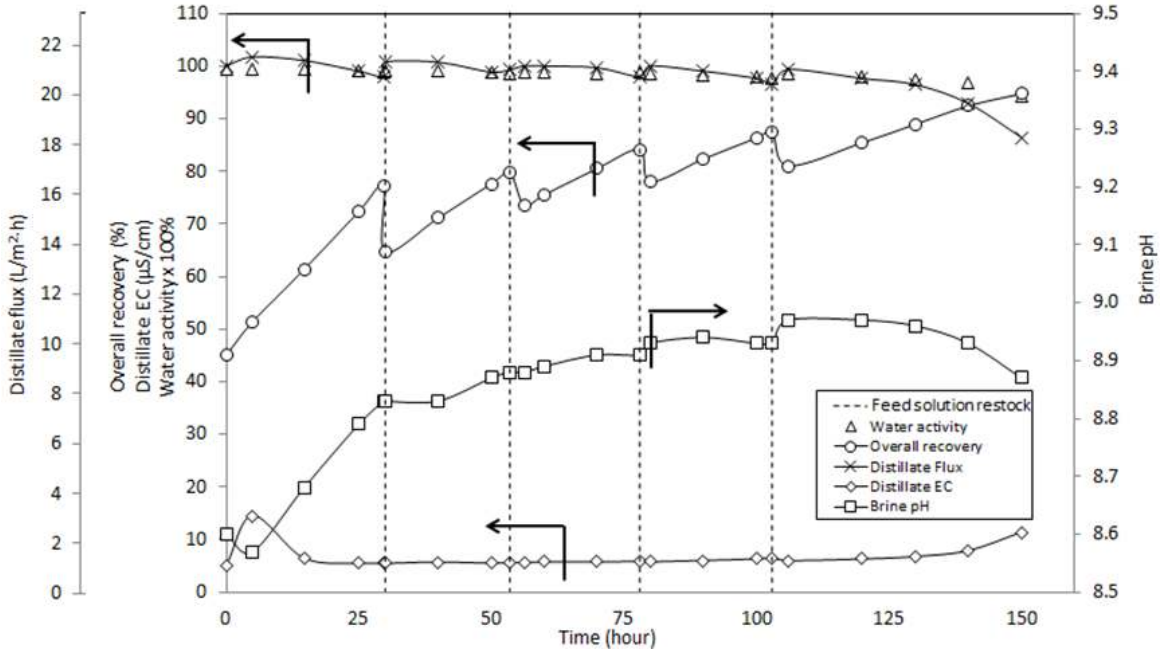

Figure 5.1 DCMD batch mode operation on CSG RO brine. Behaviour of distillate EC, overall recovery, brine pH and distillate flux and brine water activity as function of time.

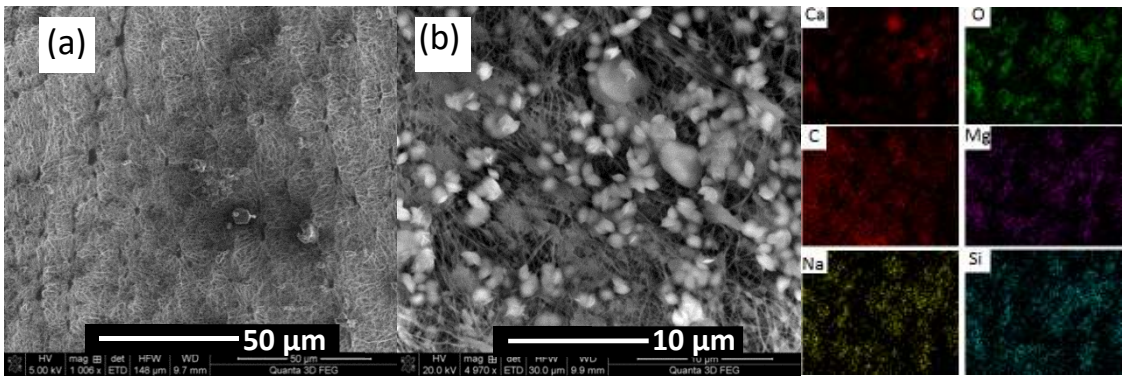

Figure 5.2 SEM micrographs and EDS analysis results of PTFE membrane surface (b) at the end of DCMD batch mode operation on CSG RO brine.

5.2 DCMD on synthetic CSG RO brines

5.2.1 Effect of Ca^{2+} and Mg^{2+} on DCMD silica fouling

Results of batch mode DCMD on 7.2 L synthetic CSG RO brine Mg4.3 (Table 3.5) are shown in Figure 5.3. In this test, the brine feed cartridge filter was not installed. The experiment was terminated at an overall recovery of 91% and the brine EC was 82 mS/cm. Distillate EC was below 15 µS/cm throughout the experiment. It can be seen from Figure

5.3 that distillate flux had a moderate drop prior to the overall recovery of 88%. Thereafter, distillate flux declined more rapidly and it reached 18.6 L/m^2·h at the end of experiment. Compared with Figure 5.1 where real CSG RO was adopted, this single batch experiment with synthetic brine showed a good degree of reproducibility to real CSG RO brine in DCMD process, and single batch operation was adopted in subsequent experiment.

ICP–AES analysis was conducted on brine water samples taken during the experiment. As it is shown in Figure 5.4, Ca^{2+} concentration decreased significantly compared to the theoretical concentration from mass balance, while dissolved silica and Mg^{2+} did not deviate from theoretical concentrations for 100% rejection of the ions with no precipitation. Results suggest that the kinetics of $CaCO_3$ formation was fast in brine. However, the rapid formation of $CaCO_3$ did not co-precipitate with dissolved silica. The mechanisms of dissolved silica co-precipitation with magnesium and calcium have not been clearly described in previous research, but it is generally considered that dissolved silica removal efficiency by $CaCO_3$ or calcium silicate is negligible compared to the removal by magnesium (Latour et al. 2014). The absence of magnesium silicate formation (Figure 5.4) contradicts the Phreeqc–3 thermodynamic calculations that indicated significant precipitation of magnesium silicates would occur at high SI (Section 5.1). A possible explanation is that high Na^+ concentration in MD brine acted as a stabilising agent that created a binding layer around dissolved silica, therefore, preventing dissolved silica from reacting with Mg^{2+} and OH^- (Lunevich et al. 2016).

To further investigate magnesium silicate precipitation kinetics, a subsequent experiment was conducted on brine solution Mg30 (Table 3.5). Batch mode DCMD was operated to

80% brine recovery followed by 24 h continuous mode operation. Magnesium, calcium and dissolved silica are presented here as wt.% which is defined below:

$$\text{wt.}\,\% = \frac{\text{wt}_\text{i}}{\text{wt}_\text{io}} \times 100\% \quad (5.1)$$

Where wt_i is total weight (mg) of the particular species (e.g., Mg^{2+}) in brine which was calculated by mass balance according to results of ICP–AES, and wt_io is total weight (mg) of the species in the initial synthetic CSG RO brine.

It can be seen in Figure 5.5a, both Mg^{2+} and dissolved silica started to deviate from 100 wt.% at Mg^{2+} concentration of 45 mg/L, suggested the formation of magnesium silicate. Mg^{2+} and dissolved silica reduced to about 90 wt.% at the end of batch mode operation followed by a slight decline during continuous mode operation. On the other hand, over 90 wt.% of Ca^{2+} was depleted during the first 10 h of operation (Figure 5.5a). As it is shown in Figure 5.5b, SEM analysis shows amorphous deposits on the membrane surface, and EDS analysis revealed that the stoichiometric ratio of silicon to magnesium was about 1 : 1, suggesting the formation of magnesium silicate compounds ($Mg_3Si_4O_{10}(OH)_2$, $Mg_3Si_2O_5(OH)_4$) as predicted by Phreeqc–3 calculations (Section 5.1).

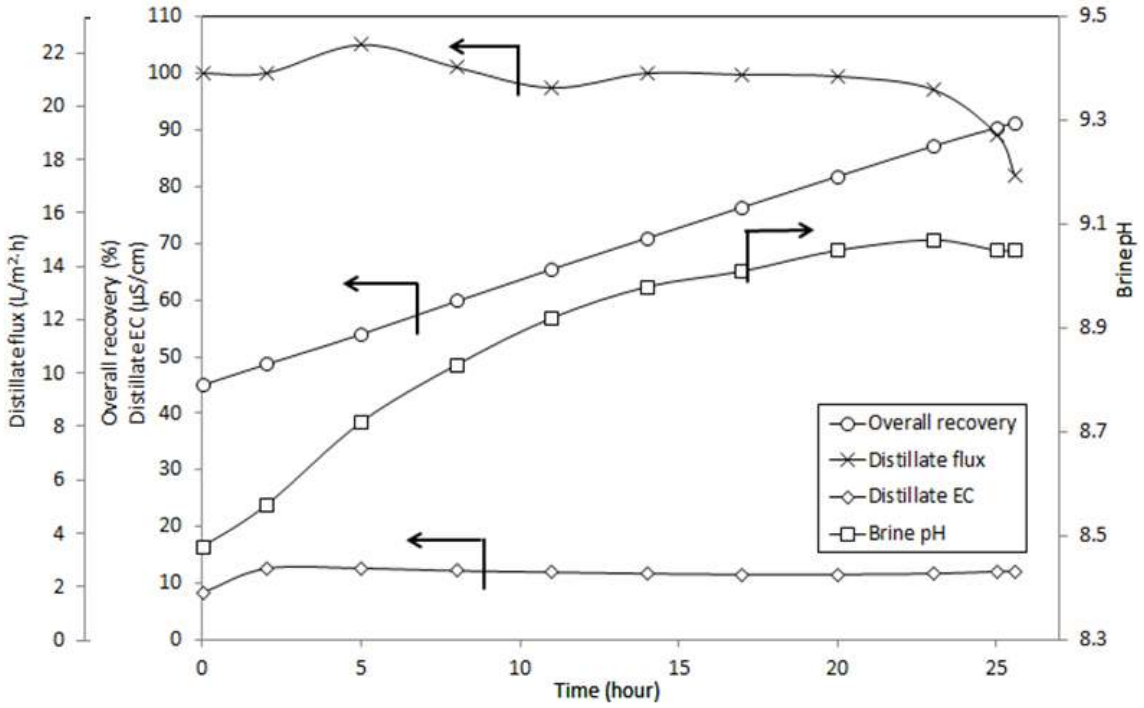

Figure 5.3 Behaviour of distillate EC, overall recovery, brine pH and distillate flux as function of time. DCMD batch mode operation on synthetic CSG RO brine Mg4.3.

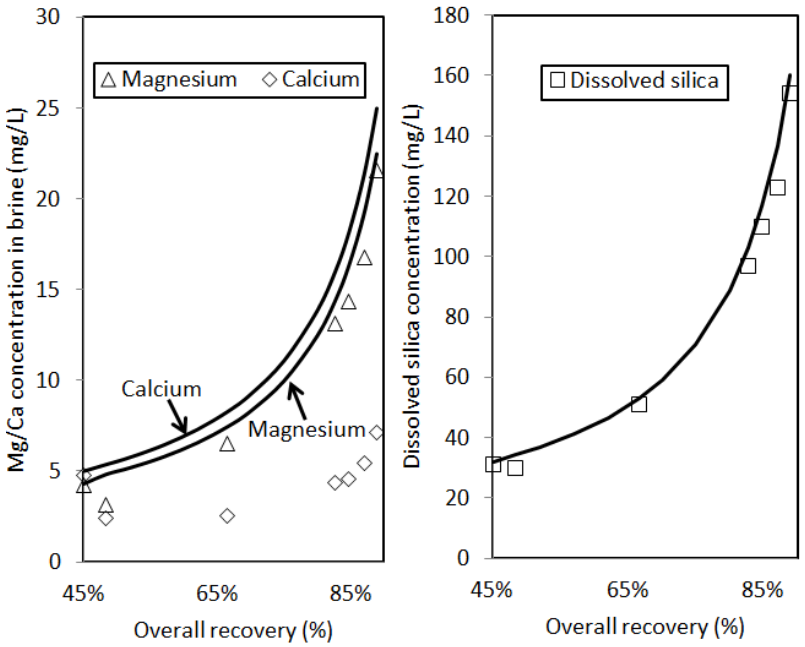

Figure 5.4 ICP–AES measured concentrations of dissolved silica, Mg^{2+} and Ca^{2+} in brine as a function of overall recovery. Solid lines represent theoretical concentrations of dissolved silica, Mg^{2+} and Ca^{2+} assuming 100% rejection and no precipitation.

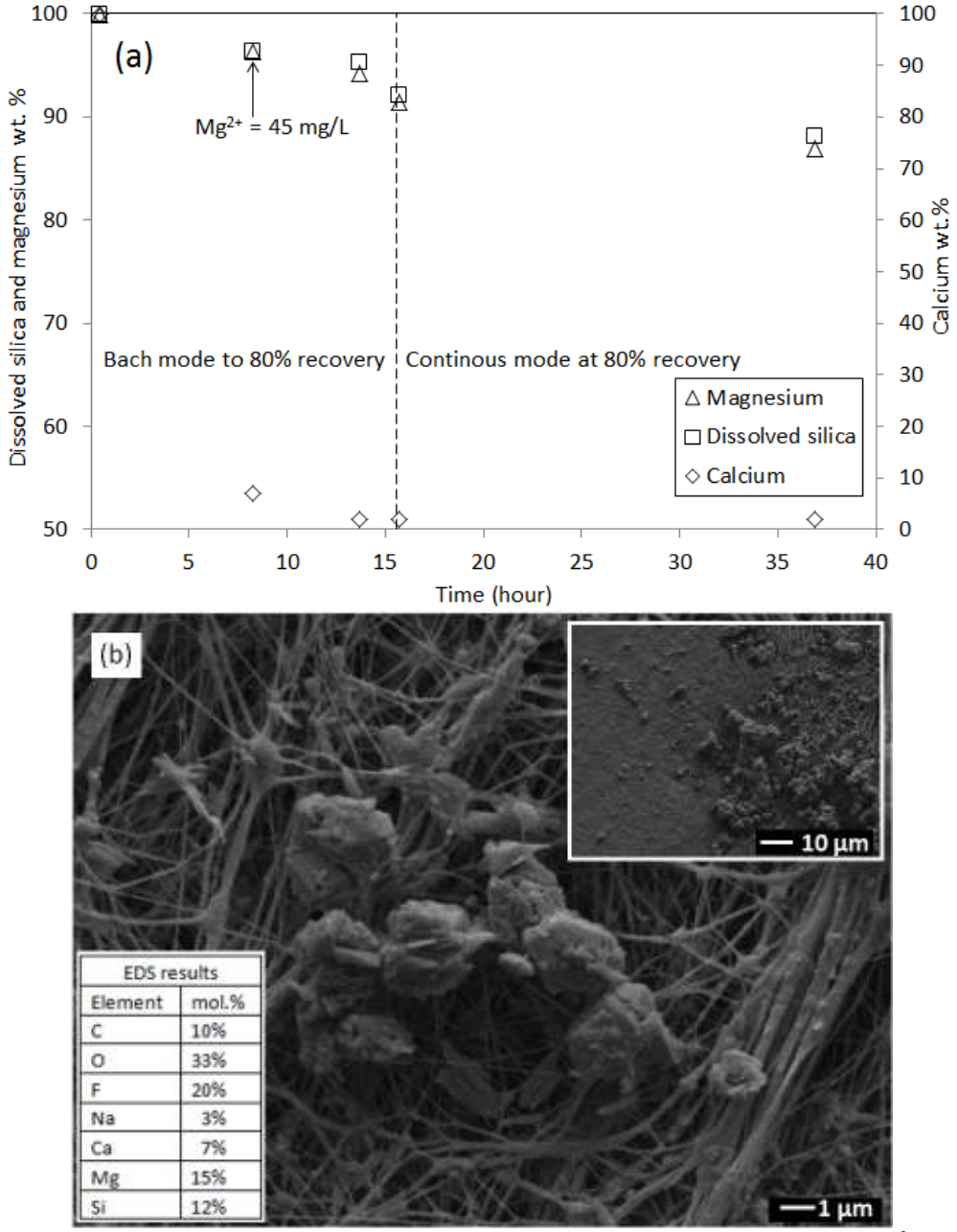

Figure 5.5 DCMD on synthetic CSG RO brine Mg30. a) wt.% of dissolved silica, Mg^{2+} and Ca^{2+} in brine as a function of time. b) SEM–EDS analysis of membrane surface.

5.2.2 Effect of $NaHCO_3$ / Na_2CO_3 and NaCl on DCMD polymerised silica fouling

Synthetic brine solutions NaCl0M and NaCl0.1M described in Table 3.6 were used in these tests. Batch mode DCMD was operated to 80% brine recovery followed by 35 h continuous mode operation. It can be seen in Figure 5.6a, both solutions demonstrated the same normalised flux trend in batch mode operation with distillate ECs less than 5 µS/cm.

However, significant flux decline and exponential distillate EC increase occurred in continuous mode operation for both solutions (Figure 5.6a). During this period, the PTFE membrane particularly the areas near the hot brine outlets turned clear so that the PP scrim support could be seen as indicative of membrane wetting phenomena (Figure 5.7), possibly due to precipitation of colloidal amorphous silica. As this experiment only had about 0.5% of feed water evaporated along the DCMD module during a single pass, concentration polarisation influence at the membrane surface was considered negligible. It was speculated that colloidal amorphous silica first reached supersaturation near the hot brine outlet due to the bulk brine temperature being the lowest at this point. Silica oligomers (e.g., 3–4 nm diameters) (Bergna and Roberts. 2005) could deposit inside the membrane pores, and encourage further silica polymerisation deeper into the pores and potentially lead to membrane wetting. Gilron et al. (2013) also reported that colloidal amorphous silica nanoparticles could not be effectively removed by a 0.2 μm in-line filter in a MD study. It can be seen in Figure 5.8, the colloidal amorphous silica precipitated and ultimately polymerised to a non-porous layer on the membrane surface. The fouling mechanisms of colloidal amorphous silica in DCMD process are illustrated in Figure 5.9. It is shown in Figure 5.6b, at the end of batch mode operation, dissolved silica concentration in solution NaCl0M and NaCl0.1M peaked at 588 and 524 mg/L, respectively. Then, dissolved silica concentrations rapidly declined and reached relatively stable states after 14 h continuous mode operation. This behaviour was described by Lunevich et al. (2016) as “pseudo-solubility” state due to the relatively fast increase in dissolved silica concentration for brine with insufficient time for dissolved silica to precipitate. At the end of experiment, dissolved silica concentration in solution NaCl0M and NaCl0.1M reached 370 and 328 mg/L, respectively (Figure 5.6b). Compared with

solution NaCl0.1M that had equal molar concentration of HCO_3^- and Cl^-, higher dissolved silica concentration in solution NaCl0M (higher HCO_3^- and no Cl^-) demonstrated less deterioration of both normalised flux and distillate EC (Figure 5.6a). These results suggest that HCO_3^- / CO_3^{2-} has greater ability to stabilise silica in dissolved form compared with Cl^-. This could be attributed to the formation of salt complex between orthosilicic acid and HCO_3^- / CO_3^{2-} as theorised by Marshall and Warakomski (1980). However, it is worth noting that dissolved CO_2 from hydrolysis of CO_3^{2-}, and the additional (< 3%) Na^+ and Cl^- introduced in brine NaCl0M via solution pH control could have detrimental influence on silica solubility. Further research is needed to understand the interactions between HCO_3^- / CO_3^{2-} and dissolved silica.

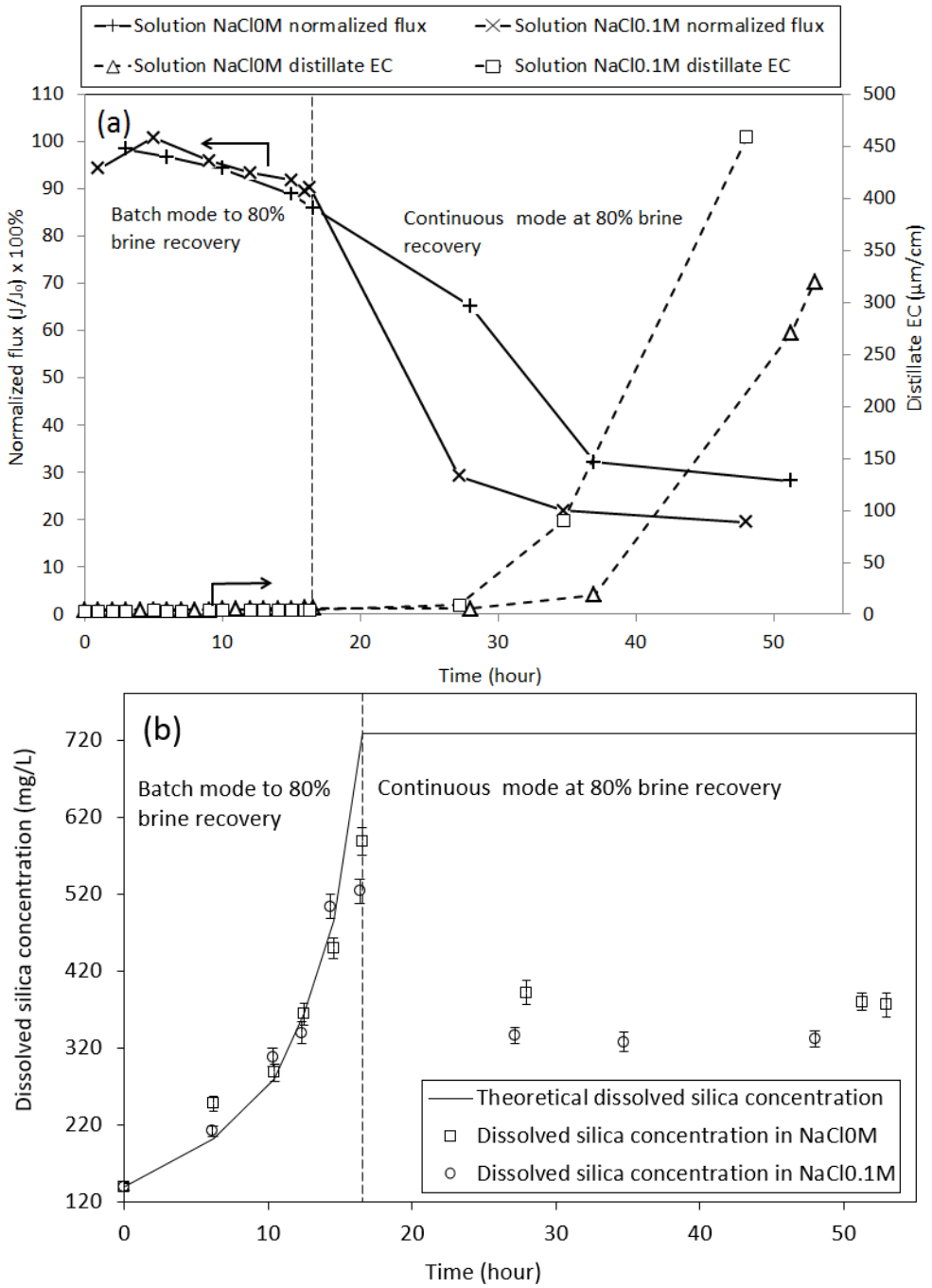

Figure 5.6 DCMD on hardness-free synthetic CSG RO brines listed in Table 3.6. a) Behaviour of distillate EC and normalised flux as function of time. b) Behaviour of dissolved silica concentrations in brine as function of time. Error bar represents the standard deviation of replicate measurements (n = 3).

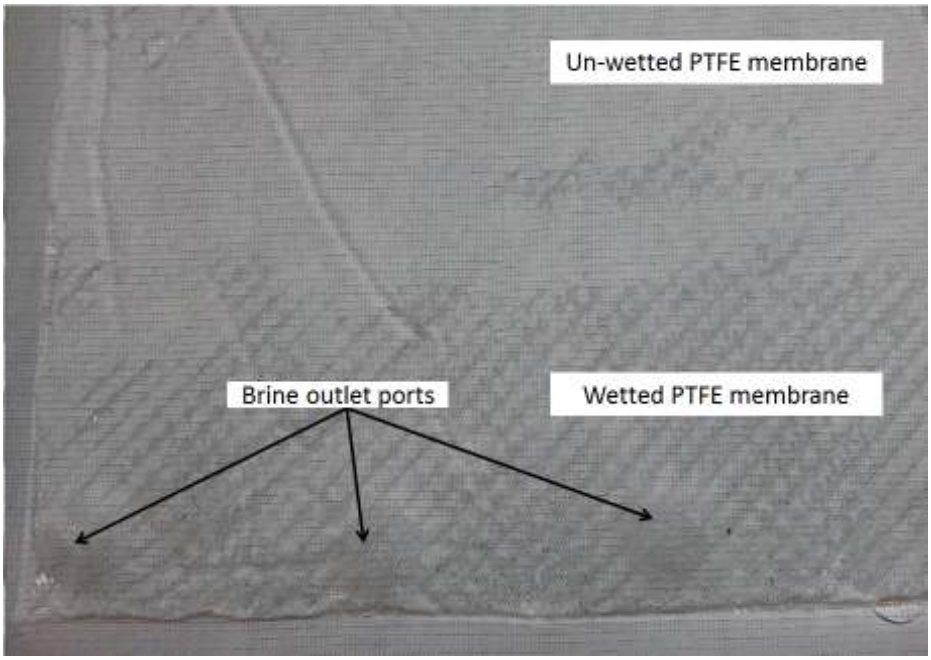

Figure 5.7 PTFE membrane surface at the end of experiment with solution of NaCl0.1M.

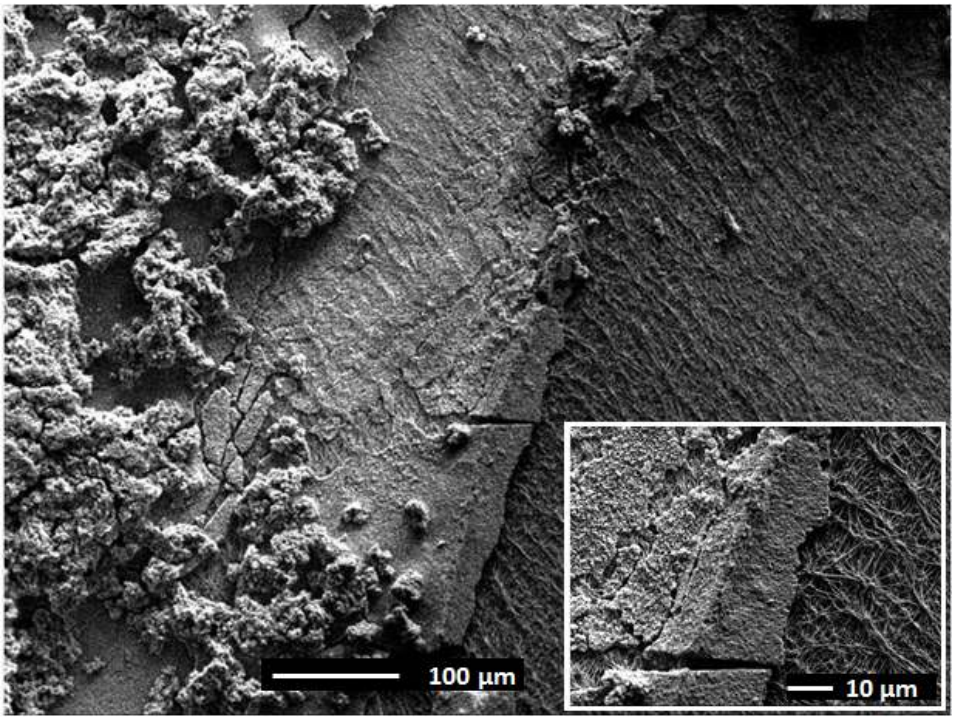

Figure 5.8 SEM micrographs of membrane surface at the end of solution NaCl0.1M (Table 3.6) DCMD operation.

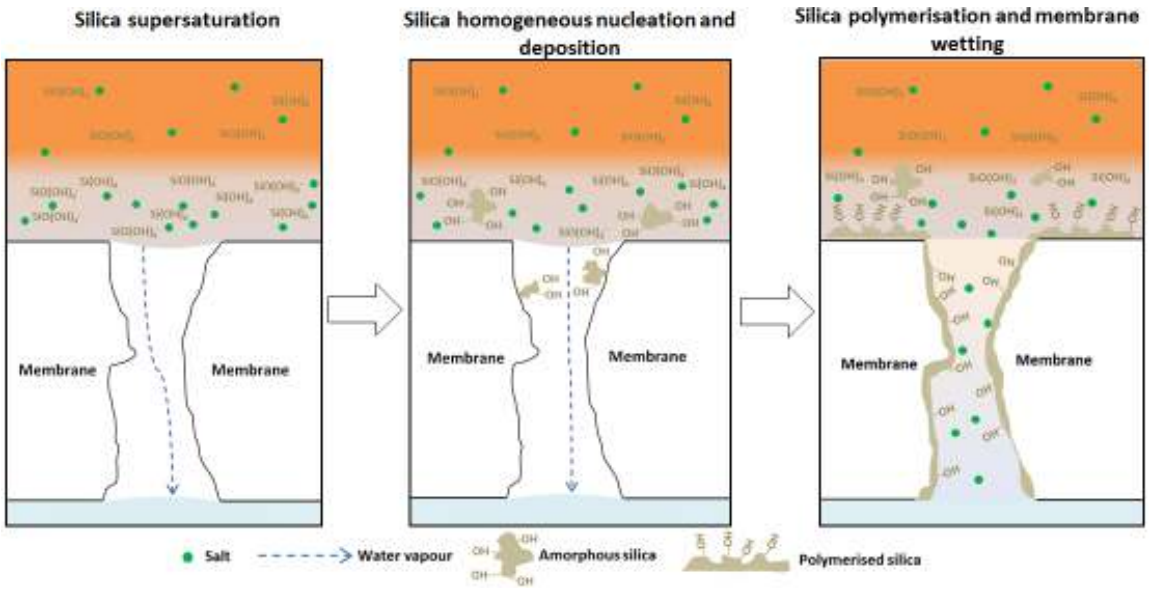

Figure 5.9 Fouling mechanisms of colloidal amorphous silica in DCMD process.

5.3 Amorphous silica solubility beaker experiments

5.3.1 Effect of temperature on amorphous silica solubility

Amorphous silica solubility beaker tests were conducted at different temperatures over a period of 100 h using synthetic waters which were made of 100 g/L $NaHCO_3$ and 12 g/L NaCl, equivalent to CSG produced water at about 88% recovery.

As can be seen in Figure 5.10a, dissolved silica concentrations declined rapidly within the first 24 h, and reached stable states after 48 h. Silica concentration at 55 and 65 ˚C dropped by 30 and 44%, respectively within the first 5 h (Figure 5.10a), and this was due to higher temperature accelerating the kinetics of silica polymerisation (Sheikholeslami et al. 2002). At the end of these tests, the dissolve silica concentration in 25, 55 and 65 ˚C brine reached 200, 330 and 440 mg/L, respectively (Figure 5.10a). RO is typically operated at brine silica concentration less than 150 mg/L at pH below 8 (Demadis 2010). Results here suggest that it is favourable to further concentrate CSG RO brine using MD at higher temperatures due to increased silica solubility at higher temperature, however,

mitigation approaches must also be taken with regards to the Mg^{2+} concentration to avoid magnesium silicate formation as discussed in Section 5.2.1.

Subsequently, 65 ˚C brine was immediately cooled to 25 ˚C by pumping the solution through a cooling coil in cold water bath controlled at temperature of 25 ˚C. It can be seen in Figure 5.10b, the dissolved silica concentration rapidly declined from 440 to 220 mg/L within 4 h. Large colloidal amorphous silica flocs were formed and settled rapidly at the bottom of solution (Figure 5.10b). Results here suggest that for MD operating in batch mode, brine recycling design needs to avoid sudden temperature decline, which will cause rapid formation of colloidal amorphous silica. Coincidently, in another DCMD experiment treating real CSG RO brine, an unplanned power outage occurred at brine recovery of 90% (dissolved silica ~ 180 mg/L). Power was restored after 4 h, and the experiment resumed under continuous mode operation with the same brine. Thereafter, it was noticed that distillate EC continuously increased from 13 to 108 μS/cm in 7 h of operation while distillate flux increased 5% (results not shown). It was speculated that during the power outage, the brine cooled to ambient temperature (~ 18 ºC) which led to the formation of colloidal amorphous silica, and this facilitated the membrane wetting at re-start of the experiment. This observation suggests that a post MD shutdown flushing with warm water is required to mitigate membrane wetting when treating solution contains high silica.

Beaker test results suggest that by incorporating heat exchangers for rapid cooling of MD brine followed by brine stabilisation (aging) and filtration / clarification to remove silica, the brine could be further treated for beneficial reuse, such as NaOH production by membrane electrolysis (ME) treating CSG MD concentrate (Lisdonk et al. 2001), where silica can present in dissolved form after re-heating filtered MD brine prior to ME process.

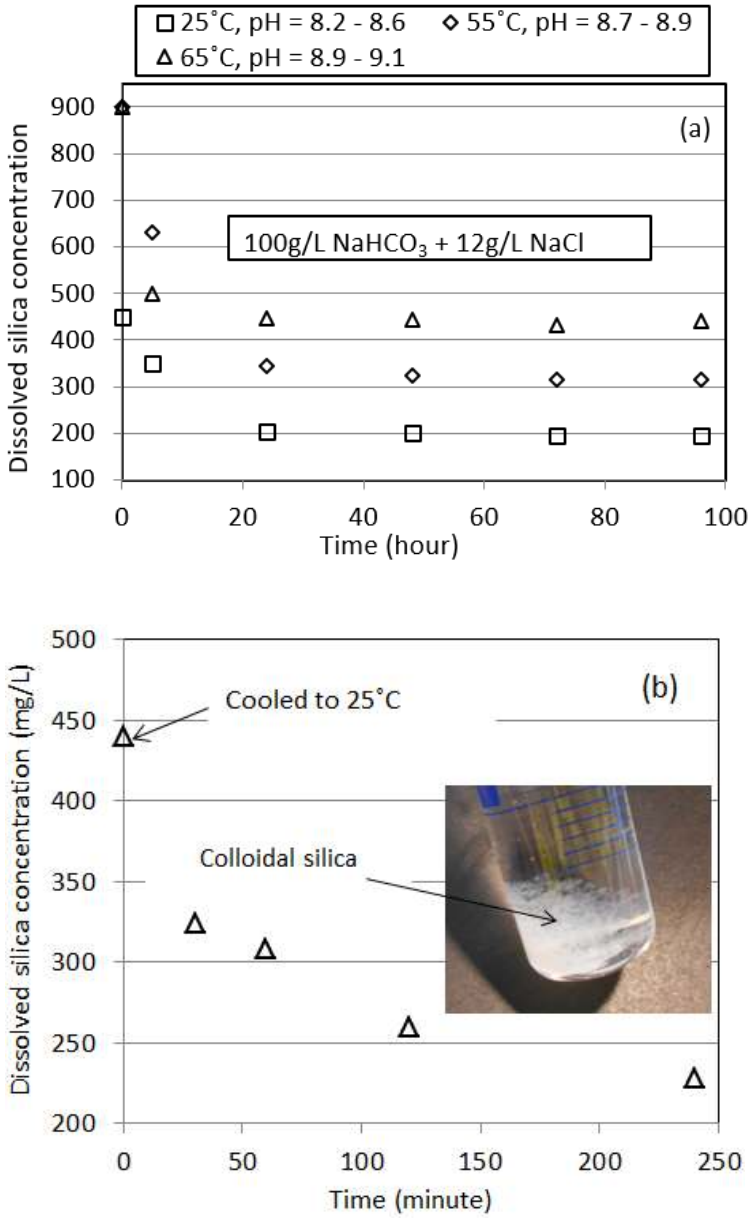

Figure 5.10 Beaker tests of amorphous silica solubility at temperature of 25, 55 and 65 ˚C, respectively, in brine solutions with 100 g/L $NaHCO_3$ and 12 g/L NaCl. a) Effect of temperature on amorphous silica solubility. b) Change of dissolved silica concentration in 65 ˚C brine solution after cooled to 25 ˚C.

5.3.2 Effects of pH and Mg^{2+} on amorphous silica solubility

Beaker tests were conducted with synthetic solutions at the same concentrations of $NaHCO_3$ and NaCl as described in Section 5.3.1, and Mg^{2+} and silica concentrations at 30 and 220 mg/L, respectively. Solution pH was adjusted using 1 N NaOH and HCl, respectively. Solution temperature was maintained at 50 ℃ throughout the test. Each test

was terminated after 24 h. The concentrations of Mg^{2+} and silica were measured at the end of each test. As it can be seen in Figure 5.11 concentrations of Mg^{2+} and silica remained same at brine pH = 9.2. However, increasing brine pH > 9.5 had a dramatic influence on both Mg^{2+} and silica concentrations (Figure 5.11). At higher pH, more dissolved silica exists in solution as reactive silicate ions which are likely to react with Mg^{2+}. The stoichiometric ratio of silicon reduction to magnesium reduction (pH 9.2 to 10) was 1.6 : 1 which is greater than 1 : 1 as observed in Section 5.2.1. Since the solubility of $Mg(OH)_2$ decreases dramatically at pH > 9.2 (Liu et al. 1973), it is likely that $Mg(OH)_2$ formed first in brine, and subsequently enhanced the adsorption of dissolved silica onto $Mg(OH)_2$ surfaces (Demadis 2010). Results here indicate that it is preferred to operate MD process at CSG brine pH < 9.2 to mitigate the formation of magnesium silicates.

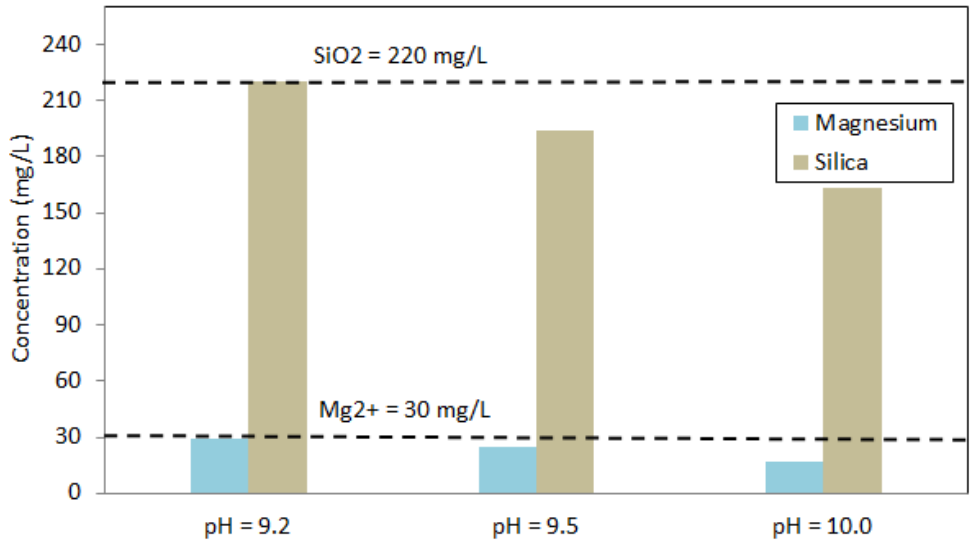

Figure 5.11 Concentrations of Mg^{2+} and silica in final brine at pH = 9.2, 9.5 and 10.0, respectively. Beaker test conditions: brine solutions with 100 g/L $NaHCO_3$ and 12 g/L NaCl; initial concentrations of Mg^{2+} and silica at 30 and 220 mg/L, respectively; temperature = 50 °C; and test time = 24 h.

5.4 Mitigation of DCMD scaling

5.4.1 DCMD with scale inhibitors

Scale inhibition tests were carried out in batch mode DCMD on brine solution Mg4.3 and brine recovery of 80%. Distillate EC less than 5 µS/cm was produced throughout all tests. The concentrations of dissolved silica, Mg^{2+} and Ca^{2+} in final MD brine were analysed by ICP–AES, and results are shown in Figure 5.12. As can be seen in Figure 5.12, phosphonate based antiscalant A demonstrated better performance for inhibiting $CaCO_3$ formation than polymer based antiscalant B. Polymeric antiscalant B could adsorb on formed $CaCO_3$, and further reduce its effectiveness for inhibiting magnesium silicate formation. However, it is important to keep in mind that the amount of inhibitor dosed and the induction period for precipitation should be properly determined to obtain the maximum effect of antiscalant for scale inhibition in MD process (He et al. 2009), and these aspects were not addressed in this study. Compared with antiscalant A and B, Na_2EDTA performed better for inhibiting magnesium silicates and $CaCO_3$ formation by maintaining more silica, Mg^{2+} and Ca^{2+} in soluble form (Figure 5.12), and this is attributed to the strong complexing ability of Na_2EDTA to Mg^{2+} and Ca^{2+}. Therefore, Na_2EDTA treatment could be a viable option for DCMD treating CSG RO brine at low concentrations of Ca^{2+} and Mg^{2+}. Continues brine treatment using EDTA could reduce the frequency of clean-in-place (CIP) process for MD membrane, and thereby extend membrane life. However, the impacts of EDTA in MD brine on the natural environment need be scrutinised prior to adopt this treatment option.

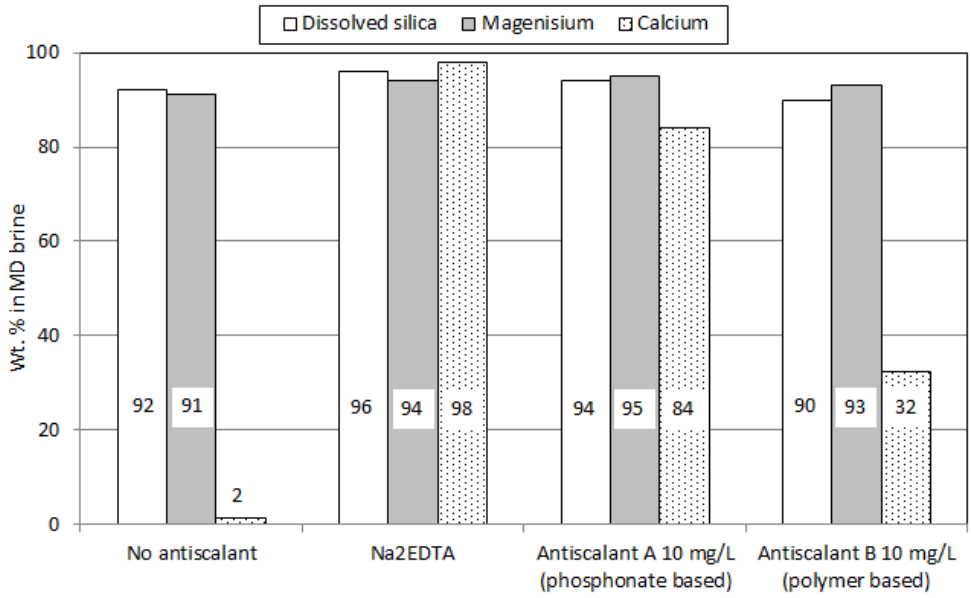

Figure 5.12 Effect of antiscalant dosing on the wt.% of dissolved silica, Mg^{2+} and Ca^{2+} in DCMD at 80% brine recovery of synthetic CSG RO brine Mg4.3.

5.4.2 DCMD with intermittent distillate flushing

Results of batch mode operation in Section 5.1 show that DCMD can achieve CSG RO brine recovery of 80% (overall recovery ~ 90%) with minimal scaling of $CaCO_3$ and magnesium silicate. Magnesium silicates and $CaCO_3$ can be removed by acid cleaning, however, chemical cleaning should be considered as the last resort, as it could lead to membrane wetting (Gryta 2005) and cleaning efficiency tends to decrease over long-term operation (Zhong et al. 2016). The results of DCMD on SWRO brine in Chapter 4 suggest that distillate flushing was effective to remove inorganic Ca and Mg related salts from PTFE membrane surface without causing membrane wetting (Section 4.5.3). The test here is to evaluate DCMD performance at high water recovery over long-term operation by applying intermittent distillate flushing. CSG RO brine was processed by batch mode DCMD to brine recovery of 80% followed by continuous mode operation. A 3 min distillate flushing was carried out to DCMD module at flowrate and temperature of 1000 ml/min and 50 °C, respectively. The experiment was terminated after 15 d of operation

and the results are shown in Figure 5.13. As can be seen in Figure 5.13, distillate flux remained relatively constant (~ 21 L/m^2·h) throughout this test. Distillate EC on the other hand, increased slightly after each flushing followed by the slow decline, and stabilised at around 7 µS/cm. Distillate EC increase post flushing could due to the CO_2 degassing from flushing solution while $CaCO_3$ was removed from membrane surface (Section 4.3). The overall EC rejection in this test was > 99.9%. The results here suggest that intermittent distillate flushing at brine temperature can effectively revert membrane inorganic scaling, and facilitate long-term MD operation at consistent distillate quality and flux.

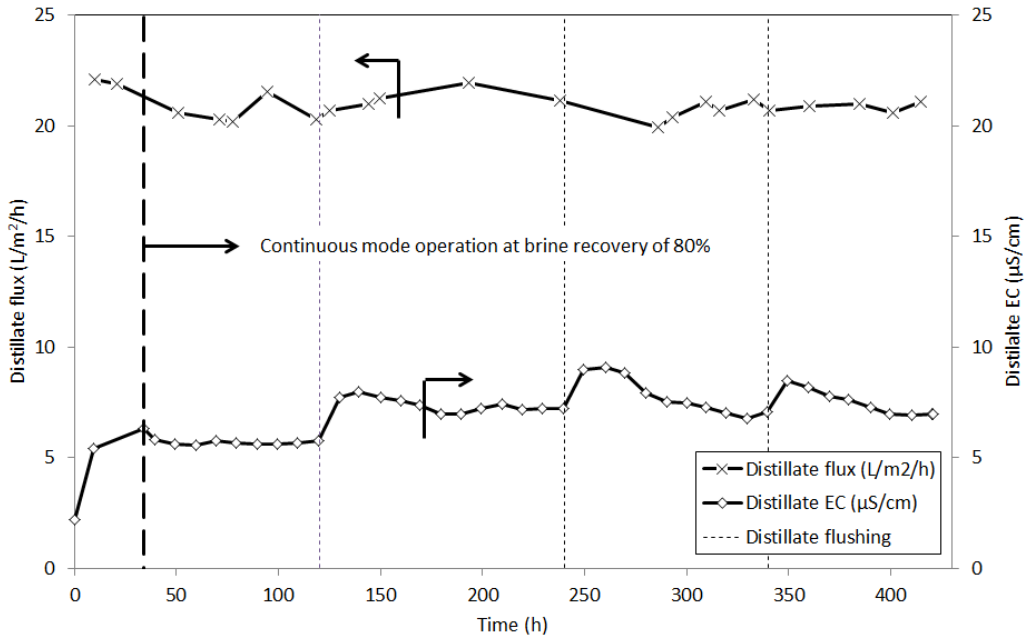

Figure 5.13 DCMD continuous mode operation on CSG RO brine at brine recovery of 80% with intermittent distillate flushing. Behaviours of distillate EC and distillate flux as function of time.

5.5 Conclusions

This study mainly investigated silica fouling behaviours in MD during treatment of CSG RO brine. The impacts of divalent cations (Mg^{2+} and Ca^{2+}) and anions (HCO_3^- / CO_3^{2-} and Cl^-) on silica fouling were examined using synthetic solutions. Thermodynamic

software Phreeqc–3 was also adopted to predict the potential foulants, and the calculation results were compared with membrane surface analysis.

Bench scale DCMD operated on CSG produced water achieved 95% overall recovery at 150 h of operation. EDS analysis revealed that precipitates on the membrane surface contained Mg, Ca and Si. Further investigations on synthetic solutions revealed that the foulants were $CaCO_3$ and magnesium silicates with stoichiometric ratio of silicon to magnesium of 1: 1. Study on synthetic solutions revealed that the formation of $CaCO_3$ was rapid and it did not co-precipitate with dissolved silica while the precipitation of magnesium silicates was strongly influenced by the concentration of Mg^{2+} (> 45 mg/L) and brine pH (> 9.2). Phreeqc–3 thermodynamic calculations successfully predicted the species of magnesium silicates. However, the delayed precipitation of magnesium silicates was possibly due to abundant Na^+ in brine which competed with Mg^{2+} to react with dissolved silica. Results also showed that HCO_3^- / CO_3^{2-} has greater ability to stabilise silica in dissolved form compared with Cl^-.

A key finding in this study is that the formation of colloidal amorphous silica was temperature sensitive, and polymerised silica fouling could drastically reduce distillate flux and potentially lead to MD membrane wetting. Therefore, industry should avoid temperature decline in MD brine recycling stream, and perform a warm distillate flushing (e.g., at brine temperature) post MD shutdown to mitigate the formation of colloidal amorphous silica. On the other hand, rapid cooling of MD brine followed by brine stabilisation (aging) and filtration / clarification could be adopted to remove silica.

To mitigate membrane fouling, Na_2EDTA treatment demonstrated better performance for inhibiting $CaCO_3$ and magnesium silicate formation compared with commercial

phosphonate and polymer RO antiscalants. Intermittent distillate flushing at brine temperature did not cause membrane wetting over 15 d of operation at CSG RO brine recovery of 80% (overall recovery of 90%). Industry could adopt EDTA treatment coupled with distillate flushing for processing CSG RO brine (with low hardness) over long-term operation.

The results present in Chapter 6 are related to a copper barren RO brine treatment using DCMD process where MD performances were assessed by employing two commercial LDPE membranes, standard and with oleophobic chemistry, respectively. The behaviour of NH_3 transfer in MD and its impact on the stabilities of metal-ammonia complexes were also assessed.

Chapter 6 DCMD of copper barren RO brine

In this study, DCMD process was explored to concentrate copper barren RO brine solution (Table 3.3) from an inland copper processing plant. The membrane performance in organic adsorption was evaluated using standard PE membrane and oleophobic PE membrane, respectively. The stability of metal-ammonia complexes was investigated with respect to ammonia equilibrium thermodynamics, followed by the membrane cleaning using commercial RO cleaning agents. In addition, thermal energy demand for the DCMD process was assessed linking to the available on-site waste heat source.

6.1 Standard PE and oleophobic PE membranes

The SEM-EDS analysis results of the virgin membranes are presented in Figure 6.1. Standard PE membrane presented mostly circular pores at membrane surface (Figure 6.1a), while oleophobic PE membrane presented with elliptical pores (Figure 6.1b) indicative of an elongation-induced pore deformation being introduced during the fabrication of oleophobic PE membrane. The fabrication of PE microporous membrane is commonly practiced using melt-extrusion-stretching method where PE polymer is heated above the melting point and extruded into thin sheet forms followed by stretching to form porous membrane structure (Lalia et al. 2013; Mitsuoka et al. 2013). Membrane pore size and associated standard deviation were estimated by measuring 20 pores randomly at each membrane. Standard PE membrane has average pore size of 0.26 µm with standard deviation of 0.13 µm, and oleophobic PE membrane has average pore size of 0.22 µm with standard deviation of 0.20 µm. Compared to oleophobic PE membrane, standard PE membrane appears to have larger membrane pore size and greater membrane pore uniformity. EDS analysis revealed that elements associated with oleophobic PE

membrane were C, F and O, while F was not found at the surface of standard PE membrane (Figure 6.1). As informed by the membrane supplier, oleophobic PE membrane was fabricated by applying a fluorinated polymer coating onto standard PE membrane to reduce membrane surface energy.

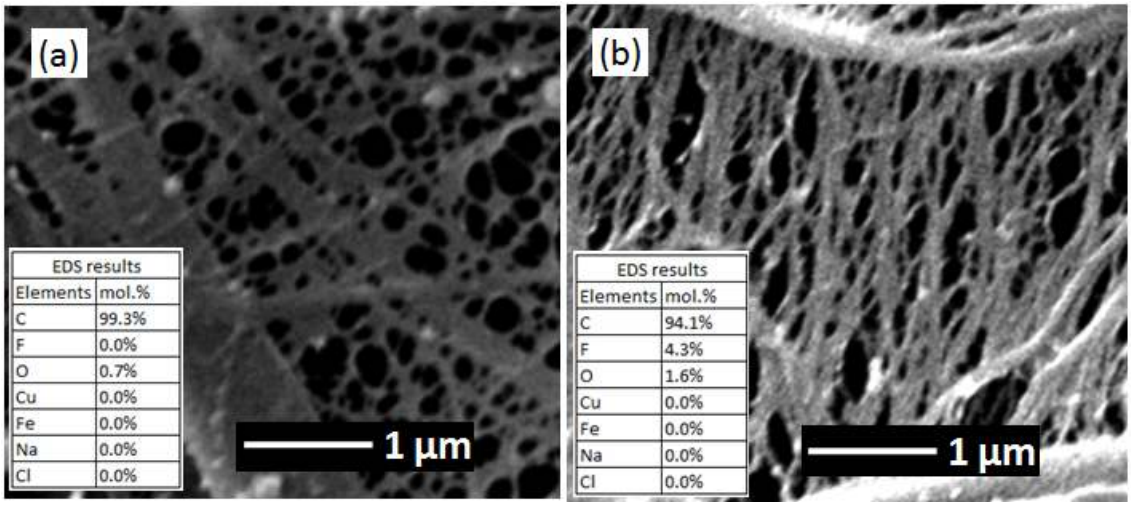

Figure 6.1 SEM–EDS analysis results of a) virgin standard PE membrane and b) virgin oleophobic PE membrane, respectively.

6.2 DCMD tests

In this test, 17 kg of brine was processed to CF = 5 followed by 72 h of constant CF mode operation. Figure 6.2a shows the distillate flux behaviour in DCMD batch mode operation. The distillate flux of standard PE membrane and oleophobic PE membrane decreased from 19.2 to 17.3 L/m^2·h and 12.2 to 9.8 L/m^2·h, respectively (Figure 6.2a). Distillate flux decline in batch mode operation may be due to rising salinity according to Raoult's law (Equation 3.4), which defines that vapour pressure of the water in the solution would drop by increased non-volatile solutes dissolved in solution. Solution total vapour pressure containing volatile components, such as NH_3, is higher than that of pure water. Studies reported that decreasing NH_3 concentration in the brine led to the decrease of distillate flux (Qu et al. 2013; Ding et al. 2006). Moreover, the pH changes in distillate

and brine influence NH_3 transfer due to ammonia equilibrium thermodynamics (Equation 2.8), and this further complicates the estimation of distillate flux in this test. During constant CF mode operation, distillate flux of standard PE membrane and oleophobic PE membrane declined from 17.3 to 16.1 L/m^2·h and 12.2 to 9.3 L/m^2·h, respectively (Figure 6.2b). Distillate flux decline during this period could be linked to scale build up on the membrane surface, which adds thermal and hydraulic resistance and this is discussed later with SEM-EDS analysis. ICP analysis showed that the distillate Na^+ concentrations were 0.68 and 0.37 mg/L for standard PE membrane and oleophobic PE membrane experiments, respectively. Overall, DCMD achieved greater than 99.9% non-volatile solute rejection by using either membrane.

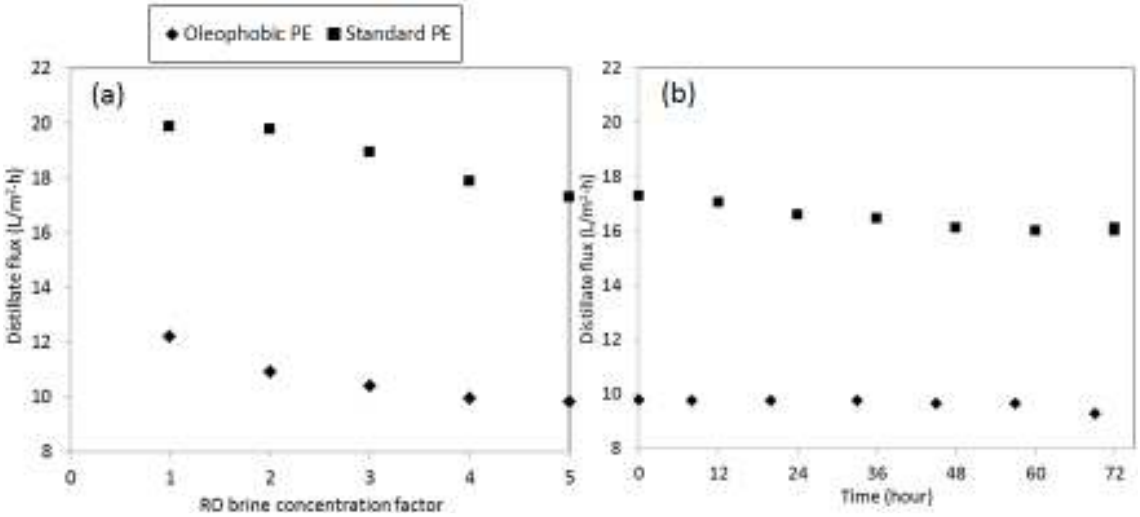

Figure 6.2 Behaviours of distillate fluxes in DCMD a) batch mode operation and b) constant CF mode (brine CF = 5) operation using standard PE membrane and oleophobic PE membrane, respectively. Experimental conditions: initial brine = 17 kg; T_f = 60 °C; T_d = 30 °C; Q_f = Q_d = 1200 ml/min (cross flow velocity = 0.09 m/s); batch mode total run times: oleophobic PE membrane = 59.6 h and standard PE membrane = 36.2 h; constant CF mode total run time = 72 h.

After the end of each experiment, the membrane was removed from DCMD module for SEM-EDS analysis and the results are shown in Figure 6.3 and Figure 6.4. The SEM micrograph of the standard PE membrane surface revealed that the majority of deposits

displayed as amorphous structure with some needle-like crystals (Figure 6.3a). EDS spectrum of the amorphous deposits (Area 2 shown in Figure 6.3a) confirmed that there was significant peak of C at 96.7 mol.%, with small peaks of O, Cl, Na and Au at 2.2 0.5, 0.4 and 0.1 mol.%, respectively (Figure 6.3c). C and O would be associated with virgin standard PE membrane as illustrated in Figure 6.1a. Au would come from the conductive coating as part of membrane sample preparation for SEM analysis. The stoichiometric ratio of Na and Cl approximately 1 : 1 indicated that amorphous deposits were likely NaCl. The formation of NaCl in this test is abnormal as NaCl concentration in brine was about 38 g/L which was well below 370 g/L, the saturation limit of NaCl at 60 ºC (Pavuluri et al. 2014). The most plausible explanation is that NaCl was introduced during the membrane drying process in preparing for SEM analysis.

EDS spectrum of crystalline deposits (Area 1 shown in Figure 6.3a) confirmed that there were significant peaks of C and O at 72.7 and 20.5 mol.%, respectively, with small peaks of Au, Sr, Ca and S at 0.1, 0.1, 0.5 and 1.8 mol.%, respectively (Figure 6.3b). C and O would come from the virgin membrane (Figure 6.1a). Au would come from SEM conductive coating. Small peaks of Sr, Ca and S suggests that the possible formation of $CaSO_4$ and $SrSO_4$ which are typically displayed as needle shape / rod-like structure (Nghiem et al. 2011), and both salts are sparingly soluble in water and have inverse solubility with respect to temperature. A small peak of Cu at 0.1 mol.% (Figure 6.3b) represents minor Cu salts deposition in this test. Again, the peaks of Na and Cl could come from NaCl which was trapped inside other foulants during the membrane drying out process (Nguyen et al. 2015).

SEM image of oleophobic PE membrane (Figure 6.4a) revealed that membrane surface was covered by amorphous deposits with no distinctive crystalline deposits. EDS

spectrum of the amorphous deposits (circled in Figure 6.4a) confirmed that the peaks were C, Na and Cl at 90.6, 4.7 and 3.0 mol.%, respectively, with other metal cations below the detection limits (Figure 6.4b). Results here seem to suggest that NaCl was the only deposit on the membrane surface. The amorphous structure of NaCl displayed in Figure 6.3 and Figure 6.4 was possibly due to organic matter in the brine (Table 3.3). Chloride components in NaCl may react with weak organic acid (e.g., carboxylic acid) and resulted in the amorphous organic salt (Laskin et al. 2012). A repeat test was conducted using oleophobic PE membrane. Again, EDS analysis showed that amorphous deposit contained Na and Cl at molar ratio approximately 1.1. The absence of membrane support layer could encourage membrane deformation and subsequently trap stagnant brine along the spacer lines (Figure 6.9a). Different techniques of membrane draining / drying also need to be accessed in future study to eliminate the interference of NaCl. Overall, the SEM-EDS analysis suggests that inorganic salt precipitation on both membrane surfaces was insignificant during these experiments.

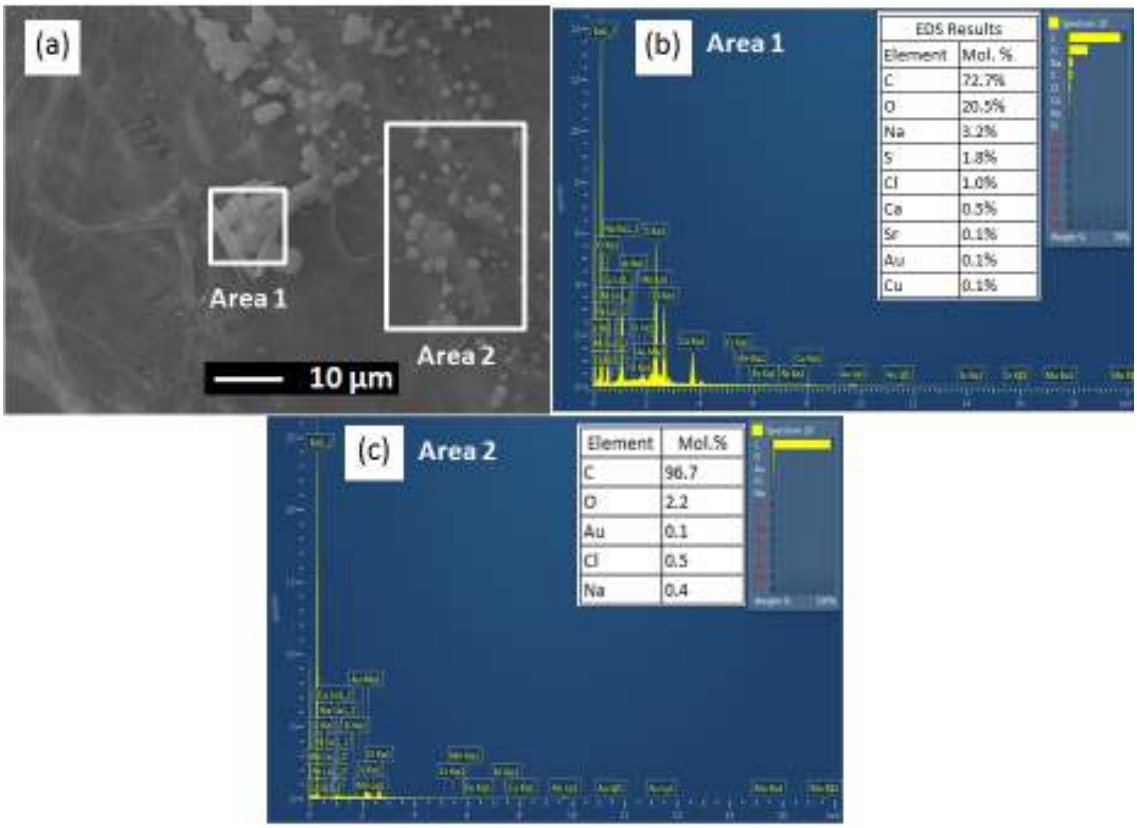

Figure 6.3 SEM–EDS analysis of standard PE membrane. Experimental conditions: initial brine = 17 kg; T_f = 60 °C; T_d = 30 °C; Q_f = Q_d = 1200 ml/min (cross flow velocity = 0.09 m/s); batch mode total run time = 36.2 h; constant CF mode total run time = 72 h.

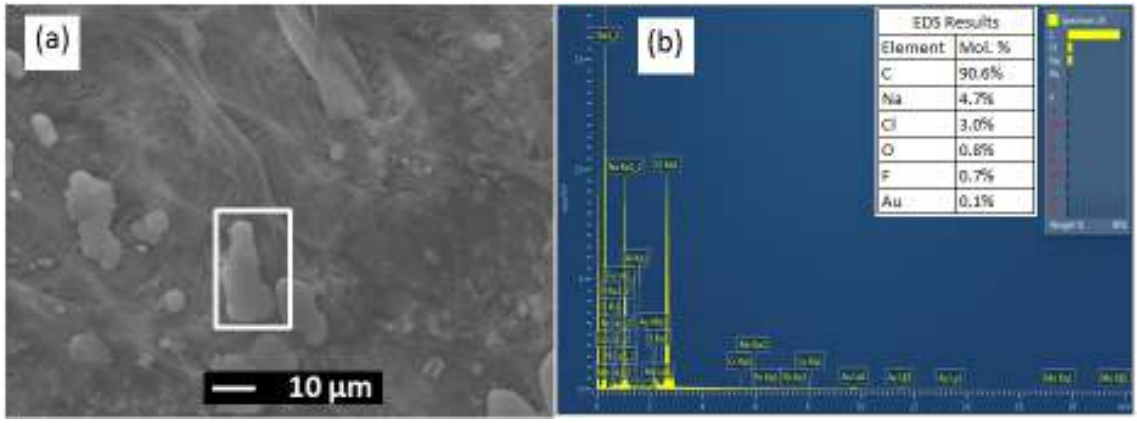

Figure 6.4 SEM–EDS analysis of oleophobic PE membrane. Experimental conditions: initial brine = 17 kg; T_f = 60 °C; T_d = 30 °C; Q_f = Q_d = 1200 ml/min (cross flow velocity = 0.09 m/s); batch mode total run time = 59.6 h; constant CF mode total run time = 72 h.

TOC concentrations were measured in brine samples throughout the experiments and the results are shown in Figure 6.5. Prior to brine CF = 4 during the standard PE membrane

experiment, brine TOC concentrations did not deviate from theoretical concentrations calculated from mass balance. At brine CF = 5, brine TOC concentration reached 223 mg/L which was lower than the theoretical TOC concentration of 235 mg/L (Figure 6.5). Thereafter, brine TOC concentration further declined to 195 mg/L at the end of constant CF mode operation (Figure 6.5). The oleophobic PE membrane experiment on the other hand, brine TOC concentrations remained the same as theoretical concentrations throughout batch mode operation and then slightly declined to 216 mg/L at the end of constant CF mode operation (Figure 6.5). It is worth noting that overall run time of oleophobic PE membrane experiment was 23 h longer than that of the standard PE membrane experiment due to its lower flux and constant feed volumes used during experiments.

TOC concentrations in UF feed and RO brine was 7.5 and 47 mg/L (Table 3.3), respectively, indicating that organics were not effectively removed by UF and RO processes at 85% RO recovery. TOC present in RO brine was possibly from degradation products or impurities of synthetic organic flocculant, which was introduced into pregnant leach solution to assist CuO removal in the thickener. Flocculant was made of anionic vinyl polymers containing acrylic acid. At higher pH, high molecular weight polyacrylic acid presents hydrophilic property due to the hydrogen bonding between carboxylic groups and water molecules (Plavšić et al. 1996). A previous study showed that hydrophilic organic matter does not have strong bonding with MD hydrophobic surfaces (Naidu et al. 2014). However, Plavšić et al. (1996) showed that the monomer unit of polyacrylic acid (acrylic acid) had strong tendency of adsorption onto hydrophobic surface due to the hydrophobic characteristic of monomer from linear – CH_2 – CH_2 – chain. Overall, TOC analysis results here suggest that oleophobic PE membrane is more

resistance against attachment of organic with both hydrophilic and hydrophobic properties, while standard PE membrane favours the adsorption of hydrophobic organic compounds. DCMD is able to concentrate RO brine at brine CF = 4 with low risk of membrane organic fouling. However, operating DCMD at brine CF > 5 increases the likelihood of organic attachment onto membrane surface which could have detrimental effect on DCMD long-term stable operation.

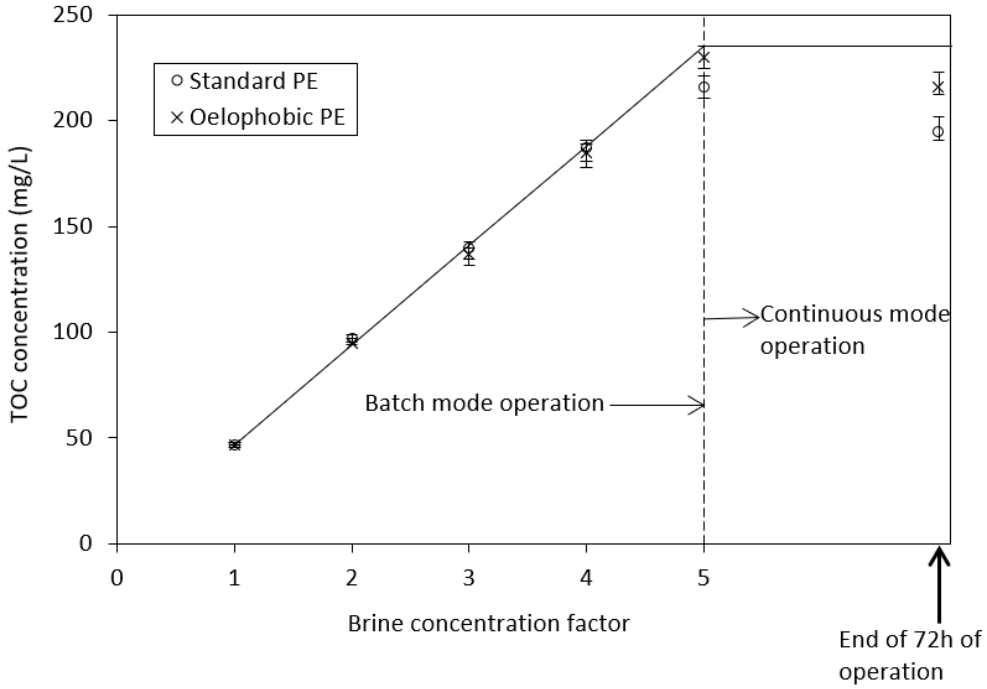

Figure 6.5 DCMD brine TOC concentrations at various CFs in batch mode operation and at the termination of constant CF mode operation, respectively. Solid line represents the theoretical TOC concentration in brine. Experimental conditions: initial brine = 17 kg; T_f = 60 °C; T_d = 30 °C; $Q_f = Q_d$ = 1200 ml/min (cross flow velocity = 0.09 m/s); batch mode total run times: oleophobic PE membrane = 59.6 h and standard PE membrane = 36.2 h; constant CF mode total run time = 72 h. Error bar represents the standard deviation of replicate measurements (n = 3).

6.3 Behaviours of NH_3 and CO_2 in DCMD process

The concentrations of NH_3 and NH_4^+ in brine are temperature, pH and salinity dependent. The relative concentration of NH_3 and NH_4^+ in brine at 60 °C can be calculated by the Equation 6.1 below:

$$NH_3\ (\%) = \frac{100}{(1+10^{(pK_{a,T}-pH-S)})}$$ (Soderberg 1995) (6.1)

Where T is the temperature in °C, pK_a is the negative log of the acid dissociation constant for ammonia, and it is calculated as:

$$pK_a = 0.09108 + \frac{2927.92}{273.2+T}$$ (Emerson et al. 1975) (6.2)

s in Equation 6.1 is the salinity correction term, which is calculated from the Lewis equation:

$$s = -A \times \left[I^{1/2}/\left(1 + I^{1/2}\right)\right] - 0.2I \quad (6.3)$$

Where A is a coefficient that is a function of the dielectric constant and temperature of water and *I* is the ionic strength (IS) of brine. A is calculated from below (Truesdell and Jones. 1974):

$$A = 1.82483 \times 10^6 \times [E \times (T + 273.16)]^{-1.5} \quad (6.4)$$

E is calculated from following formula:

$$E = 87.74 - 0.4008\,T + 9.398 \times 10^{-4} \times T^2 - 1.41 \times 10^{-6} \times T^3 \quad (6.5)$$

s was calculated as 0.1 according to Equation 6.3, therefore, the impact of brine salinity on the portion of volatile ammonia is negligible as compared to brine pH (Equation 6.1). As can be in Figure 6.6, at brine pH = 9.1 (Table 3.3), > 80% of total ammonia exists in brine as NH_3 (volatile ammonia), and this indicates that a significant amount of NH_3 could be released from brine in MD process, and subsequently influences brine and distillate pH.

Figure 6.7a illustrates the pH behaviours of brine and distillate in batch mode experiments using oleophobic PE membrane. In the early stages of the experiments (CF = 1.1), brine pH declined rapidly from 9.1 to 7.8 while distillate pH increased from 6.5 to 9.4 (Figure 6.7a). Thereafter, brine pH gradually reduced to 6.9 at the end of this test, distillate pH on the other hand, stabilised at 9.0 from brine CF = 2 (Figure 6.7a). The brine pH rapid decline at the beginning of the experiment was attributed to the release of NH_3 from solution (Equation 2.8). More volatile ammonia presented in brine at sudden temperature increase, and this enhanced the driving force of ammonia across the membrane. The rapid ammonia transfer led to pH increase in the distillate as the equilibrium reaction shifted towards the left side of Equation 2.8. As it is shown in Figure 6.6, for brine pH < 8, more ammonia existed in brine in the form NH_4^+ while more NH_3 existed in distillate due to pH > 9, and this caused the reduction of overall driving force for ammonia across the membrane. As shown in Figure 6.7b, the proportion of total ammonia to the starting ammonia in brine batch that was processed reduced by 40% at brine CF = 2. From then on, the rate of ammonia reduction slowed, and 25% of the initial total ammonia remained in the brine at the end of the experiment. Figure 6.7b also shows that the fraction of brine TIC sharply declined to 20% at brine CF = 2, and only 2% of the initial TIC remained in the brine at the end of this run. TIC reduction in brine was attributed to CO_2 degassing. Sudden increase in brine temperature encourages CO_2 liberation (Zhang et al. 2015). Reduced brine pH also facilitates CO_2 generation (Equation 2.9). In addition, dissolved ammonia at high distillate pH acted as a "strip" solution for CO_2, and led to the formation of non-volatile species such as CO_3^{2-}, HCO_3^- and $NHCOO^-$ (Equation 2.9, 2.10 and 2.11). This facilitated continuous CO_2 degassing across the membrane driven by the CO_2 partial pressure difference between the feed and distillate. CO_3^{2-} and HCO_3^- are well-known as

pH buffer factors, therefore, pH remained stable in distillate after brine CF = 2 (Figure 6.7a). According to Equation 2.9, CO_2 degassing will increase the pH of solution. However, the reduced pH in brine (Figure 6.7a) suggests that ammonia transfer in this experiment was significant and therefore dominated the pH changes in both brine and distillate. The rate of ammonia transfer appeared to be correlated with TIC removal (Figure 6.7), therefore, it was speculated that over long-term DCMD operation, brine pH could be plateaued at near neutral pH after the complete removal of TIC (as CO_3^{2-} / HCO_3^-). At this pH, nearly 100% total ammonia exists in brine as NH_4^+ (Figure 6.6), and free Cu^{2+} could be released from Cu–NH_3 complexes and eventually form copper salts on membrane surface. To assess the stability of Cu–NH_3 complexes and the associated membrane fouling potential, following test (Section 6.4) was performed by compensating the distillate lost in brine using deionised water to encourage the conversion from NH_3 to NH_4^+.

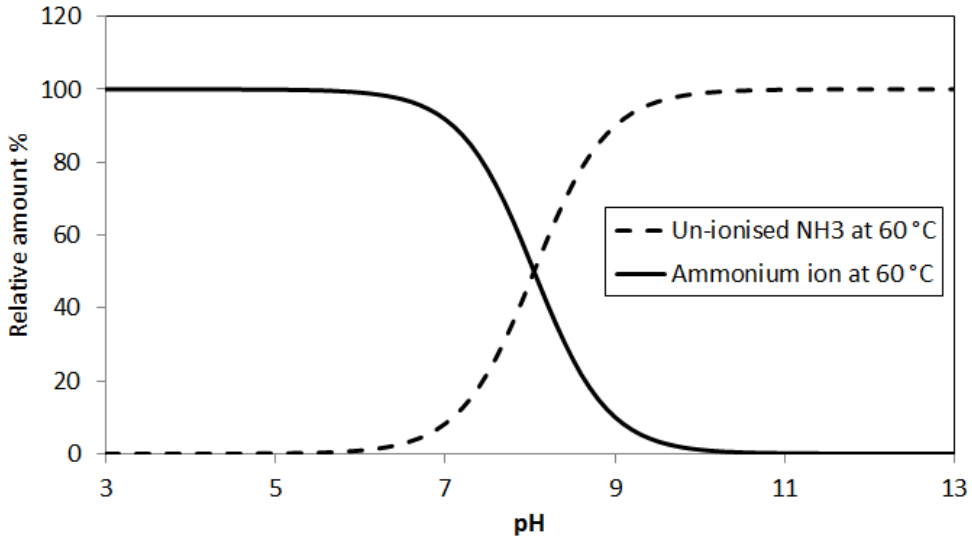

Figure 6.6 Relative speciation (%) of NH_3 and NH_4^+ in brine (Table 3.3) at 60 °C.

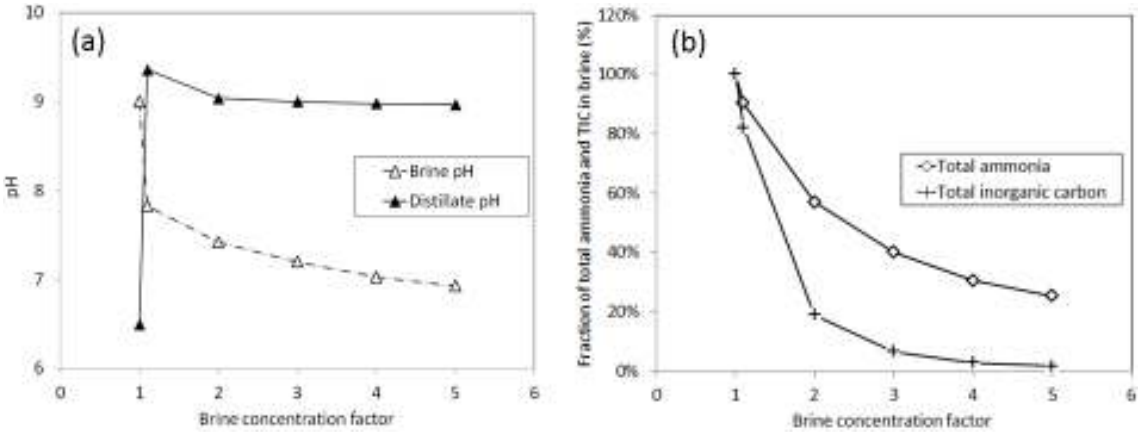

Figure 6.7 Behaviours of a) brine and distillate pH, and b) fractions of total ammonia and TIC in brine at various brine CFs in DCMD batch mode experiment using oleophobic PE membrane. Experimental conditions: initial RO brine = 17 kg; T_f = 60 °C; T_d = 30 °C; Q_f = Q_d = 1200 ml/min (cross flow velocity = 0.09 m/s); batch mode total run time = 59.6 h.

6.4 Stability of Cu–NH_3 complexes in DCMD process

In this test, RO brine was first processed to brine CF = 5, then, deionised water was added in the brine intermittently to compensate the water loss. The experiments lasted 74 h and deionised water top up and measured brine pH and distillate flux are illustrated in Figure 6.8. Distillate flux for the standard PE membrane experiment remained stable at 18 L/m^2·h until sudden flux decline occurred after 48 h of operation, and flux further reduced to 10 L/m^2·h at the end of the experiment (Figure 6.8). Brine pH on the other hand, gradually dropped from 7.1 to 6.1 over this period (Figure 6.8). Figure 6.8 also shows that distillate flux for the oleophobic PE membrane experiment remained at about 10 L/m^2·h throughout the run and brine pH declined from 7.0 to 6.4. Sudden distillate flux decline for the standard PE membrane experiment could be due to copper salts (e.g., $Cu(OH)_2$) precipitation as inadequate NH_3 presented in brine to form stable complexes with copper. Compared with performance of standard PE membrane, less brine pH decline in oleophobic PE membrane experiment was likely attributed to the lower distillate flux, therefore, less deionised water top up. Ammonia solution is a weak base,

adding deionised water will reduce solution pH due to reduced concentration of OH^-. However, this reaction will not cause solution pH < 7. The continuous pH decline below 7 could due to the formation of metal hydroxides which resulted in a reduced concentration of OH^-. At pH < 7, CO_2 transfer could potentially elevate solution pH (e.g., > 8.5) in the brine side boundary layer, therefore, faciliating volatile ammonia removal (Yang et al. 2017) and releasing free metal ions from metal-ammonia complexes.

At the end of oleophobic PE membrane experiment, visual inspection of used membrane revealed brown deposits along the spacer lines (Figure 6.9a). However, no deposit was observed on previously used membrane (Chapter 6.2). It was concluded that brown deposits were unlikely introduced from experimental environment (e.g., dust) in the laboratory. In addition, large brown deposits were discovered at the bottom of feed container. Final brine was filtered through a 0.45 μm filter, and SEM-EDS analysis was performed on the filtered deposits and results are shown in Figure 6.10. SEM image (Figure 6.10a) shows that deposits displayed as amorphous structure. EDS spectrum of amorphous deposits (circled in Figure 6.10a) revealed that the most significant peaks are C and O at 53.0 and 43.2 mol.%, respectively (Figure 6.10b). C and O would come from 0.45 μm cellulose acetate filter material (Figure 6.10e). Small peaks of Fe (2.1 mol.%), Cr (0.7 mol.%), Cu (0.1 mol.%) and Ni (0.1 mol.%) also appeared in EDS results (Figure 6.10b). Studies have shown that the relative stability of metal-ammonia complexes is in the sequence of Mn < Fe < Co < Ni < Cu (Irving and Williams. 1952). Therefore, it was speculated that with NH_3 gradually removed from brine, metal ions such as Fe^{2+} and Ni^{2+} were firstly released from metal-ammonia complexes and subsequently dropped out of the solution as metal salts followed by Cu^{2+} salts precipitation. The Fe deposits were likely accumulated near the spacers where relevant stagnant brine existed. It is worth

noting that the very small peak of Cu shown in Figure 6.10b represents negligible Cu salts deposition in this test. Moreover, the small peaks of Al and Si both at 0.3 mol.% (Figure 6.10b) seem to point at the formation of aluminum silicate (e.g., $Al_2Si_2O_5(OH)_4$) which is highly insoluble in water.

Visual inspection of used standard PE membrane revealed that a large portion of membrane surface was covered with green deposits (Figure 6.9b). SEM image (Figure 6.10c) confirmed that membrane surface was covered by a thick layer of amorphous deposits. EDS analysis results (Figure 6.10d) revealed that apart from major peaks of C (60.3 mol.%) and O (22.6 mol.%), a significant peak of Cu at 10.1 mol.% presented along with a very low peak of Fe at 0.1 mol.%. It was speculated that at brine pH < 6.5, Cu^{2+} was released from Cu–NH_3 complexes, and subsequently formed copper salts due to concentration polarisation and elevated pH near membrane surface (Yang et al. 2017). A very small peak of Mo (0.1 mol.%) also presented in Figure 6.10d. Mo concentration in RO brine was below the detection limit of 0.01 mg/L. The element of Mo could come from raw RO brine due to a five-fold concentration. In addition, the 316L heating coil used in this study could leach Mo into solution due to corrosion. Moreover, small peak of P (0.1 mol.%) could come from RO phosphonate based antiscalant.

Results in this test suggest that brine pH is an important process monitoring parameter. For this particular application, it is recommended to operate DCMD process at above neutral pH to avoid metal salts precipitation. DCMD could be ideal candidate compared with other membrane configurations because unlike VMD which continuously maintains low pressures on the distillate side (Yang et al. 2016), in DCMD, dissolved ammonia in distillate reduces the overall driving force of ammonia across the membrane, therefore,

slowing the ammonia release from brine and keeping metal ions in stable metal-ammonia complexes.

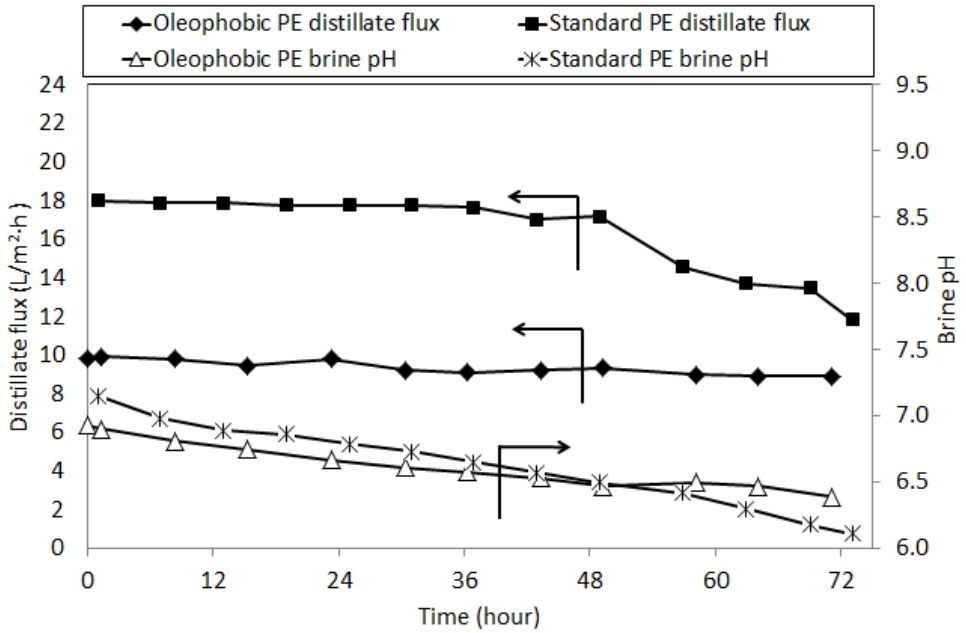

Figure 6.8 Distillate flux and brine pH as function of time at brine CF = 5. Experimental conditions: initial brine = 17 kg; T_f = 60 °C; T_d = 30 °C; Q_f = Q_d = 1200 ml/min (cross flow velocity = 0.09 m/s); total run time = 74 h; brine tank with intermittent deionised water top up.

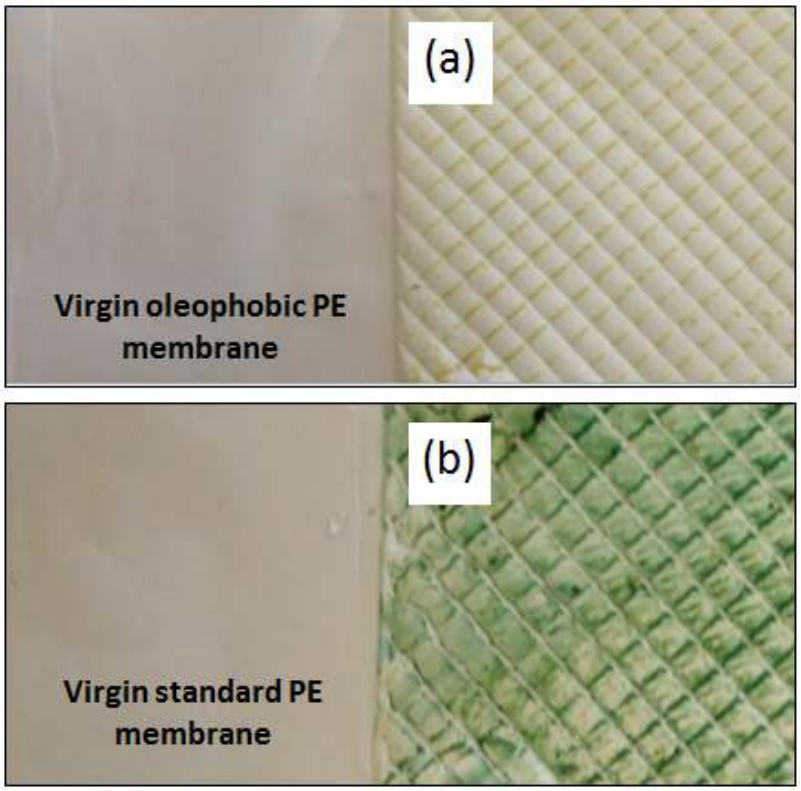

Figure 6.9 Membrane surfaces of a) fouled oleophobic PE membrane and b) standard PE membrane in comparison with virgin membranes.

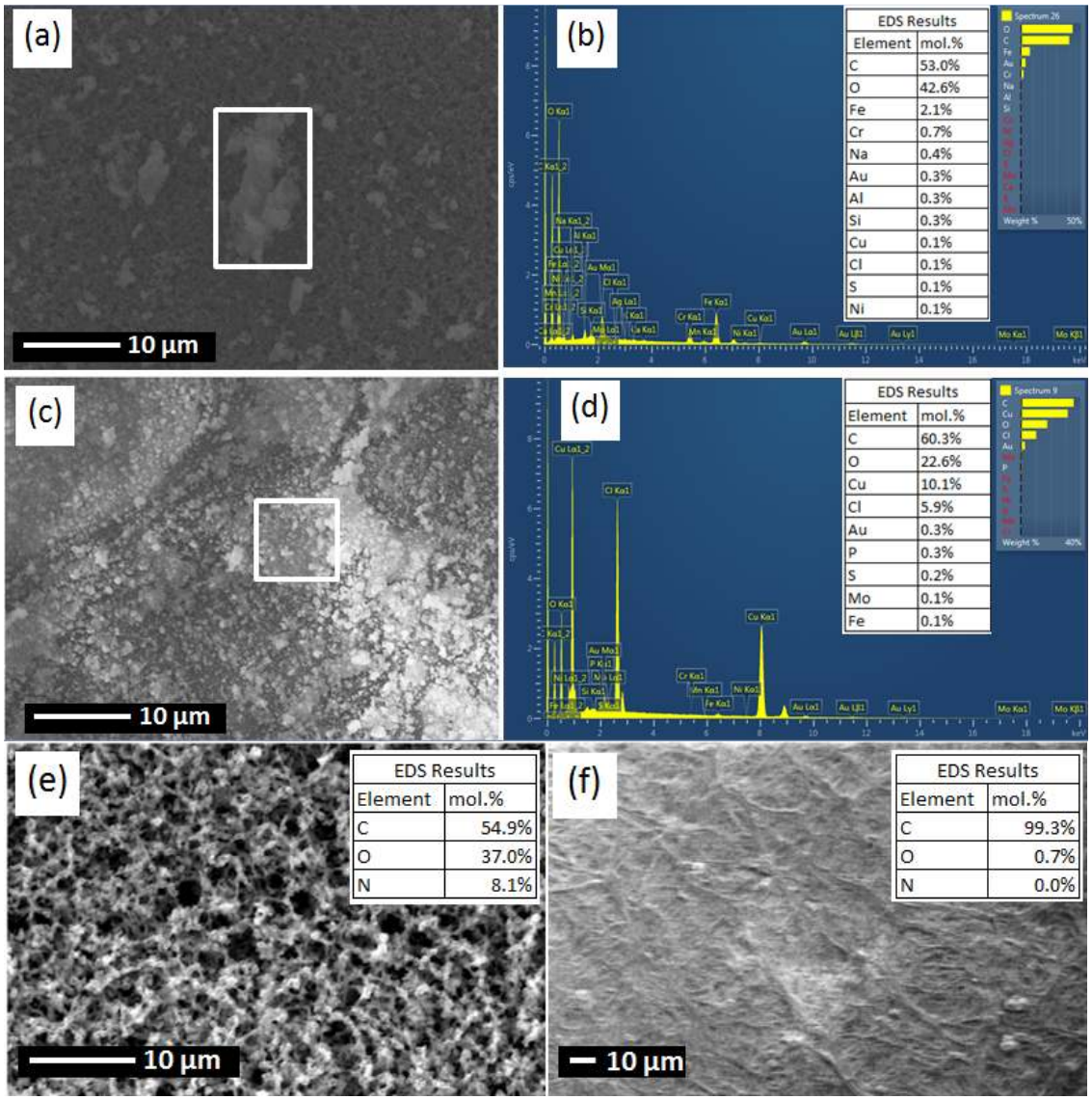

Figure 6.10 SEM-EDS analysis: a) and b) are for 0.45µm nitrocellulose filter from oleophobic PE membrane experiment in comparison with e) virgin nitrocellulose filter; and c) and d) are for standard PE membrane in comparison with f) virgin standard PE membrane.

6.5 Membrane cleaning tests

Cleaning test was performed on the used standard PE membrane sample from Section 6.4, and the effectiveness of cleans were evaluated by SEM-EDS analysis. The results of this test are summarised in Figure 6.11. It can be seen that the fouled membrane surface

was covered by green deposits (Figure 6.11a). EDS analysis results (Figure 6.11b) revealed that the most significant element was Cu at 43.5 wt.%. Cupper (II) salts often display as green color. After chemical cleaning, visual inspection did not observe any green deposits on the entire membrane surface (Figure 6.11c) and EDS analysis revealed that the only peaks associated with C and O were present, reflecting the structure of virgin PE membrane (Figure 6.1a). Interestingly, it was found that deposits displayed as black colour after alkaline clean using 1 wt.% NaOH + 1 wt.% Na_4EDTA (Figure 6.11g). This was likely due to the decomposition of copper compounds (e.g., $Cu_2(OH)_2CO_3$) with formation of CuO (Brown et al. 1984; Radmehr et al. 2013). It is encouraging to see that the proposed chemical cleaning regime was capable of removing foulants from membrane surface at 100% efficiency. Membrane cleaning by adopting weak organic acids (e.g., citric acid) that are readily available for cleaning membrane plants could also be trialed in future studies. From an occupational health and safety perspective, organic acids are less harmful to humans and the environment compared with mineral acid (e.g., HCl). Moreover, organic acids can behave as chelators and form stable complexes with metal ions which accelerate metal salts removal from membrane surface.

The fouled standard PE membrane sample cleaned by RO brine demonstrated that the majority of green deposits were removed from membrane surface (Figure 6.11e). However, a brown fouling layer was observed after cleaning (Figure 6.11e). EDS analysis results revealed a significant reduction of Cu (43.5 to 11.7 wt.%) before and after cleaning (Figure 6.11b and 6.11e), and this was likely due to the reaction between copper salts with ammonia and re-forming of copper-ammonia complexes. EDS analysis also revealed that brown fouling layer contained Fe at 5.0 wt.% (Figure 6.11f), however, Fe was not detected by EDS analysis in Figure 6.11b. This could due to the thickness of Cu salts

fouling layer formed on top of Fe salts exceeded EDS analysis effective depth of 1-2 micrometers. Results in this test suggest that raw RO brine can be used to assist copper salts removal from membrane surface, however, it is not effective for entire fouling layer removal due to the no/weak bond interaction between dissolved ammonia and other foulants, such as Fe salts, aluminum silicates and organics.

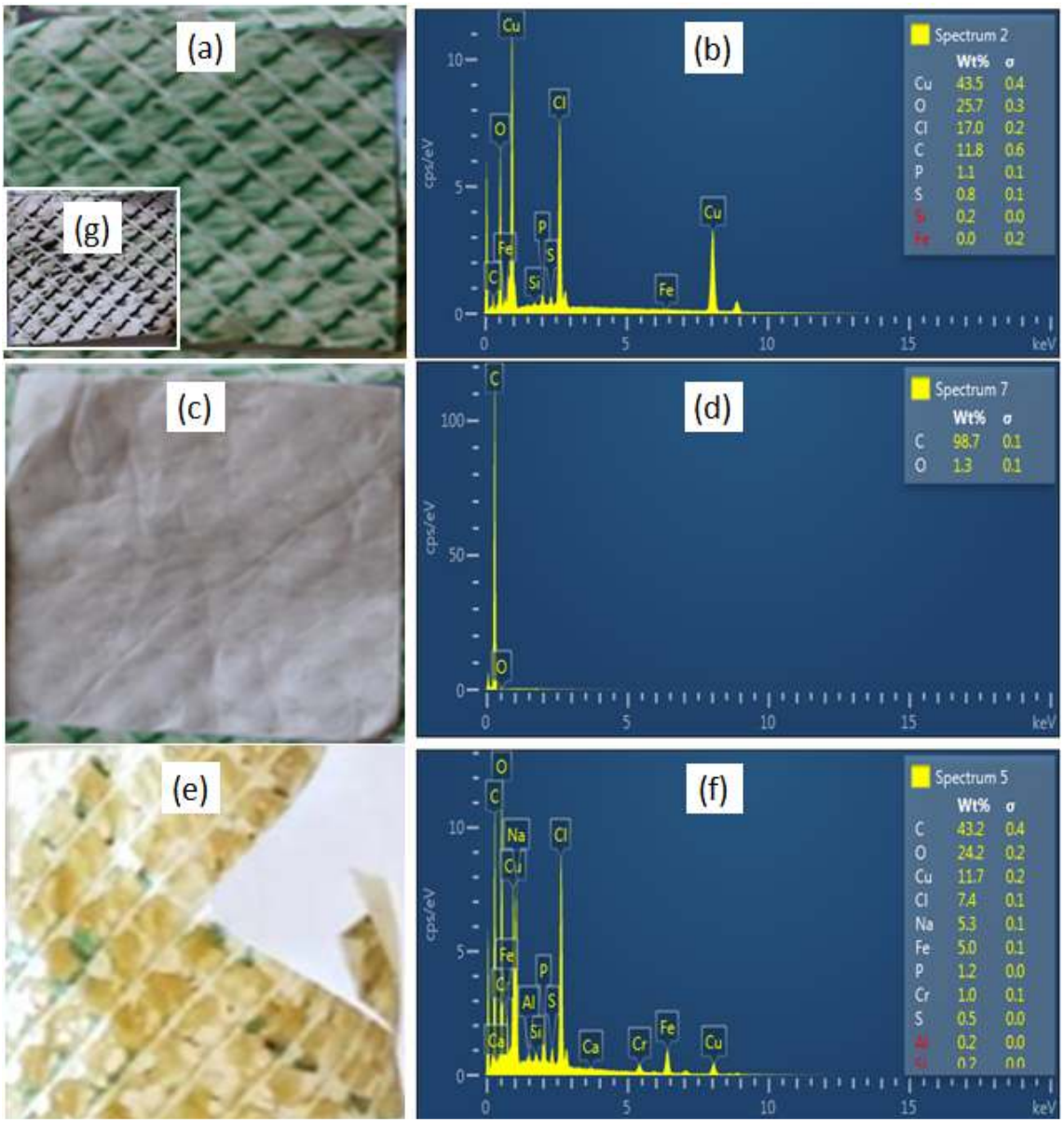

Figure 6.11 SEM–EDS analysis: a) and b) are for fouled standard PE membrane; c) and d) are for chemical cleaned membrane using 1 wt.% NaOH + 1 wt.% Na_4EDTA followed by 1 wt.% HCl; and e) and f) are for RO brine cleaned membrane. SEM micrograph: g) membrane cleaned using 1 wt.% NaOH + 1 wt.% Na_4EDTA.

6.6 Energy assessment of DCMD using standard PE membrane

Compared with oleophobic PE membrane, standard PE membrane nearly doubled the distillate flux (Figure 6.2), which leads to lower STEC according to Equation 3.7. The average STEC of standard PE membrane for DCMD experiment was calculated at approximately 1308 KWh/m^3, and this value is less than the STEC of 1500-1600 KWh/m^3 reported by Dow et al. (2016) for a DCMD pilot study using PTFE membrane with brine feed temperature less than 40 °C and distillate temperature of 20 °C. Lower STEC in this study could due to higher brine feed temperature as well as higher temperature difference between brine and distillate streams (Zaragoza et al. 2014). The waste thermal energy from copper processing plant is estimated at 1.86 MW including processing wastewater thermal energy and exhaust heat from boiler. Therefore, the maximum water production of a DCMD plant (with no heat recycling) is estimated at 34.2 m^3/day according to Equation 6.6, and this equates to 35.6% water recovery from brine.

$$\dot{V}_{prod.max} = 24{,}000 \frac{Q_{wastewater}}{STEC} \quad (6.6)$$

Where $\dot{V}_{prod.max}$ is the maximum production of DCMD plant. $Q_{wastewater}$ is the available thermal energy.

For industrial sites constrained by waste heat sources, using high thermal efficiency MD systems can enhance RO brine recovery. The spiral-wound AGMD module manufactured by Aquastill using standard PE membrane has demonstrated STEC of 175 to 250 kWh/m^3 at distillate flux range of 1.7 to 2.4 L/m^2·h (Duong et al. 2015). Using AGMD can potentially operate MD at higher RO brine recovery utilising existing waste heat source but with much lower flux and therefore, possibly higher Capex. The trade-off of using

DCMD is simpler to install and operate with high flux. In addition, due to the low fouling potential of brine, a hybrid system could be employed to concentrate brine to some fixed level using VMD (low STEC) to improve water recovery and avoid membrane fouling, then, DCMD (high STEC) to achieve desired overall water recovery with higher flux (shorter run time) and higher crossflow to mitigate membrane fouling (Dow et al. 2017).

6.7 UHP RO for brine treatment

With inadequate waste heat on site, UHP RO was explored to concentrate brine to a certain level prior to DCMD. Experiment was conducted using a custom made UHP RO rig (Figure 3.6) to process brine to CF = 3. RO feed and permeate conditions (e.g., flow, pressure, temperature, pH and EC) were recorded and normalised using FTNorm.xls software (Dow Chemical Pty Ltd), and results are shown in Figure 6.12. Throughout the experiment, the permeate flows were maintained at about 0.02 m^3/h which equates to permeate flux of 25 $L/m^2 \cdot h$ (Figure 6.12). Constant normalised permeate flows illustrated in Figure 6.12 indicated that negligible membrane fouling occurred during this test. It appeared that UHP RO is capable to concentrate brine to CF > 3 for a longer operation time. In addition, it was noticed that brine pH only dropped 0.2 throughout the run. Operating RO at much lower temperature than MD could reduce NH_3 degassing from brine and thereby minimising membrane fouling from metal salts. Results here suggest that it is possible to achieve high water recovery from brine at high flux using a hybrid UHP RO + DCMD process.

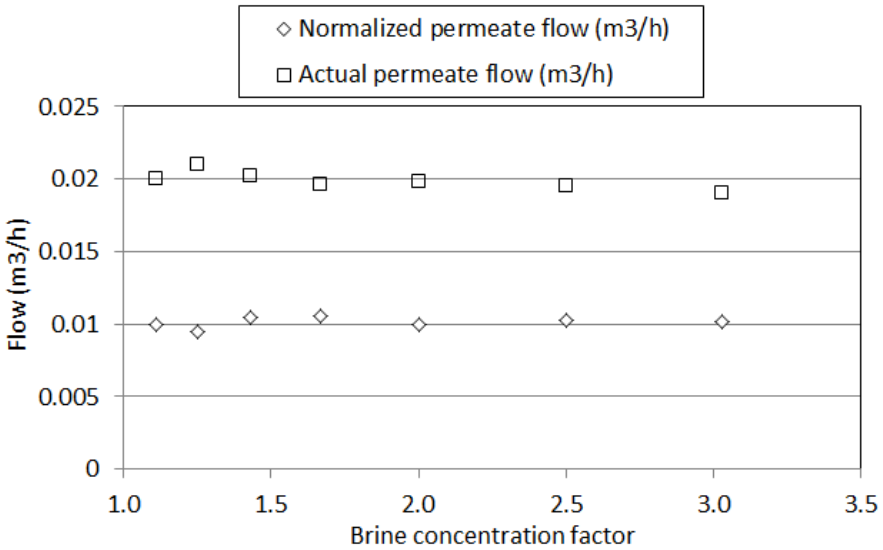

Figure 6.12 Actual permeate flow and normalised permeate flow in UHP RO experiment treating copper barren RO brine. Experiment conditions: feed pressure = 100 bar, feed flow = 5 L/min, total run time = 13 h.

6.8 DCMD of aged brine

It is worth mentioning that at the early stage of this study, an aged brine sample was inadvertently supplied from copper processing manufacturer, and this brine was processed by DCMD using oleophobic PE membrane to brine CF = 5. The behaviour of distillate flux was almost identical as it is shown in Figure 6.2a (results not shown). However, SEM analysis revealed that rod shaped bacteria colonies formed on membrane surface (Figure 6.13). It is shown in Figure 6.13 that all bacteria demonstrated rod shape with rounded ends at approximately 1 μm in length, and these are typical characteristics of nitrifying bacteria includes ammonia-oxidizing bacteria (AOB) and nitrite oxidizing bacteria (NOB) (Koops et al. 1991; Tomiyama et al. 2001). The presence of such bacteria in aged brine is not surprising due to the abundant dissolved NH_3 and exposure to air. It was reported that the optimum growth temperature of nitrifying bacteria is around 30 °C, and nitrifying bacteria dies at > 50 °C (Koops et al. 1991). Therefore, it is important to operate MD process at higher temperature (> 50 °C) to mitigate membrane biofouling.

Cu compound (e.g., $CuSO_4$) is well known as an effective algaecide. Although brine contained 120 mg/L of Cu (Table 3.3), however, Cu did not exist in brine as free Cu^{2+} rather as Cu–NH_3 complexes which has less ability in inhibiting the potential high growth rate of nitrifying bacteria as compared to free Cu^{2+} (Lee et al. 2009).

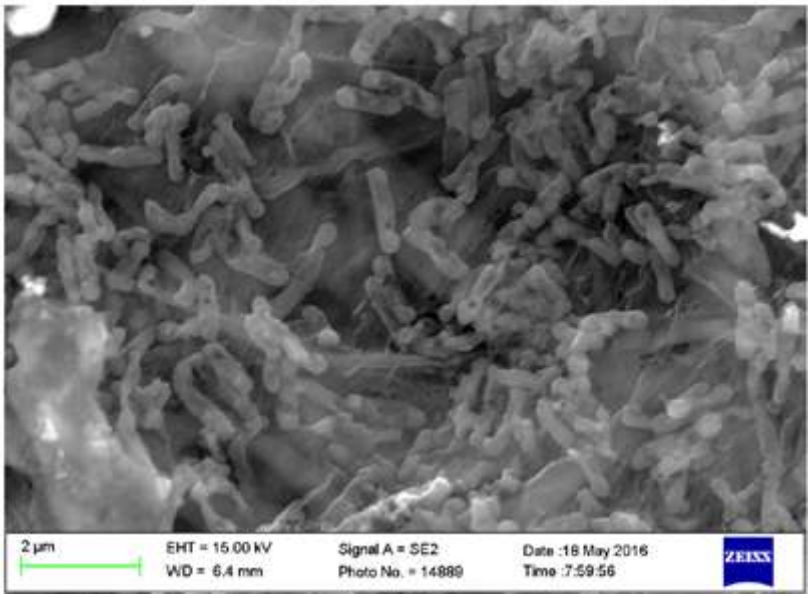

Figure 6.13 SEM image of biological fouling on oleophobic PE membrane surface from DCMD experiment processing aged brine.

6.9 Conclusions

This study investigated MD fouling kinetics while concentrating copper barren RO brine at high water recovery, particularly the behaviour of metal salts precipitation in relation to NH_3 removal from brine. The effectiveness of foulant removal using commercial RO cleaning agents was also evaluated. In addition, the tendency of organic adsorption was compared using two commercial LDPE membranes, with and without oleophobic coating, respectively.

At brine CF = 5, membrane surfaces demonstrated negligible inorganic crystal formation and relatively stable distillate flux was achieved at 17 $L/m^2 \cdot h$ (standard PE membrane)

and 10 L/m^2·h (oleophobic PE membrane), respectively. NH_3 transfer from brine was significant, and it had dominant influence over pH changes in brine and distillate. Dissolved NH_3 at distillate acted as a "strip" solution for CO_2 and achieved near complete removal of inorganic carbon from brine. With NH_3 gradually removed from brine, metal ions such as Fe^{2+} and Ni^{2+} were firstly released from metal-ammonia complexes followed by Cu^{2+}, and this was due to the relative stability of metal-ammonia complexes. Organic adsorption did not occur on both membranes at brine CF = 4 (overall water recovery = 96%). Standard PE membrane favoured the adsorption of organic compounds at brine CF = 5.

Results from this study revealed that it is important to operate DCMD process at above neutral pH to ensure that sufficient free NH_3 is present in brine to from stable metal-ammonia complexes. However, due to high STEC of DCMD process, DCMD can only achieve 35.6% water recovery from brine utilising on-site waste heat source. Without additional thermal energy input, higher water recovery can be obtained by implementing a UHP RO process prior to DCMD.

In the aspect of fouling management, membrane cleaning using 1 wt.% NaOH + 1 wt.% Na_4EDTA followed by 1 wt.% HCl was capable to achieve complete removal of foulants from membrane surface. Using RO brine for cleaning was only effective to remove Cu salts fouling layer. Moreover, in order to mitigate membrane biological fouling, it is recommended to process fresh brine with minimum aging time and operate MD at temperature > 50 ºC.

Overall, this study showed that dissolved ammonia plays an important role in the inhibition of metal salts formation. Both standard PE membrane and oleophobic PE

membrane were capable to treat copper barren RO brine at a four-fold brine concentration with negligible membrane fouling. The flux of oleophobic PE membrane was nearly half of standard PE membrane's flux, and this means much larger membrane surface area is required for oleophobic PE membrane on full-scale installation. Therefore, it is recommended that standard PE membrane to be selected for treatment of copper barren RO brine.

Chapter 7 Conclusion and future research

7.1 Conclusion

In Chapter 4, scaling formation behaviours were investigated for DCMD during SWRO brine treatment. DCMD achieved distillate EC of less than 5 µS/cm and good flux (above 20 L/m^2·h) prior to rapid flux reduction at a brine feed EC of approximately 160 mS/cm. Membrane surface analysis revealed that the major foulants were $CaCO_3$ and $CaSO_4$. Negligible calcium salts crystallisation occurred prior to the critical brine EC. Upon brine EC reached 160 mS/cm, the homogeneous nucleation of calcium salts proceeded rapidly and subsequently formed a thick and highly compacted scaling layer on membrane surface within 4 h of operation. Rapid $CaCO_3$ formation was correlated to the pH variation in brine due to the dissociation of HCO_3^-. In the study of MD fouling mitigation, 5 mg/L of antiscalant in 120 mS/cm brine effectively maintained $CaCO_3$ at supersaturated condition (with S&DSI = 1.24) for 50 h of continuous mode operation. Implementation of a 0.45 µm cartridge filter at the brine feed inlet extended water recovery from 45% to 60% due to the removal of precipitating salts. In addition, simple chemical free membrane cleaning regime involving distillate flushing restored MD initial flux to 98%. Periodic raw SWRO brine feed flushing also restored membrane initial flux to 84% over 133 h of operation. Therefore, a cleaning regime consisting of distillate and SWRO brine flushing of the MD membrane can minimise the chemical cleaning frequency and chemical consumption.

Chapter 5 investigated the silica fouling in DCMD of CSG RO brine. At brine EC of 17.8 mS/cm, DCMD achieved 90% brine recovery (overall recovery of 95%) with distillate flux decline of 16%, and distillate EC of 15 µS/cm over 150 h of operation. The deposits

on membrane surface contained Mg, Ca and Si. Further investigations of DCMD on synthetic CSG RO brine revealed that the salt species were $CaCO_3$ and magnesium silicates. The formation of $CaCO_3$ was rapid and it did not co-precipitate with dissolved silica. On the other hand, the precipitation of magnesium silicates was strongly influenced by the concentration of Mg^{2+} (> 45 mg/L) and brine pH (> 9.2). The species of magnesium silicates appeared consistent with the projection results of Phreeqc–3 software. However, Phreeqc–3 thermodynamic calculations did not successfully predict the precipitation of magnesium silicates. It was hypothesised that abundant Na^+ in brine competes with Mg^{2+} to react with dissolved silica, therefore, postponing the formation of magnesium silicate. Compared to metal silicate fouling, polymeric silica fouling has more profound impact in MD. It was found that polymerised silica formed a non-porous layer on the membrane, which led to rapid flux decline and exponential increase of distillate EC. Moreover, results showed that HCO_3^- / CO_3^{2-} has greater ability to stabilise silica in dissolved form compared with Cl^-. To mitigate membrane fouling, Na_2EDTA treatment demonstrated better performance for inhibiting $CaCO_3$ and magnesium silicate formation compared with commercial phosphonate and polymeric RO antiscalants. Therefore, EDTA addition in MD process could be a feasible option for processing CSG RO brine containing low hardness.

In Chapter 6, DCMD process was explored to concentrate copper barren RO brine solution from an inland copper processing plant. The membrane performance in organic adsorption was evaluated using standard PE membrane and oleophobic PE membrane, respectively. At a five-fold brine concentration, both membrane surfaces demonstrated negligible inorganic crystal formation, and standard PE membrane showed a slight favour for adsorption of organic compounds as compared to oleophobic PE membrane. NH_3

transfer in DCMD process was significant, and it had dominant influence over pH changes in brine and distillate. Dissolved NH_3 at distillate acted as a "strip" solution for CO_2 and achieved near complete removal of inorganic carbon from brine. With NH_3 gradually removed from brine, metal ions such as Fe^{2+} and Ni^{2+} were firstly released from metal-ammonia complexes followed by Cu^{2+}. Results revealed that it is important to operate DCMD process at above neutral pH to ensure that sufficient free NH_3 is present in brine to from stable metal-ammonia complexes. In the aspect of fouling management, membrane cleaning using 1 wt.% NaOH + 1 wt.% Na_4EDTA followed by 1 wt.% HCl was capable to achieve complete removal of foulants from membrane surface. On the other hand, using RO brine for cleaning was only effective to remove copper salts fouling layer.

Overall, the key findings from this study can be summarised as below:

- The implementation of MD in all three brines significantly reduced brine volume and produced high quality distillate. MD demonstrated as a sustainable technology for industry growth, particularly the traditional industries where abundant waste heat is being exhausted.
- For brine with the high potential for $CaCO_3$ and $CaSO_4$ precipitation, antiscalant prolonged MD operational time by mitigating salt precipitation. However, significant homogeneous nucleation of $CaCO_3$ and $CaSO_4$ occurred at critical brine EC level even in the presence of antiscalant. The rapid formation of crystal deposits was correlated to the pH variation in brine, where pH was an early indicator of rapid flux decline. Although distillate flushing was effective in removing inorganic scaling from membrane surface, however, organic fouling showed resistance to non-chemical flushing.

- For brine containing dissolved silica, low hardness and high $NaHCO_3$, Mg^{2+} demonstrated stronger bond with dissolved silica as compared to Ca^{2+}. The precipitation of magnesium silicates was strongly influenced by the concentration of Mg^{2+} and brine pH. HCO_3^- / CO_3^{2-} on the other hand, showed greater ability to stabilise silica in dissolved form compared with Cl^-. In addition, polymeric silica fouling significantly affected MD performances, demonstrated by rapid flux decline and exponential increase of distillate EC.
- MD achieved stable performance with negligible fouling over a relative long period of operation for concentrating brine with high dissolved ammonia and metal ions. At above neutral pH, dissolved ammonia reacted with metal ions and formed stable metal-ammonia complexes in soluble form which prevented membrane fouling from metal deposits.
- Commercial RO antiscalants did not demonstrate fouling potential and cause any pore wetting problem under experimental conditions during DCMD.

Based on the knowledge gained from this research, following recommendations can be made for industrial MD process on RO brine treatment:

- For brine with the high potential for $CaCO_3$ and $CaSO_4$ precipitation, it is a key to determine the critical brine TDS concentration via bench scale / pilot study.
- For brine contains high level of dissolved silica but low hardness, EDTA treatment could be adopted to mitigate the formation of metal-silicates. To reduce the risk of colloidal amorphous silica formation, it is important to avoid sudden temperature drop at MD brine recycling stream.

- In copper processing industry where abundant waste heat is being exhausted and plentiful cooling capacity from existing cooling tower, DCMD is the ideal MD configuration concentrating copper barren RO brine by simultaneously recovering ammonia and water. However, it is important to operate DCMD at above neutral pH to ensure that sufficient free NH_3 is present in brine.
- Intermittent distillate flushing at brine temperature can effectively revert membrane inorganic scaling, and facilitate long-term MD operation at consistent distillate quality and flux.
- Standard PE membrane is ideal for treatment of copper barren RO brine due to high flux and low fouling tendency at a four-fold brine concentration. Oleophobic membrane could be adopted to tackle the high organic containing brines.

From the conclusions stated above, the primary objective of understanding the fouling mechanisms of MD process in RO brine treatment was accomplished well through the study of three real RO brines. The new knowledge on fouling kinetics gained from this thesis have wider implementations of MD fouling research. In addition, findings in MD fouling management strategies, such as cartridge filtration, distillate / raw brine flushing, EDTA / antiscalant treatment and chemical cleaning have practical implications of operating MD process.

7.2 Recommendation for future research

The current research has led to an improved understanding of MD fouling chemistry and mechanisms as well as management of this fouling by inorganic salts, such as $CaCO_3$, $CaSO_4$ and metal silicates. Today, research of practical MD fouling on real solutions is still in its early stage. More focused research on understanding MD fouling and wetting

in the context of real solutions where MD may find application are needed. Several specific research tasks can be further investigated in future, and they include the following:

- Results in Chapter 4 showed that possible organic fouling developed over long-term MD operation. The mechanisms and impacts of NOM fouling in MD process require further understanding. In addition, during the flushing of MD full hot cycle, it was observed that white salt precipitates from heat exchanger were carried to MD module by flushing water, and large undissolved precipitates were trapped in the feed spacer. Scaling of the heat exchanger can be an issue since the highest temperatures in the hot cycle occur inside the heat exchanger. Therefore, future study is needed on mitigating scale formation in heat exchanger.
- It was reported in Chapter 5 that polymerised silica fouling can significantly impact on MD performance and possibly lead to membrane wetting. Research is necessary to improve the understanding of silica polymerisation in MD process and determine the best practice (including operational limits / conditions) for silica fouling mitigation in MD. In addition, beaker test results suggested that silica removal could be obtained by incorporating heat exchangers for rapid cooling of MD brine followed by brine stabilisation (aging) and filtration / clarification. Assessment of this proposed treatment is recommended to improve water recovery from RO brine.
- Results in Chapter 6 showed that oleophobic PE membrane has advantage in treating RO brine containing high organic content. However, the distillate flux was only about 50% of the standard PE membrane. Further membrane material optimisation is needed to improve the distillate flux of oleophobic membrane.

Membrane biological fouling was also reported in Chapter 6. So far, the research of biological fouling in MD is very scarce, and study needs to be undertaken in this specific area.

- In this study, RO spacer was used at brine feed with the intention of providing more turbulent flow and therefore less fouling. However, spacer demonstrated a tendency to trap deposits. In addition, in all experiments the membrane module was placed in the horizontal position with feed side facing up, and this may enhance membrane fouling due to salt precipitation. Therefore, the effects of feed spacer configurations and module orientations on MD fouling need further evaluation.
- The current study has identified the water recovery limits of all three RO brines using MD process. It would be advantageous to develop a mathematical model to predict the MD internal heat recoveries in different MD module designs. The Capex of MD system can be estimated based on the specific site conditions (e.g., available heat source) and the complexity of MD module design. The Opex of MD system can be estimated by incorporating the fouling mitigation strategies that were proposed in the present research. Then, the suitability of RO brine treatment using MD technology can be determined in each case.

Reference

Abu-Zeid M A E-R, Zhang Y, Dong H, Zhang L, Chen H-L, Hou L. A comprehensive review of vacuum membrane distillation technique. Desalination 2015; 356: 1-14.

Ahmed M, Shayya W H, Hoey D, Al-Handaly J. Brine disposal from reverse osmosis desalination plants in Oman and the United Arab Emirates. Desalination 2001; 133: 135-147.

Alklaibi A M, Lior N. Membrane distillation desalination: status and potential. Desalination 2004; 171: 111-131.

Al-Obaidani S, Drioli E. Potential of membrane distillation in seawater desalination: thermal efficiency, sensitivity study and cost estimation. Journal of Membrane Science 2008; 323: 85-98.

Alsogair S. Reverse osmosis and nano-filtration innovation for water reuse. 5th Water Arabia Conference and Exhibition. 17th – 19th October 2017. Al-Khobar, Saudi Arabia. Available from http://sawea.org/waterarabia2017/.

Ang W S, Lee S, Elimelech M. Chemical and physical aspects of cleaning of organic fouled reverse osmosis membranes. Journal of Membrane Science 2006; 272: 198-210.

Australian Water Association fact sheet: desalination. 2018. Available from http://www.awa.asn.au/AWA_MBRR/Publications/Fact_Sheets/Desalination_Fact_Sheet.aspx.

Bandini S, Sarti G C. Concentration of must through vacuum membrane distillation. Desalination 2002; 149: 253-259.

Bansal V, Keller C. Membrane distillation modules during oleophobically and antimicrobially treated microporous membranes 2013; Patent US8801933B2.

Bergna H E, Roberts W O. Colloidal silica: fundamentals and application. CRC Press, 2005.

Blandin G, Verliefde A R D, Tang C Y, Childress A E, Le-Clech P. Validation of assisted forward osmosis (AFO) process: impact of hydraulic pressure. Journal of Membrane Science 2013; 447: 1-11.

Bouchrit R, Boubakri A, Hafiane A, Bouguecha S A-T. Direct contact membrane distillation: capability to treat hyper-saline solution. Desalination 2015; 376: 117-129.

Bremere I, Kennedy M, Mhyio S, Jaljuli A, Witkamp G-J, Schippers J. Prevention of silica scale in membrane systems: removal of monomer and polymer silica. Desalination 2000; 132: 89-100.

Brown I W M, Mackenzie K J D, Gainsford G J. Thermal decomposition of the basic copper carbonates malachite and azurite. Thermochimica Acta 1984; 74: 23-32.

Camacho L M, Dumee L, Zhang J, Li J, Duke M, Gomez J, and Gray S. Advances in membrane distillation for water desalination and purification applications. Water 2013 (5), 94–196.

Cameron D. Coal seam gas. Engineers Media 2011. Available from http://www.engineersmedia.com.au.

Cath T Y, Adams D, Childress A E. Experimental study of desalination using direct contact membrane distillation: a new approach to flux enhancement. Journal of Membrane Science 2003; 228: 5-16.

Chester S P, Morton P, Fazel M. Membrane and minewater: waste or revenue stream. Proceedings IMWA 2016.

Clesceri L S, Greenberg A E, Eaton A D. Standard method for the examination of water and wastewater. 20th ed. American Water Works Association.

Curcio E, Ji X, Profio G D, Sulaiman A O, Fontananova E, Drioli E. Membrane distillation operated at high seawater concentration factors: role of the membrane on $CaCO_3$ scaling in presence of humic acid. Journal of Membrane Science 2010; 346: 263-269.

Demadis K D. The Science and Technology of Industrial Water Treatment – Chapter 10 recent development in controlling silica and magnesium silicate fouling in industrial water systems. CRC Press, 2010.

Deshmukh A, Boo C, Karanikola V, Lin S, Straub A P, Tong T, Warsinger D M, Elimelech M. Membrane distillation at the water-energy nexus: limits, opportunities, and challenges. Energy & Environmental Science 2018; 11: 1177-1196.

Ding Z, Liu L, Li Z, Ma R, Yang Z. Experimental study of ammonia removal from water by membrane distillation (MD): the comparison of three configurations. Journal of Membrane Science 2006; 286: 93-103.

Dow N, Gray S, Li J-D, Zhang J, Ostarcevic E, Liubinas A, Atherton P, Roeszler G, Gibbs A, Duke M. Pilot trial of membrane distillation driven by low grade waste heat: membrane fouling and energy assessment. Desalination 2016; 391: 30-42.

Dow N, Garcia J V, Niadoo L, Milne N, Zhang J, Gray S, Duke M. Demonstration of membrane distillation on textile waste water: assessment of long term performance, membrane cleaning and waste heat integration. Environmental Science: Water Research & Technology 2017; 3: 433-449.

Dow N, Duke M, Zhang J, O'Reilly T, Li J-D, Ostarcevic E, Atherton P. Demonstration of solar driven membrane distillation in remote Victoria. Ozwater'10: 08-10 March 2010.

Drioli E, Ali A, Macedonio F. Membrane distillation: recent development and perspectives. Desalination 2015; 356: 56-84.

Drioli E, Ali A, Macedonio F. Membrane operations for process intensification in desalination. Applied Science 2017; 7 (1), 100.

Duong H C, Chivas A R, Nelemans B, Duke M, Gray S, Cath T Y, Nghiem L D. Treatment of RO brine from CSG produced water by spiral-wound air gap membrane distillation: a pilot study. Desalination 2015; 366: 121-129.

Duong H C, Duke M, Gray S, Nelemans B, Nghiem L D. Membrane distillation and membrane electrolysis of coal seam gas reverse osmosis brine for clean water extraction and NaOH production. Desalination 2016; 197: 108-115.

Emerson K, Russo R C, Lund R E, Thurston R B. Aqueous ammonia equilibrium calculations: effects of pH and temperature. Journal of the Fisheries Research Board of Canada. 1975; 32: 2379-2383.

Falini G, Fermani S, Tosi G, Dinelli E. Calcium carbonate morphology and structure in the presence of seawater ions and humic acids. Crystal Growth and Design 2009; 9: 2065-2072.

Fell C. Water treatment and coal seam gas 2014. Available from http://www.chiefscientist.nsw.gov.au/__data/assets/pdf_file/0005/56858/Water-treatment-and-CSG_Final.pdf.

Forbes R J. A short history of the art of distillation: from the beginnings up to the death of Cellier Blumenthal. 2nd ed. Brill Academic Publishers; 1970.
Francis L, Ghaffour N, Al-Saadi A A, Amy G L. Material gap membrane distillation: a new design for water vaour flux enhancement. Journal of Membrane Science 2013; 448: 240-247.
Gilron J, Ladizansky Y, Korin E. Silica fouling in direct contact membrane distillation. Ind. Eng. Chem. Res. 2013; 52: 10521−10529.
Giwa A, Dufour V, Marzooqi F A. Kaabi A, Hasan S W. Brine management methods: recent innovations and current status. Journal of Desalination 2017; 407: 1-23.
Glater J and Cohen Y. Brine disposal from land based membrane desalination plants: a critical assessment, a report prepared for the Metropolitan Water District of South California. 2003.
Global water intelligence. Global water market 2017. Available from http://www.globalwaterintel.com.
Gloede M, Melin T. Physical aspects of membrane scaling. Desalination 2008; 224: 71-75.
Glueckstern P, Priel M. Optimized brackish water desalination plants with minimum impact on the environment. Desalination 1996; 108: 19-26.
Greenlee L F, Testa F, Lawler D F, Freeman B D, Moulin P. The effect of antiscalant addition on calcium carbonate precipitation for a simplified synthetic brackish water reverse osmosis concentrate. Water Research 2010; 44: 2957-2969.
Gryta M. Alkaline scaling in the membrane distillation process. Desalination 2008; 228: 128-134.
Gryta M. Influence of polypropylene membrane surface porosity on the performance of membrane distillation process. Journal of Membrane Science 2007; 287: 67-78.
Gryta M. Fouling in direct contact membrane distillation process. Journal of Membrane Science 2008; 325: 383-394.
Gryta M. Polyphosphates used for membrane scaling inhibition during water desalination by membrane distillation. Desalination 2012; 285: 170-176.
Gryta M. Long-term performance of membrane distillation process. Journal of Membrane Science 2005; 265: 153-159.
Gryta M. Calcium sulphate scaling in membrane distillation process. Chemical Papers 2009; 63: 146-151.
Gude G. Renewable energy powered desalination handbook: application and thermodynamics. 1st ed. Butterworth-Heinemann: Oxford; 2018, P287.
Guillen-Burrieza E, Thomas R, Mansoor B, Johnson D, Hilal N, Arafat H. Effect of dry-out on the fouling of PVDF and PTFE membranes under conditions simulating intermittent seawater membrane distillation (SWMD). Journal of Membrane Science 2013; 438: 126-139.
Guillen-Burrieza E, Ruiz-Aguirre A, Zaragoza G, Arafat H A. Membrane fouling and cleaning in long term plant-scale membrane distillation operations. Journal of Membrane Science 2014; 468: 360-372.
Gunnarsson I, Arnórsson S. Amorphous silica solubility and the thermodynamic properties of $H_4SiO_4^\circ$ in the range of 0° to 350°C at P_{sat}. Geochimica et Cosmochimica Acta 2000; 64: 2295-2307.
Hamawand I, Yusaf T, Hamawand S G. Coal seam gas and associated water: a review paper. Renewable and Sustainable Energy Reviews 2013; 22: 550-560.

Hao Y, Moriya A, Maruyama T, Ohmukai Y, Matsuyama H. Effect of metal ions on humic acid fouling of hollow fiber ultrafiltration membrane. Journal of Membrane Science 2011; 376: 247-253.
Hasson D, Drak A, Semiat R. Induction times induced in an RO system by antiscalants delaying CaSO4 precipitation. Desalination 2003; 157: 193-207.
Hausmann A, Sanciolo P, Vasiljevic T, Weeks M, Schroën K, Gray S, Duke M. Fouling mechanisms of dairy streams during membrane distillation. Journal of Membrane Science 2013; 441: 102-111.
Hausmann A, Sanciolo P, Vasijevic T, Kulozik U, Duke M. Journal of Dairy Science 2014; 97: 56-71.
He F, Sirkar K K, Gilron J. Studies on scaling of membrane in desalination by direct contact membrane distillation: $CaCO_3$ and mixed $CaCO_3/CaSO_4$ systems. Chemical Engineering Science 2009; 64: 1844-1859.
Hoch A R, Reddy M M, Aiken G R. Calcite crystal growth inhibition by humic substances with emphasis on hydrophobic acids from the Florida Everglades. Geochimica et Cosmochimica Acta 2000; 64: 61-72.
Hsu S T, Cheng K T, Chiou J S. Seawater desalination by direct contact membrane distillation. Desalination 2002; 143: 279-287.
Hwang H J, He K, Gray S, Zhang J H, Moon I S. Direct contact membrane distillation (DCMD): Experiment study on the commercial PTFE membrane and modelling. Journal of Membrane Science 2011; 371: 90-98.
Iler R K. The chemistry of silica: solubility, polymerisation, colloid and surface properties and biochemistry. John Wiley and Sons, New York, USA, 1979.
Irving H, William J P. The stability of transition-metal complexes. Inorganic Chemistry 1953; 0: 3192–3210.
Jermann D, Pronk W, Boller M M. Interplay of different NOM fouling mechanisms during ultrafiltration for drinking water production. Water Research 2007; 41: 1713-1722.
Karlapudi R. Process for treating concentrated brine. 2015, Patent US2015/0158748 A1.
Khalifa A E, Lmteyaz B A, Lawal D U, Abido M A. Heuristic optimisation techniques for air gap membrane distillation system. Arabian Journal for Science and Engineering 2017; 5: 1951-1965.
Khan S, Kordek G. Coal seam gas: produced water and solids 2014. Available from http://www.chiefscientist.nsw.gov.au/__data/assets/pdf_file/0017/44081/OCSE-Final-Report-Stuart-Khan-Final-28-May-2014.pdf.
Khayet M, Velázquez A, Mengual J I. Direct contact membrane distillation of humic acid solutions. Journal of Membrane Science 2004; 240: 123-128.
Koo T, Lee Y J, Sheikholeslami R. Silica fouling and cleaning of reverse osmosis membranes. Desalination 2001; 139: 43-56.
Koops H P, Böttcher B, Möller U C, Pommerening-Röser, Stehr D. Classification of eight new species of ammonia-oxidizing bacteria:*Nitrosomonas communis sp.nov., Nitrosomonas ureae sp. nov., Nitrosomonas aestuarii sp. nov., Nitrosomonas marina sp. nov., Nitrosomonas nitrosa sp. nov., Nitrosomonas eutropha sp. nov., Nitrosomonas oligotropha sp. nov. and Nitrosomonas halophila sp. nov.* Journal of General Microbiology 1991; 137: 1689-1699.
Lalia B S, Kochkodan V, Hashaikeh R, Hilal N. A review on membrane fabrication: structure, properties and performance relationship. Desalination 2013; 326: 77-95.

Laskin A, Moffet R C, Gilles M K, Fast J D, Zaveri R A, Wang B, Nigge P, Shutthanandan J. Tropospheric chemistry of internally mixed sea salt and organic particles: surprising reactivity of NaCl with weak organic acids. Journal of Geophysical Research 2012; 117: D15302.

Latour I, Miranda R, Blanco A. Silica removal with sparingly soluble magnesium compounds. Part I. Separation and Purification Technology 2014; 138: 210-218.

Lawson K W, Lloyd D R. Membrane distillation. Journal of Membrane Science 1997; 124: 1-25.

Le H. Innovative commercial and technical solutions for CSG produced water treatment project. Chemical Engineering World Magazine. April 2017.

Lee S, Choi J, Park Y-G, Shon H, Ahn C H, Kim S-H. Hybrid desalination processes for beneficial use of reverse osmosis brine: current status and future prospects 2018. Desalination; article in press.

Lee S, Cho J, Elimelech M. Combined influence of natural organic matter (NOM) and colloidal particles on nanofiltration membrane fouling. Journal of Membrane Science 2005; 262: 27-41.

Lee Y-W, Tian Q, Sato C, Chung J. Inhibitory effects of copper on nitrifying bacteria in suspended and attached growth reactors. Water Air and Soli Pollution 2009; 203: 17-27.

Lisdonk C A C, Rietman B M, Heijman S G J, Sterk G R, Schippers J C. Prediction of supersaturation and monitoring of scaling in reverse osmosis and nanofiltration membrane systems. Journal of Desalination 2001; 138: 259-270.

Liu S-T, Nancollas G H. The crystallisation of magnesium hydroxide. Desalination 1973; 12: 75-84.

Lunevich L, Sanciolo P, Dumée L F, Gray S. Silica fouling in high salinity waters in reverse osmosis desalination (sodium-silica system). Environmental Science: Water Research & Technology 2016; 2: 539-548.

Marshall W J, Warakomski J M. Amorphous silica solubility – II. Effect of aqueous salt solutions at 25 ºC. Geochimca et Cosmochimica Acta 1980; 44: 915-924.

Martinetti C. R, Childress A E, Cath T Y. High recovery of concentrated RO brines using forward osmosis and membrane distillation. Journal of Membrane Science 2009; 331: 31-39.

McCain W D. The properties of petroleum fluids. 2nd ed, PennWell Books, Tulsa, Oklahoma, 1990.

Mehta S, Nicoll P. Novel technology for concentration of brine using membrane-based system. Water Today Magazine. January 2018.

Meng S, Ye Y, Mansouri J, Chen V. Fouling and crystallisation behaviour of superhydrophobic nano-composite PVDF membranes in direct contact membrane distillation. Journal of Membrane Science 2014; 463: 102-112.

Mericq J-P, Laborie S, Cabassud C. Vacuum membrane distillation of seawater reverse osmosis brines. Water Research 2010; 44: 5260-5273.

Millar G J, Couperthwaite S J, Moodliar C D. Strategies for the management and treatment of coal seam gas associated water. Renewable and Sustainable Energy Reviews 2016; 57: 669-691.

Milne N A, O'Reilly T, Sanciolo P, Ostarcevic E, Beighton M, Taylor K, Mullett M, Tarquin A J, Gray S R. Chemistry of silica scale mitigation for RO desalination with particular reference to remote operations. Water Research 2014; 65: 107-133.

Mitsuoka H, Kikuchi S. Polyethylene microporous membrane and process for manufacturing same. 2013, European Patent EP2832781B1.
Morillo J, Usero J, Rosado D, Bakouri H E, Riaza A, Bernaola F-J. Comparative study of brine management technologies for desalination plants. Journal of Desalination 2014; 336: 32-49.
Mudd G M. Water and mining in Australia: towards an improved future? 2007. Available from http://www.civil.eng.monash.edu.au.
Naidu G, Jeong S, Vigneswaran S. Interaction of humic substances on fouling in membrane distillation for seawater desalination. Chemical Engineering Journal 2015; 262: 946-957.
Naidu G, Jeong S, Kim S-J, Kim I S, Vigneswaran S. Organic fouling behaviour in direct contact membrane distillation. Desalination 2014; 347: 230–239.
Nghiem L D, Elters C, Simon A, Tatsuya T, Price W. Coal seam gas produced water treatment by ultrafiltration, reverse osmosis and multi-effect distillation: a pilot study. Separation and Purification Technology 2015; 146: 94-100.
Nghiem L D, Cath T. A scaling mitigation approach during direct contact membrane distillation. Separation and Purification Technology 2011; 80: 315-322.
Nguyen Q M, Lee S. Fouling analysis and control in a DCMD process for SWRO brine. Desalination 2015; 367: 21-27.
Nguyen Q-M, Jeong S, Lee S. Characteristics of membrane foulants at different degrees of SWRO brine concentration by membrane distillation. Desalination 2017; 409: 7-20.
Ning R Y. Discussion of silica speciation, fouling, control and maximum reduction. Desalination 2002; 151: 67-73.
Nowack B, Sigg L. Adsorption of EDTA and metal-EDTA complexes onto goethite. Journal of Colloid and Interface Science 1996; 177: 106-121.
Oh H-J, Choung Y-K, Lee S, Choi J-S, Hwang T-M, Kim J H. Scale formation in reverse osmosis desalination model development. Desalination 2009; 238: 333-346.
Oztekin E, Altin S. Wastewater treatment by electrodialysis system and fouling problems. Journal of Science and Technology. 2016; 6: 91-99.
Pavuluri et al. Kinetic approach for modeling salt precipitation in porous-media. Master Thesis. 2014 Available from https://www.researchgate.net/publication/262495450_Kinetic_approach_for_modeling_salt_precipitation_in_porous-media.
Phattaranawik J, Jiraratananon R, Fane A G. Heat transport and membrane distillation coefficients in direct contact membrane distillation. Journal of Membrane Science 2003; 212: 177-193.
Plavšić M, Ćosović B, Rodić S. Adsorption of polyacrylic acid on hydrophobic and hydrophilic surfaces. Colloidal and Polymer Science 1996; 274: 548-554.
Qu D, Sun D, Wang H, Yun Y. Experiment study of ammonia removal from water by modified direct contact membrane distillation. Desalination 2013; 326: 135-140.
Radmehr V, Koleini S M J, Khalesi M R, Mohammadi M R T. Ammonia leaching: a new approach of copper industry in hydrometallurgical processes. J. Inst. Eng. India Ser. D 2014; 94 (2): 95–104.
Richardson W H. Handbook of copper compounds and applications. CRC Press; 1997.
Rioyo J, Aravinthan V, Bundschuh J, Lynch M. A review of strategies for RO brine minimisation in inland desalination plants. Desalination and Water Treatment 2017; 90: 110-123.

Saffarini R B, Summers E K, Arafat H A, Lienhard V J H. Technical evaluation of stand-alone solar powered membrane distillation systems. Desalination 2012; 286: 332-341.
Sharqawy M H, Lienhard J H, Zubair S M. Thermophysical properties of seawater: a review of existing correlations and data. Desalination and Water Treatment 2010; 16: 354-380.
Sheikholeslami R, Tan S. Effect of water quality on silica fouling of desalination plants. Desalination 1999; 126: 267-280.
Sheikholeslami R, Al-Mutaz I.S, Koo T, Young A. Pretreatment and the effect of cations and anions on prevention of silica fouling. Desalination 2001; 139: 83-95.
Sheikholeslami R, Ong H W K. Kinetics and thermodynamics of calcium carbonate and calcium sulfate at salinities up to 1.5 M. Desalination 2003; 157: 217-234.
Sheikholeslami R, Al-Mutaz I S, Tan S, Tan S D. Some aspects of silica polymerisation and fouling and its pretreatment by sodium aluminate, lime and soda ash. Desalination 2002; 150: 85-92.
Soderberg R W. Flowing water fish culture. 1995, Lewis Publishers, Boca Raton, Florida.
Stillwell A, Webber M. Predicting the specific energy consumption of reverse osmosis. Water 2016;. 8, 601.
Subramani A, Jacangelo J G. Treatment technologies for reverse osmosis concentrate volume minimisation: a review. Separation and Purification Technology 2014; 122: 472-489.
Szyplinska P. Thirsty World of Mining: harvesting New Water Solutions. 2011. Available from http://www.waterworld.com/articles/wwi/print/volume-27/issue-1/regulars/creative-finance/thirstyworld-of-mining.html.
Thomas N, Mavukkandy M O, Loutatidou S, Arafat H A. Membrane distillation research and implementation: lessons from the past five decades. Separation and Purification Technology 2017; 189: 108-127.
Tijing L D, Woo Y C, Choi J-S, Lee S, Kim S-H, Shon H K. Fouling and its control in membrane distillation: a review. Journal of Membrane Science 2015; 475: 215-244.
Tomiyama H, Ohshima M, Ishii S, Satoh K, Takahashi R, Isobe K, Iwano H, Tokuyama T. Characteristics of newly isolated nitrifying bacteria from Rhizoplane of Paddy Rice. Microbes and Environments 2001; 16: 101-108.
Trevani L N, Roberts J C, Tremaine P R. Copper (II)-ammonia complexation equilibria in aqueous solutions at temperatures from 30 to 250 ºC by visible spectroscopy. Journal of Solution Chemistry 2001; 30: 585-622.
Tsiakis P, Papageorgiou L G. Optimal design of an electrodialysis brackish water desalination plant. Desalination 2005; 173: 173-186.
Truesdell A H, Jones B F. WATEQ, a computer program for calculating chemical equilibria of natural waters. Journal of Research, U.S. Geological Survey, 1974; v. 2, 233-274.
Tun C M, Fane A G, Matheickal J T, Sheikholeslami R. Membrane distillation crystallisation of concentrated salts: flux and crystal formation. Journal of Membrane Science 2005; 257: 144-155.
Ugrozov V V, Elkina I B, Nikulin V N, Kataeva L I. Theoretical and experimental research of liquid-gap membrane distillation process in membrane module. Desalination 2003; 157: 325-331.

Waly T, Kennedy M D, Witkamp G-J, Amy G, Schippers J C. The role of inorganic ions in the calcium carbonate scaling of seawater osmosis systems. Desalination 2012; 284: 279-287.

Wang Z, Hou D, Lin S. Composite membrane with underwater-oleophobic surface for anti-oil-fouling membrane distillation. Environmental Science and Technology 2016; 50 (7) : 3866-3874.

Warsinger D M, Swaminathan J, Guillen-Burrieza E, Arafat H A, Lienhard V J H. Scaling and fouling in membrane distillation for desalination application: a review. Desalination 2015; 356: 294-313.

Weres O, Yee A, Tsao L. Kinetics of silica polymerisation. Prepared for the U.S. Department of Energy under Contract W-7405-ENG-48. 1980.

Woldemariam D, Kullab A, Fortkamp U, Magner J, Royen H, Martin A. Membrane distillation pilot plant trials with pharmaceutical residues and energy demand analysis. Chemical Engineering Journal 2016; 306: 471-483.

Xie Z, Duong T, Hoang M, Nguyen C, Bolto B. Ammonia removal by sweep gas membrane distillation. Water Research 2009; 43: 1693-1699.

Yang X, Ding L, Wolf M, Velterop F, Bouwmeester H J M, Smart S, Diniz da Costa J C, Liubinas A, Li J-D, Zhang J, Duke M, Pervaporation of ammonia solution with γ-alumina supported organosilica membranes. Separation and Purification Technology 2016; 168: 141-151.

Yang X, Pang H, Zhang J, Liubinas A, Duke M. Sustainable wastewater deammonification by vacuum membrane distillation without pH adjustment: Role of water chemistry. Chemical Engineering Journal 2017; 328: 884–893.

Yu X, Yang H, Lei H, Shapiro A. Experimental evaluation on concentrating cooling tower blowdown water by direct contact membrane distillation. Desalination 2013; 323:134-141.

Zaragoza G, Ruiz-Aguirre A, Guillén-Burriea E. Efficiency in the use of solar thermal energy of small membrane desalination systems for decentralized water purification. Applied Energy 2014; 130: 491–499.

Zhang J, Dow N, Duke M, Ostarcevic E, Li J-D, Gray S. Identification of material and physical features of membrane distillation membranes for high performance desalination. Journal of Membrane Science 2010; 349: 295-303.

Zhang J, Duke M, Ostarcevic E, Dow N, Gray S, Li J-D. Performance of new generation membrane distillation membranes. Water Science & Technology: Water Supply – WSTWS 2009; 9: 501-508.

Zhang J, Gray S, Li J-D. Predicting the influence of operating conditions on DCMD flux and thermal efficiency for incompressible and compressible membrane systems. Desalination 2013; 323: 142-149.

Zhang J, Gray S, Li J-D. Modelling heat and mass transfers in DCMD using compressible membranes. Journal of Membrane Science 2017; 387-388: 7-16.

Zhang P, Knötig P, Gray S, Duke M. Scale reduction and cleaning techniques during direct contact membrane distillation of seawater reverse osmosis brine. Desalination 2015; 374: 20-30.

Zhong W, Li H, Ye Y, Chen V. Evaluation of silica fouling for coal seam gas produced water in a submerged vacuum membrane distillation system. Desalination 2016; 393: 52-64.

Appendix A Design of DCMD module flow channels